NUMERICAL SOLUTION OF THE STAGNATION POINT FLOW AND HEAT TRANSFER WITH SEVERAL EFFECTS

HASMAWANI BT HASHIM

MASTER OF SCIENCE (MATHEMATICS)

UNIVERSITI MALAYSIA PAHANG

UNIVERSITI MALAYSIA PAHANG

<div style="border:1px solid black">

DECLARATION OF THESIS AND COPYRIGHT

Author's Full Name : <u>HASMAWANI BT HASHIM</u>

Date of Birth : <u>24 MARCH 1982</u>

Title : <u>NUMERICAL SOLUTION OF THE STAGNATION POINT</u>
<u>FLOW AND HEAT TRANSFER WITH SEVERAL EFFECTS</u>

Academic Session : <u>SEM II 2019/2020</u>

I declare that this thesis is classified as:

☐ CONFIDENTIAL (Contains confidential information under the Official Secret
Act 1997)*

☐ RESTRICTED (Contains restricted information as specified by the
organization where research was done)*

☒ OPEN ACCESS I agree that my thesis to be published as online open access
(Full Text)

I acknowledge that Universiti Malaysia Pahang reserves the following rights:

1. The thesis is the property of Universiti Malaysia Pahang.
2. The Library of Universiti Malaysia Pahang has the right to make copies of the
thesis for the purpose of research only.
3. The Library has the right to make copies of the thesis for academic exchange.

Certified by:

_____   _____
(Student's Signature)   (Supervisor's Signature)

820324-03-6100   Professor Dr. Mohd Zuki Salleh
_____   _____
New IC/Passport Number   Name of Supervisor
Date: Date:

</div>

NOTE : * If the thesis is CONFIDENTIAL or RESTRICTED, please attach a thesis declaration
letter.

SUPERVISOR'S DECLARATION

We hereby declare that we have checked this thesis and in our opinion, this thesis is adequate in terms of scope and quality for the award of the degree of Master of Science (Mathematics).

_____

(Supervisor's Signature)

Full Name   : DR. MOHD ZUKI SALLEH

Position   : PROFESSOR

Date   :

_____

(Co-supervisor's Signature)

Full Name   : DR. NORHAFIZAH MD SARIF

Position   : SENIOR LECTURER

Date   :

STUDENT'S DECLARATION

I hereby declare that the work in this thesis is my original work except for quotations and citation which have been duly acknowledged. I also declare that it has not been previously or concurrently submitted for any other degree at Universiti Malaysia Pahang or any other institutions.

_____

(Author's Signature)

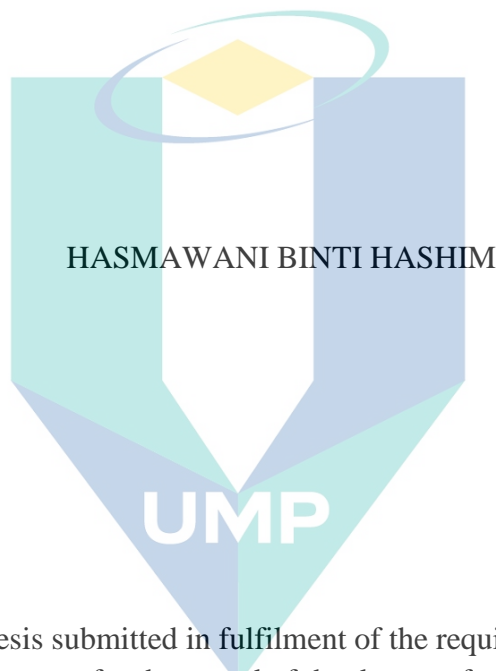Full Name   : HASMAWANI BINTI HASHIM
ID Number   : MSE14001
Date   :

NUMERICAL SOLUTION OF THE STAGNATION POINT FLOW AND HEAT
TRANSFER WITH SEVERAL EFFECTS

HASMAWANI BINTI HASHIM

Thesis submitted in fulfilment of the requirements
for the award of the degree of
Master of Science (Mathematics)

Centre for Mathematical Sciences
UNIVERSITI MALAYSIA PAHANG

SEPTEMBER 2020

ACKNOWLEDGEMENTS

ABSTRAK

Masalah melibatkan aliran lapisan sempadan dan pemindahan haba adalah penting disebabkan oleh pelbagai aplikasi praktikal yang terdapat dalam bidang kejuruteraan dan perindustrian. Sistem penyejukan, reaktor nuklear, elektronik, proses hidrodinamik, penghasilan kertas, dan lapisan sempadan dalam proses pemeluwapan cecair bagi filem adalah sebahagian daripada contoh kepelbagaian aplikasi yang berkaitan dengan aliran lapisan sempadan dan pemindahan haba. Tesis ini menyelesaikan tiga masalah secara penyelesaian berangka bagi masalah aliran lapisan sempadan di titik genangan pada permukaan meregang dengan mempertimbangkan bendalir Newtonan (bendalir likat) dan bendalir tak Newtonan (bendalir Williamson). Selain itu, tesis ini memberi perhatian kepada pengaruh keadaan gelincir, radiasi haba, magnetohidrodinamik (MHD) dan kesan pelepasan likat yang berkaitan dengan syarat sempadan suhu malar tempatan. Kesemua persamaan separa dijelmakan kepada persamaan pembezaan biasa dengan menggunakan penjelmaan keserupaan yang sesuai. Persamaan pembezaan biasa yang diperoleh telah diselesaikan secara berangka dengan menggunakan kaedah Luruan dalam perisian Maple. Penyelesaian berangka diperoleh untuk nombor Nusselt setempat dan pekali geseran kulit serta profil suhu dan halaju. Ciri-ciri aliran dan pemindahan haba untuk pelbagai nilai lapan parameter yang berkaitan iaitu nombor Prandtl, parameter regangan, nombor Eckert, parameter gelincir halaju, parameter gelincir haba, parameter radiasi, parameter magnetik dan parameter bendalir tak Newtonan Williamson telah dianalisis dan dibincangkan. Perbandingan juga dibuat dengan mengesahkan melalui penyelidikan yang sedia ada supaya keputusan yang diperoleh adalah sesuai dan boleh dipercayai. Sebagai kesimpulan, peningkatan nilai nombor Prandtl, parameter regangan, haba tanpa dimensi dan halaju tak berdimensi menyebabkan penurunan dalam suhu dinding dan juga ketebalan lapisan sempadan haba. Sementara itu, peningkatan parameter bendalir tak Newtonan Williamson dan parameter radiasi haba, lapisan sempadan halaju juga meningkat.

ABSTRACT

Problems related to boundary layer flow and heat transfer is important due to its various practical applications in engineering and industrial area. Cooling systems, nuclear reactor, electronic, hydrodynamics process, paper production and the boundary layer in liquid film condensation process are some of the example of various applications related to boundary layer flow and heat transfer. Present thesis solved numerically three problems of boundary layer flow on stagnation point over a stretching by considering the Newtonian fluid (viscous fluid) and non-Newtonian fluid (Williamson fluid). Besides, this thesis concern of the influence of slip flow, thermal radiation, magnetohydrodynamic (MHD) and viscous dissipation effects associated with constant wall temperature as boundary conditions. All gorvening equations in the form partial differential equations are transformed into ordinary differential equations by employing the suitable similarity transformation. The transformed ordinary differential equations obtained are solved numerically using a Shooting method in Maple software. Numerical solutions are obtained for the local Nusselt number and skin friction coefficient as well as the temperature and velocity profiles. The features of the flow and heat transfer characteristics for various values of eight pertinent parameters which are the Prandtl number, the stretching parameter, the Eckert number, the velocity slip parameter, the thermal slip parameter, the radiation parameter, the magnetic parameter and the non-Newtonian Williamson fluid parameter are analyzed and discussed. The comparison is also done by verifying through existing research so that the results obtained are a good agreement and reliable. As conclusion, the increases of Prandtl number, stretching parameter, dimensionless thermal and velocity slip parameter result to the decreasing in the wall temperature and also thermal boundary layer thickness. Meanwhile, increasing the non-Newtonian Williamson fluid parameter and thermal radiation parameter, the thermal boundary layer also increases.

TABLE OF CONTENT

LIST OF TABLES

UMP

اونيۏرسيتي مليسيا ڤهڠ

UNIVERSITI MALAYSIA PAHANG

LIST OF FIGURES

xii

LIST OF SYMBOLS

a,b,c	Positive constant for stretching rate
$u_e(x)$	External velocity
$u_w(x)$	Stretching velocity
$\underline{u}, u$	Velocity components along the x directions
$\underline{v}, v$	Velocity components along the y directions
γ^*	Dimensional velocity slip parameter
β^*	Dimensional thermal slip parameter
k	Thermal conductivity
C_p	Specific heat
Ec	Eckert number (Viscous dissipation parameter)
$\Pr$	Prandtl number
C_f	Skin friction coefficient
Nu_x	Local Nusselt number
q_w	Surface heat flux
Re_x	Local Reynolds number
L	Length of plate surface
x, y	Cartesian coordinate
T	Temperature in boundary layer / fluid temperature
T_w	Wall temperature
T_∞	Ambient temperature
U_∞	Free stream velocity
B_o	Uniform magnetic field strength
Nr	Radiation parameter
q_r	Radiative heat flux
σ^*	Stefan-Boltzmann parameter
k^*	Mean absorption coefficient
T^4	Linear function of temperature

M	Magnetic parameter
$\dfrac{D}{D_t}$	Material derivative
$\underline{F}$	Force components
p	Pressure
t	Time
ρ_∞	Fluid Density at ambient temperature
$\overline{V}$	Velocity vector directions
$F_x,\ F_y$	Components of body force per unit volume
τ_w	Surface shear stress
δ_h	Velocity boundary layer thickness
δ_T	Thermal boundary layer thickness

Greek Symbol

ε	Stretching parameter
μ	Dynamic viscosity
η	Dimensionless similarity variable
ψ	Stream function
ρ	Fluid density
ν	Kinematic viscosity
θ	Dimensionless temperature
δ	Boundary layer thickness
τ	Frictional shear stress
$\overline{\Phi}$	Viscous dissipation function
$\overline{\nabla}^2$	Laplacian operator
γ	Dimensionless velocity slip parameter
β	Dimensionless thermal slip parameter
λ	Williamson fluid parameter
Γ	Time constant
∇	Vector operator

xiv

Subscript

w	Condition at the surface
∞	Ambient/free stream condition

Superscript

'	Differentiation with respect to η
‾	Dimensional variables

LIST OF ABBREVIATIONS

MHD   Magnetohydrodynamics

PDEs   Partial Differential Equations

ODEs   Ordinary Differential Equations

RKF45   Runge-Kutta-Fehlberg Method

bvp4c   Boundary Value Problem-fourth order method
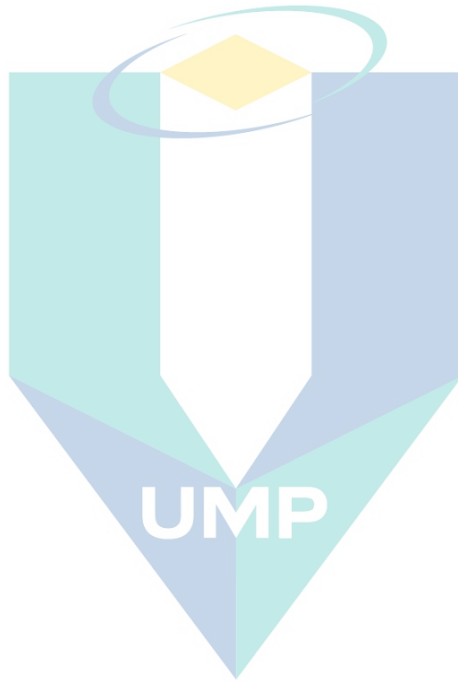
CHAPTER 1

PRELIMINARIES

1.1   Introduction

Transition energy is a term used to describe heat transfer. According to Incropera (1996) and Ishak (2008), heat is energy in transit due to a temperature difference. Heat in the form of energy is related to the movement of atoms, molecules and other particles that contain mass. When one system is making contact with another system with different temperature, heat flows spontaneously and at the same time, the thermal interaction will occur. Heat is also synonymous with thermal transportation (heat transfer) which can move between objects or areas within an object. Basically, heat transfer may occur in three conditions which are conduction, convection and radiation. Heat flow by conduction refers to the transfer of heat in the form of energy through direct or physical contact between atoms and molecules within objects that are touching. In other words, when adjacent atoms and molecules vibrate against one another, the heat will flow. The example of heat conduction is touching a hot iron, where the heat will pass from iron to our hands. Solid is a better conductor compared to liquid or gas since the array of molecules in solid are very compactly packed together. Meanwhile, heat flow by convection refers to heat passes through the movement of fluids. Liquids and gases are categorical in fluids. The actual movement or the circulation of the up and down motion helps the heat to spread in fluids. An example of heat flow by convection is the temperature of the water inside a pool, where it is warm at the top of the pool but as we swim deeper, we can feel the water gets colder. Lastly, heat flow by radiation refers to the heat in the form of electromagnetic energy which is moving in waves through any transparent medium or empty space. Radiation does not need any molecules or contact between the heat sources to pass the energy along. The sun is the biggest source of heat radiation that transfers energy into the solar system. The radiation heat moves through empty space or any transparent medium and we can

feel the heat. According to Baehr and Stephen (2006) and Lienhard IV and Lienhard V (2011), heat transfer by conduction and radiation from a solid surface to a fluid named is called the convective heat transfer process. In this study, the convection heat flow will be considered.

1.1.1 Convective Heat Transfer Process

The convective refers to heat transfer that occurs between surfaces with a moving fluid when both are at different temperatures (Incopera, 1996; Ishak, 2008). Heating can reduce fluid density because when heat transfers from the solid surface into fluid, the density of fluid decreases and the molecules will also move, spread out and rise. The cold fluid with more density will sink, and these up and down motions create circulation movements of heat to spread out. The above phenomena are also described as a mechanism from convection where the energy is transferred by movement and random motion of molecules (diffusion). This process will continue until both the surface and the fluid have the same temperature (Darus, 1994; Ishak, 2008).

Convection can be separated into two types; the forced convection and the free convection which is also known as natural convection (Pop and Ingham, 2001; Mohamed, 2017). The forced convection occurs when fluid motion circulation is generated with the influence of external agents such as fan, blower or nozzle through the fluid. The example of forced convection by a fan is a snow machine. While for free convection, there is no external agent that influences the heat transfer process, but fluid motion circulation is generated by the gravitational field and temperature changes. The fluid with different temperatures can cause variation of fluid density. The example of free convection is sea-wind formation.

In addition, mixed convection occurs when both free and force convection take parts or occur simultaneously. The buoyancy parameter $\lambda = \dfrac{Gr}{Re^n}$ as a scalar to measure the influence of forced and free convection in a flow with Re as a Reynold's number, Gr as Grashof number and $(n \gg 0)$ as a constant. The forced convection is dominant

when $\lambda = \dfrac{Gr}{Re^n} \to 0$, while free convection take part as $\lambda = \dfrac{Gr}{Re^n} \to \infty$ (Pop and Ingham, 2001; Mohamed, 2017).

1.1.2 Boundary Layer Theory

Ludwig Prandtl (1875 – 1953) is the first person to introduce the boundary layer theory with a paper entitled "On the Motion of Fluid with Very Little Friction". According to Anderson (2005), based on Prandtl theory, a thin layer (region) is adjacent to the plate surface that is embedded in the fluid motion field and this region is known as the boundary layer.

Prandtl theory describes the fluid flows past a body can be divided into two parts, one is the thin layer adjacent to the plate surface and another one is outside the boundary layer (major part), this concept can be delineated in Figure 1.1. Furthermore, in thin layer adjacent to the plate surface or known as boundary layer, the effects of viscosity and the frictional force should not be neglected and must be considered. The outside of the boundary layer (major part) is defined as inviscid. According to Schlichting (1979), inviscid flow refers to fluid flow where the viscosity is neglected because the frictional force is too small.
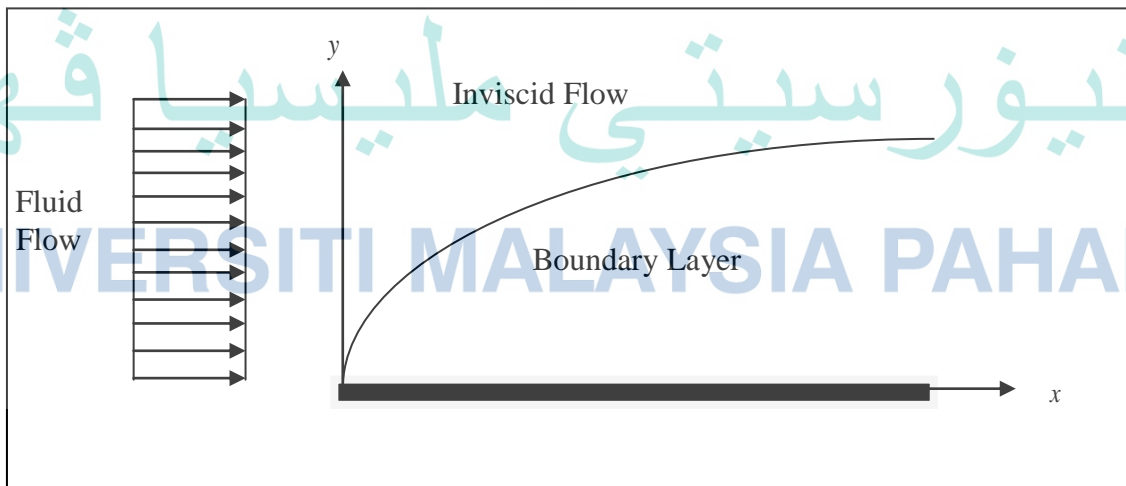
Figure 1.1   Inviscid flow and boundary layer

There are two types of boundary layer which are the velocity boundary layer and the thermal boundary layer (Ozisik, 1985). For boundary layer theory, Figure 1.2 shows the consideration of fluid flows past over a plate surface. When the fluid molecule is making contact with the plate surface, it is assumed that the velocity of the molecule equals zero. The molecule with zero velocity then delays the movement of other fluid in the layer next to it. This process will continue until the distance of $y = \delta_h$ from the plate surface and after that, this effect can be neglected. By increasing the distance from the surface in y, fluid velocity in x component also increases the free stream velocity U_∞ outside the boundary layer. This quantity δ_h is called the velocity boundary layer thickness, and usually is defined by y. Meanwhile, the thermal boundary layer is formed when the temperature between the fluid flow and plate surface is different. Based on Figure 1.2, there is an existence of a region where the temperature changes from $T(y)$ at $y = 0$ to T_∞ which is at a free flow outside the boundary layer. The quantity δ_T is representing the thermal boundary layer thickness. This region can be characterized by the temperature of gradient and heat transfer (Incropera, 1996; Kreith et al., 2010; Mohamed, 2017).
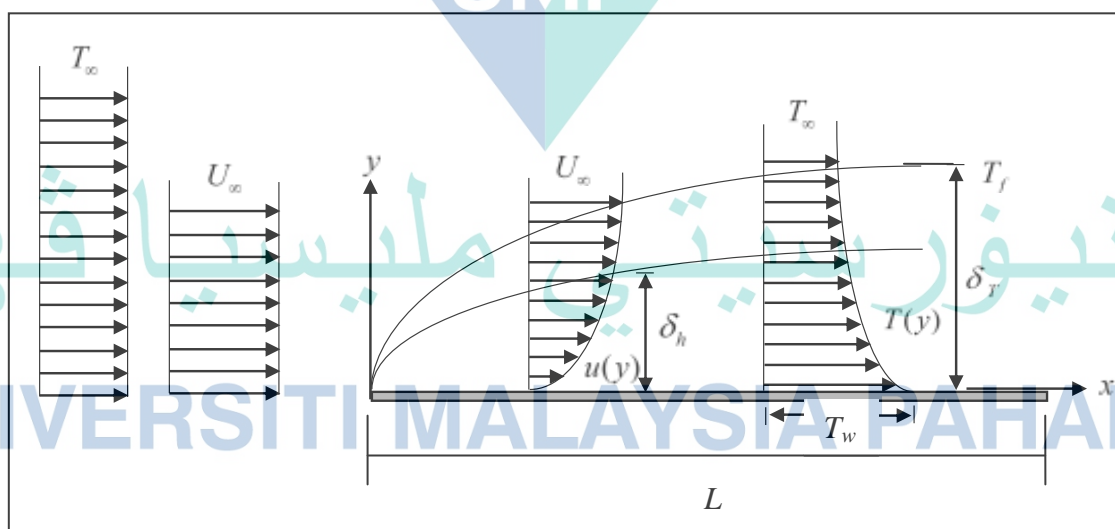
Figure 1.2   Velocity and thermal boundary layers

Acceptable only to the boundary layer, Prandtl disclosed that the Navier-Stokes equations can be changed to a simpler form and identified as the boundary layer

equations. There are a few assumptions need to be made for the derivation of boundary layer equations (Schlichting, 1979; Ishak, 2008; Mohamed, 2017):

i. The viscous effects are limited in a boundary layer only, while for the outside boundary layer, the viscous effects are not important so that flow can be determined by inviscid solutions such as potential flow or Euler's equations.

ii. The boundary layer is smaller than the plate surface. If δ is a boundary layer thickness and L is plate surface, hence $\delta / L \leq 1$. Also, $x = O(L)$ and $y = O(\delta)$, where O is called as of order.

iii. The boundary conditions:
   - at boundary layer: $u(x,0) = 0$ and $v(x,0) = 0$, the fluid obeys the no-slip condition on plate surface,
   - free stream condition at infinity: $u(x,\infty) = U_\infty$ and $v(x,\infty) = 0$, where u and v are velocity components in x and y directions, respectively and U_∞ embodies the free stream velocity.

iv. In the boundary layer, $u = O(U_\infty)$.

1.1.3 Viscous Fluid

Fluid can be classified into the Newtonian fluid (viscous fluid) and non-Newtonian fluid. For a Newtonian fluid, it must agree with Newton's equation (Newton's law of viscosity) where the frictional force per unit area, denoted by τ frictional shear stress, is linearly proportional to velocity gradient $\dfrac{du}{dy}$, which

$$\tau = \mu \frac{du}{dy}, \qquad\qquad 1.1$$

where μ is a coefficient of dynamic viscosity (Schlichting, 1979; Mohamed, 2017). The examples of Newtonian fluid are water and air.

Figure 1.3 portrays the fluid flow on a flat plate, where u is a fluid velocity in a boundary layer, U_∞ is a stream velocity (free flow outside of boundary layer) and x, y are Cartesian coordinates.
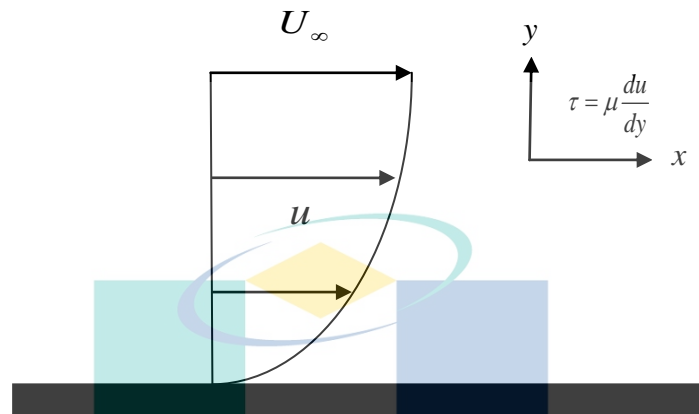
Figure 1.3   Laminar velocity profile on a flat plate

In addition, inviscid flow refers to fluid flow where, if the viscosity is neglected and μ in Equation 1.1 is set to 0. However, in real life, the inviscid flows with zero viscosity do not exist. Furthermore, some other fluids can be classified as a non-Newtonian fluid since their equations do not satisfy Equation 1.1. In non-Newtonian fluids, the viscosity can change when it is under force. The examples of non-Newtonian fluid are paint and polymer (Ishak, 2008).

1.1.4   Viscous Dissipation

The irreversible process by means of which the work done by a fluid on adjacent layers due to the action of shear forces is transformed into heat is defined as viscous dissipation (Reddy et al., 2015). In other words, the viscosity from a viscous fluid flow will take energy from the motion (kinetic energy) and transform it into thermal energy. Viscous dissipation is also called internal friction and it is important to study in order to understand the behavior of temperature distributions when internal friction is not neglected. According to Gebhart (1962), the effects of viscous dissipation in free convection flow with large decelerations from high rotating speeds, high-velocity flow and highly viscous flow with moderate velocity. Meanwhile, Soundalgekar (1972)

6

found the outcome in modeling boundary layer flow and heat transfer where the effects of viscous dissipation into the energy equation are neglected.

Viscous dissipation is represented as an Eckert number, Ec in an energy equation and it is the ratio of the kinetic energy over the boundary layer which shows differences in enthalpy. Viscous dissipation changes the temperature distribution by playing a role like an energy source, which leads to affected heat transfer rates.

1.1.5 Williamson Fluid

In this study, Williamson fluid (pseudoplastics fluids) has been chosen into consideration. Williamson (1929) was the first to discuss the flow of pseudoplastic materials and developed a model equation to illustrate the flow of pseudoplastic fluids. From the outcome of his study, there are similarities among the flow properties of this fluid and plastic fluid in certain aspects. In addition, this fluid cannot be molded and there is no influence of yield stress on fluid behavior. This fluid is categorized as non-Newtonian fluid. A Newtonian fluid is a fluid that follows Newton's equation (Newton's law of viscosity), but as for non-Newtonian, the fluids are not in accordance with Newton's equations. According to Metzner (1965), the non-Newtonian fluid can be separated into three types which are viscoelastic, time-dependent viscosity and purely viscous fluid. The behavior of non-Newtonian fluid is shear thinning, where the viscosity decreases under shear stress and it is synonymous with pseudoplastic fluid. The viscosity of pseudoplastic fluid decreases instantaneously under shear rate but stays constant in the end. The examples of this kind of fluid are blood, paint and whipped cream.

There are other studies that consider Williamson fluid. This includes a study by Hayat et al. (2016a) who analyzed the effect of an inclined magnetic field on the peristaltic flow of Williamson fluid in an inclined channel with convective boundary conditions. The effect of chemical reaction on MHD boundary layer flow and melting heat transfer of Williamson nanofluid in porous medium has been elaborated by Krishnamurthy et al. (2016). Amanulla et al. (2018) investigated numerical exploration of thermal radiation and Biot number effects on the flow of a non-Newtonian MHD Williamson fluid over a vertical convective surface. Thermal radiation effects on

Williamson fluid flow due to an expanding/contracting cylinder with nano materials: dual solutions were presented by Hamid et al. (2018b). Jain and Parmar (2018) analyzed radiation effect on MHD williamson fluid flow over stretching cylinder through porous medium with heat source.

1.1.6 Slip Condition

In no-slip conditions, a solid body will not be having any velocity relative to the body at the control surface of the moving fluid in contact (Prabhakara and Deshpande, 2004). According to Bhattacharyya et al. (2011), the no-slip assumptions are not applicable for all cases of fluid flow. It is due to some situations where the no-slip conditions may be replaced with partial or slip conditions. The slip condition is the action when the fluid at the plate surface will have non-zero velocity. Martin and Boyd (2006) analyzed the momentum and heat transfer in a laminar boundary layer with slip flow. Furthermore, Aman et al. (2011) studied the slip effects in mixed convection boundary layer flow on the vertical surface near the stagnation-point while Sahoo (2010) considered partial slip on stretching sheet embedded in the non-Newtonian fluid. Moreover, Raisi et al. (2011) investigated forced convection laminar flow of nanofluid through a microchannel in the presence as well as in the absence of slip effects. Recently, Mahmoud and Waheed (2012) as well as Nandy and Mahapatra (2013) observed the slip and heat generation/absorption effects on MHD stagnation flow past a stretching surface in nanofluid and micropolar fluid, respectively.

Other related works that focus on slip condition include Ellahi et al. (2016) that analyzed the numerical study of magnetohydrodynamics generalized Couette flow of Eyring-Powell fluid with heat transfer and slip condition. Next, Imran et al. (2018) studied the boundary layer flow of MHD generalized Maxwell fluid over an exponentially accelerated infinite vertical surface with slip and Newtonian heating at the boundary. Sobamowo et al. (2018) studied magnetohydrodynamic squeezing flow analysis of nanofluid under the effect of slip boundary conditions using variation of parameter method. Majeed et al. (2019) analyzed the impact of the magnetic field and second-order slip flow of Casson liquid with heat transfer subject to suction/injection and convective boundary conditions. Thermal radiation and slip effects on MHD

stagnation point flow of non-Newtonian nanofluid over a convective stretching surface were observed by Besthapu et al. (2019).

1.2   Research Objectives

This study investigates numerically the flow and heat transfer on the stagnation point with several effects and the main objectives are as follows:

i.   to improve by adding the new related parameter for selected problem and solve numerical algorithms for the computations by using shooting method in Maple software.

ii.   to analyze the influences of Prandtl number, Eckert number, stretching parameter, Williamson fluid parameter, thermal and velocity slip parameter, viscous dissipation parameter, magnetic parameter, thermal radiation parameter on the velocity and temperature profiles, the skin friction coefficient as well as the local Nusselt number.

1.3   Research Scope

The research is limited to the problems which involve a steady, two-dimensional stagnation point flow over a stretching sheet immersed in an incompressible viscous and Williamson fluid. The governing boundary layer equations which occupy ordinary differential equations for these problems are formulated using the similarity transformation and will be solved numerically using shooting method. Three (3) problems have been considered in this study which are:

i.   Flow and heat transfer analysis of viscous fluid on the stagnation point over a stretching surface with viscous dissipation and slip conditions.

ii.   Flow and heat transfer analysis of Williamson fluid on the stagnation point over a stretching surface with viscous dissipation and slip conditions.

iii.   Flow and heat transfer analysis of Williamson fluid on MHD stagnation point flow over a stretching surface with thermal radiation effects.

1.4   Research Significance

This study can increase the understanding and promote the development of boundary layer flow on a stagnation point over a stretching sheet with the presence of slip flow, thermal radiation, magnetohydrodynamic (MHD) and viscous dissipation effects in a viscous and Williamson fluid. Numerical solutions for each mathematical model are obtained and completely analyzed. The importance of applications of fluid flow in both areas of technology and engineering is mentioned in this chapter.

The outcomes of this study are in terms of modeling, theoretical predictions, numerical formulations and solutions. There are no physical outcomes or products produced in this study and the important finding regarding the temperature and fluid flow behavior including the effects of several parameters will help to explain and to validate numerical results as well as verify the experimental results in the future.

1.5   Literature Review

1.5.1   Stagnation Point Flow

Stagnation point flow is an attractive topic in the research area due to its applications in both the industrial and sciences areas. A point in a flow field where the local velocity of the fluid is zero is called the stagnation point (Abu Bakar et al., 2019). Hiemenz (1911) was the first to propose a problem involving stagnation point and come up with the exact solution for Navier-Stokes equations. Chao and Jeng (1965) investigated the unsteady stagnation point heat transfer while Mahapatra and Gupta (2002) investigated the stagnation point flow with heat transfer and solved using a finite difference method known as Thomas algorithm. Nazar et al. (2004a) extended the same problem of Mahapatra and Gupta (2002) by considering micropolar fluid. The Keller-box method was used to solve the system of nonlinear ordinary differential equations and as a matter of fact, it was incredibly concurrence with Mahapatra and Gupta (2002) for a resultant Newtonian fluid. In addition, Ishak et al. (2006) considered the mixed convection stagnation-point flow towards a vertical stretching sheet. The transformed ordinary differential equations are solved numerically by using the Keller-box method. Furthermore, Bachok et al. (2012) investigated the stagnation-point boundary layer heat

transfer flow over an exponentially stretching/shrinking sheet in a nanofluid. Three types of nanoparticles, especially copper, alumina and titanium were solved numerically by the transformation of the governing mathematical equations. The conclusion of an increase in the skin friction and heat transfer coefficients was produced from nanoparticles into the water-based fluid. The copper water nanofluid's skin friction coefficient and the local Nusselts number are higher compared to the others. Additionally, Suali et al. (2012) analyzed the numerical solutions of unsteady two-dimensional stagnation point heat transfer flow towards a shrinking or stretching surface with prescribed heat flux. They discussed the special effects of stretching/shrinking parameter, Prandtl number and unsteadiness parameter on the skin friction and local Nusselt number. Mohamed et al. (2013) studied the effects of convective boundary conditions on stagnation point flow instead of prescribed heat flux. In addition, a steady two-dimensional heat transfer stagnation point flow over a nonlinearly moving plate with partial slip condition was discussed by Roşca et al. (2014). In this work, dual solutions obtained for some values of the governing parameter and compared to the results of Weidman et al. (2006) which have strong excellent agreement.

Other related works focusing on the stagnation point flow include Mansur et al. (2015) who have analyzed the magnetohydrodynamic stagnation point flow of a nanofluid over a stretching/shrinking sheet with suction where boundary value problem - fourth order method (bvp4c) in MATLAB has been used to solve the boundary layer problem. The numerical results show that dual solutions exist for the shrinking case, while for the stretching case, the solution is unique. Non-aligned MHD stagnation point flow of variable viscosity nanofluids past a stretching sheet with radiative heat was studied numerically by Khan et al. (2016). The transformed equations are numerically integrated using the fourth–fifth order Runge–Kutta–Fehlberg (RKF45) method. Mehmood et al. (2018) examined the non-aligned stagnation point flow of radiating Casson fluid over a stretching surface. The comparison with previously published literature that has reached an excellent agreement is reported. Kamal et al. (2019) investigated the numerical study of a stability analysis of MHD stagnation-point flow towards a permeable stretching/shrinking sheet in a nanofluid with chemical reactions effect by using bvp4c in MATLAB software to solve the boundary layer problem. Abu Bakar et al. (2019) examined a stability analysis of boundary layer stagnation-point flow over a stretching/shrinking cylinder in a nanofluid. A shooting method in Maple

11

software and a bvp4c method in MATLAB software are applied to solve this boundary layer problem. The result shows that non-unique (dual) solutions exist for a shrinking cylinder and a unique solution exists for a stretching cylinder.

Motivated by the above-cited works, this study considers the flow and heat transfer analysis on the stagnation point over a stretching surface. In addition, the effects of slip conditions and viscous dissipation had been taken into account for further investigation.

1.5.2   Stretching Surface

Due to numerous applications of fluid over a stretching sheet in the industrial manufacturing and engineering process, many researchers have great interest to explore this area and theoretical studies have increased. According to Salleh et al. (2010), the fluid dynamics due to a stretching sheet is important in extrusion processes. In addition, there is an extrusion of a polymer sheet from the die, the boundary layer in liquid film condensation process and emulsion coating on photographic films, and these application examples of stretching sheet flows in engineering part (Nadeem et al., 2013). Crane (1970) was the first to examine the flow past a stretching plate. In his investigation, there are certain similarities with Hiemenz (1911) which the main velocity in the outer flow is proportional to the distance from the stagnation point. Later, theoretical studies have been carried out such as by Gupta and Gupta (1977), where they studied the heat and mass transfer on a stretching sheet with suction or blowing. Buoyancy effects on MHD stagnation point flow and heat transfer of a nanofluid past a convectively heated stretching/shrinking sheet were examined by Makinde et al. (2013). They were using the Runge-Kutta fourth-order (RKF45) method with shooting technique to solve coupled nonlinear ordinary differential equations. They also found both the skin friction coefficient and local Sherwood number had decreased while the local Nusselt number had increased with the expansion intensity of the buoyancy force. Next, Ibrahim and Shankar (2013) analyzed MHD boundary layer flow and heat transfer of a nanofluid past a permeable stretching sheet with velocity, thermal and solutal slip boundary conditions. The comparison has been made with the previous literature and excellent agreement has been reached. Pal et al. (2014) presented the flow and heat transfer of

nanofluids at a stagnation-point flow over a stretching/shrinking surface in a porous medium with thermal radiation.

Other studies considering a stretching sheet include the investigation by Abbas et al. (2015) on the stagnation-point flow of a hydromagnetic viscous fluid over stretching/shrinking sheet with generalized slip condition in the presence of homogeneous–heterogeneous reactions. Next, Abd El-Aziz (2015) numerically analyzed dual solutions in hydromagnetic stagnation point flow and heat transfer towards a stretching/shrinking sheet with non-uniform heat source/sink and variable surface heat flux. The thermal radiation and slip effects on MHD stagnation point flow of nanofluid over stretching sheet have been elaborated by Haq et al. (2015). They used the Runge-Kutta fourth-order (RKF45) method along with the shooting technique to solve coupled ordinary differential equations. Sandeep et al. (2016) presented a stagnation-point flow of a Jeffery nanofluid over a stretching surface with the induced magnetic field and chemical reaction and the Runge-Kutta scheme has been used to solve this problem. Next, Rehman et al. (2018) investigated thermo physical analysis for three-dimensional MHD stagnation-point flow of nano-material influenced by an exponentially stretching surface. They found the best example where the flow caused by a stretching plate near stagnation point could be detected through spinning, floating and blowing of fiber glass. Their study concluded that the stagnation point parameter increases produced velocity and thermal profile whereas decreases induced boundary layer thickness.

Inspired by the above literature, the present study aims to analyze the problems regarding boundary layer flow over a stretching surface. The investigation in this study will consider several effects.

1.5.3 Radiation and Magnetohydrodynamic (MHD)

The interaction of conducting fluids with electromagnetic waves is referred to as Magnetohydrodynamics (MHD) (Reddy et al., 2015). Due to the wide application of fluid affected by a magnetic field in technology and engineering, many researchers have investigated such study. Reddy et al. (2015) and Hayat et al. (2016b) have listed MHD power generation, MHD flow meters and MHD pump as well as plasma studies and

13

petroleum industries, as application examples of MHD in various areas of technology and engineering. Alfven (1942) was the first to explore and find electromagnetic-hydrodynamic waves in his study. On the other hand, literature on the effect of radiation on the flow and heat transfer has attracted the attention of researchers because of its important applications in rocket combustion chamber, power plants for interplanetary flight, gas-cooled nuclear reactors (Reddy et al., 2015), electrical power generation, solar power technology and astrophysical flows (Hayat et al., 2016b).

Other studies consider MHD and radiation, while Hayat and Qasim (2010) considered the influence of thermal radiation and Joule heating on MHD flow of a Maxwell fluid in the presence of thermophoresis. Khan et al. (2012) solved the problem of unsteady MHD free convection boundary layer flow of a nanofluid along a stretching sheet with thermal radiation and viscous dissipation effects. Slip effects on MHD boundary layer flow over an exponentially stretching sheet with suction/blowing and thermal radiation have been noticed by Mukhopadhyay (2013). Rashidi et al. (2014) have noticed the buoyancy effects on MHD flow of nanofluid over a stretching sheet in the presence of thermal radiation. Sheikholeslami et al. (2016) have studied MHD free convection of Al_2O_3–water nanofluid considering thermal radiation: a numerical study, the results show that the enhancement in heat transfer has a direct relationship with Hartman number, viscous dissipation parameter and radiation parameter but it has reversed relationship with Rayleigh number. Bhatti et al. (2016a) deliberated on the numerical simulation of entropy generation with thermal radiation on MHD Carreau nanofluid towards a shrinking sheet. The basic equations are solved numerically with the help of the successive linearization method and Chebyshev spectral collocation method. It is observed that the influence of the magnetic field and fluid parameters oppose the flow. It is also analyzed that thermal radiation effects and the Prandtl number show opposite behavior on the temperature profile.

Nayak (2017) numerically analyzed MHD 3D flow and heat transfer analysis of nanofluid by shrinking the surface inspired by thermal radiation and viscous dissipation. Thermal radiation of Ferro fluid in the existence of Lorentz forces considering variable viscosity has been investigated by Sheikholeslami and Shehzad (2017). Daniel et al. (2018) obtained the impact of thermal radiation on the electrical MHD flow of nanofluid over a nonlinear stretching sheet with variable thickness. Numerical study of

14

unsteady MHD flow of Williamson nanofluid in a permeable channel with heat source/sink and thermal radiation was examined by Hamid et al. (2018c). Babu et al. (2018) solved the problem of thermal radiation and heat source effects on MHD non-Newtonian nanofluid flow over a stretching sheet. Thermal management of MHD nanofluid within the porous medium enclosed in a wavy shaped cavity with square obstacle in the presence of a radiation heat source was analyzed by Alkanhal et al. (2019). Raju et al. (2019) investigated MHD viscoelastic fluid flow past an infinite vertical plate in the presence of radiation and chemical reaction.

Motivated from the above literature, the present study will focus on the problems regarding MHD and radiation as one of the parameters. Besides, constant wall temperature will be considered as a boundary condition.

1.6   Thesis Outline

This thesis is divided into six chapters. In Chapters 3 to 5, three problems have been investigated and the obtained solutions are analyzed and discussed by observing the temperature with velocity distribution, skin friction coefficient and Nusselt number. The descriptions for all chapters are as follows:

Chapter 1:   The first chapter begins by preliminaries with general introduction such as convective heat transfer process, boundary layer theory, viscous fluid, viscous dissipation, Williamson fluid and slip condition. The literature reviews are briefly elaborated which include stagnation point flow, stretching surface and radiation as well as MHD. Next, the objectives, scope and significance of research are explained to increase the understanding towards the purpose of the research.

Chapter 2:   This chapter discusses problem formulation and numerical procedure. The shooting method in Maple software has been used to solved numerically all the problems. This method is suitable and flexible to deal with all the problems discussed in this thesis. In addition,

regarding the governing equations which are in the form of elliptical non-linear partial differential equations are reduced to hyperbolic form and this is done by the order of magnitude analysis. Next, the similarity transformation is applied and lastly, the transformed ordinary differential equations obtained are solved numerically using the shooting method.

Chapter 3:   The flow and heat transfer analysis of viscous fluid on the stagnation point over a stretching surface with viscous dissipation and slip conditions are considered in this chapter. This chapter is divided into four section which include an introduction, mathematical formulation, results and discussion as well as a conclusion. The temperature and velocity field are elucidate by tables and graphs. The influence of Prandtl number, stretching parameter, Eckert number, thermal and velocity slip parameter on the flow and heat transfer characteristics are analyzed and discussed.

Chapter 4:   This chapter discusses the second problem that is the flow and heat transfer analysis of Williamson fluid on the stagnation point over a stretching surface with viscous dissipation and slip conditions. Williamson fluid is chosen as a medium fluid problem with a similar discussion in the previous problem.

Chapter 5:   Flow and heat transfer analysis of Williamson fluid on MHD stagnation point flow over a stretching surface with thermal radiation effects are discussed in this chapter. In addition, magnetic and thermal radiation are considered in this problem. The influence related parameter will be discussed in this chapter.

Chapter 6:   Lastly, this chapter includes a summary, contributions of the research and suggestion for future studies based on the present solutions. The list of references is attached at the end of this chapter.

CHAPTER 2

PROBLEM FORMULATION AND NUMERICAL PROCEDURE

2.1   Introduction

The main discussion in this chapter will be on the mathematical formulation and derivation of the governing equations of steady forced convection on the stagnation point flow of a viscous fluid over a stretching surface with slip effects as given in Section 2.2. Next, the shooting method in Maple software is carried out to solve the numerical procedures.

2.2   Governing Equations

Governing equations consist of three basic equations, i.e. continuity equation, momentum equation and energy equation. All three basic equations will be briefly discussed in the following sub-topic.

2.2.1   Basic Equations

According to Bejan (1984), the basic continuity equations can be expressed as

Continuity equation:

$$\frac{\partial \rho}{\partial t} + \nabla.(\rho \underline{u}) = 0, \qquad\qquad 2.1$$

Momentum equation:

$$\rho \frac{D\underline{u}}{Dt} = -\nabla p + \mu \nabla^2 \underline{u} + \underline{F}, \qquad\qquad 2.2$$

Energy equation:

$$\rho C_p \frac{DT}{Dt} = k\nabla^2 T + \mu\Phi,$$ 2.3

with

$$\frac{D}{Dt} = \frac{\partial}{\partial t} + \underline{u}.\nabla = \frac{\partial}{\partial t} + u\frac{\partial}{\partial x} + v\frac{\partial}{\partial y} + w\frac{\partial}{\partial z},$$ 2.4

$$\nabla = \frac{\partial}{\partial x}i + \frac{\partial}{\partial y}j + \frac{\partial}{\partial z}k,$$ 2.5

$$\mu\Phi \equiv 2\mu\left[\left(\frac{\partial u}{\partial x}\right)^2 + \left(\frac{\partial v}{\partial y}\right)^2 + \left(\frac{\partial w}{\partial z}\right)^2\right] + \\ \mu\left[\left(\frac{\partial u}{\partial y} + \frac{\partial v}{\partial x}\right)^2 + \left(\frac{\partial u}{\partial z} + \frac{\partial w}{\partial x}\right)^2 + \left(\frac{\partial v}{\partial z} + \frac{\partial w}{\partial y}\right)^2\right],$$ 2.6

where $\frac{D}{Dt}$ $\theta(\eta)$ denotes the material derivative, ∇ (del) is the vector operator and Φ is the viscous dissipation function, while $\underline{u}$ and $\underline{F}$ are velocity component and force, respectively, ρ is a fluid density, p for pressure, μ is dynamic viscosity, t is time, T is temperature, C_p is specific heat at constant pressure, k is thermal conductivity, and lastly x and y represent the Cartesian coordinates along the surface and normal to the surface, respectively.

In discussing the mathematical model considered in Chapter 3, the flow and heat transfer analysis of viscous fluid on the stagnation point over a stretching surface with viscous dissipation and slip conditions, derivatives with respect to t is neglected because it is a steady flow. In this study, it is assumed that the flow is steady and two-dimensional in an incompressible viscous fluid where the fluid properties such as specific heat, thermal conductivity and viscosity are constant. From the above considerations, Equations 2.1 to 2.3 becomes

$$\frac{\partial u}{\partial x} + \frac{\partial v}{\partial y} = 0,$$

2.7

$$u\frac{\partial u}{\partial x} + v\frac{\partial u}{\partial y} = -\frac{1}{\rho}\frac{\partial p}{\partial x} + v\left(\frac{\partial^2 u}{\partial x^2} + \frac{\partial^2 u}{\partial y^2}\right) + F_x,$$

2.8

$$u\frac{\partial v}{\partial x} + v\frac{\partial v}{\partial y} = -\frac{1}{\rho}\frac{\partial p}{\partial y} + v\left(\frac{\partial^2 v}{\partial x^2} + \frac{\partial^2 v}{\partial y^2}\right) + F_y,$$

2.9

$$u\frac{\partial T}{\partial x} + v\frac{\partial T}{\partial y} = \frac{k}{\rho C_p}\left(\frac{\partial^2 T}{\partial x^2} + \frac{\partial^2 T}{\partial y^2}\right) +$$
$$2\mu\left[\left(\frac{\partial u}{\partial x}\right)^2 + \left(\frac{\partial v}{\partial y}\right)^2\right] + \mu\left[\left(\frac{\partial u}{\partial y} + \frac{\partial v}{\partial x}\right)^2\right],$$

2.10

where u and v are the velocity in $x-$ and $y-$ direction, respectively. F_x and F_y are the components of the body force per unit volume, $v = \frac{\mu}{\rho}$ as the kinematic viscosity, $\frac{k}{\rho C_p} = \alpha$ is the thermal diffusivity. In the case of free convection, it is found that $F_x = -\rho g$ and $F_y = 0$. The term $F_x = -\rho g$ on the right hand side in momentum equations represents the body force on the negative $x-$ direction (Ishak, 2008; Mohamed, 2017). For this case, which is the case of forced convection, the body force is considered $F_x = F_y = 0$.

2.2.2 Boundary Layer Approximation

Equations 2.7 to 2.10 are non linear partial differential equations which are elliptical. These equations can be transformed into parabolic nature by eliminating the second derivatives with respect to x or y. The parabolic partial differential equations are easier to solve (Tannehill et al., 1997; Ishak, 2008; Mohamed, 2017).

19

Regarding the transformation of the elliptic equations to the parabolic equations, one of the second derivative terms must be eliminated by the analysis of the magnitude and the smallest term compared to the others in the same equation will also be eliminated (Ahmad, 2009). This is because the small values give a small effect which can be neglected from the boundary layer flow.

2.2.3 Order of Magnitude Analysis

Considering the assumptions of boundary layer flow state in Section 1.1.2, (Bejan, 2013) suggested that

$$x = O(L), \; y = O(\delta), \; T = O(T_\infty), \; u = O(U_\infty), \qquad 2.11$$

where L is the length of the plate, δ is the boundary layer thickness, U_∞ is the free stream velocity and T_∞ is the temperature of fluid.

From continuity Equation 2.7,

$$\frac{\partial u}{\partial x} + \frac{\partial v}{\partial y} = 0,$$

by using analysis of magnitude, $\frac{\partial u}{\partial x}$ and $\frac{\partial v}{\partial y}$ are defined as $\frac{U_\infty}{L}$ and $\frac{v}{\delta}$ respectively. Note that $\frac{\partial v}{\partial y}$ must be in the same order with $\frac{\partial u}{\partial x}$ in boundary layer and $\frac{\partial u}{\partial x} \neq 0.$ Therefore, v is given by

$$v = O\left(\frac{U_\infty \delta}{L}\right). \qquad 2.12$$

Now, the process of order of magnitude analysis for the x and y components of momentum Equations 2.8 and 2.9 are detailed in Tables 2.1 and 2.2 using Equations 2.11 and 2.12.

20

Table 2.1   Order of magnitude analysis for x component of the momentum equation

Terms of equation	Used Equations 2.8	Magnitude Order $\times \dfrac{L}{U_\infty^{2}}$	Decision $\delta \leq L$
$u \dfrac{\partial u}{\partial x}$	$U_\infty \dfrac{U_\infty}{L}$	$O(1)$	remain
$v \dfrac{\partial u}{\partial y}$	$\dfrac{U_\infty \delta}{L} \dfrac{U_\infty}{\delta}$	$O(1)$	remain
$\dfrac{1}{\rho} \dfrac{\partial p}{\partial x}$	$\dfrac{1}{\rho} \dfrac{\rho U_\infty^{2}}{L}$	$O(1)$	remain
$v \left(\dfrac{\partial^{2} u}{\partial x^{2}} \right)$	$v \dfrac{U_\infty}{L^{2}}$	$O\left(\dfrac{v}{U_\infty L} \right)$	can be negligible (≈ 0)
$v \left(\dfrac{\partial^{2} u}{\partial y^{2}} \right)$	$v \dfrac{U_\infty}{\delta^{2}}$	$O\left(\dfrac{v}{U_\infty L} \left(\dfrac{L}{\delta} \right)^{2} \right)$	remain
$\dfrac{1}{\rho}(\rho g)$	$\dfrac{1}{\rho} \dfrac{\rho U_2^{\infty}}{L}$	$O(1)$	remain

From Table 2.1, the magnitude for $\dfrac{\partial p}{\partial x} = O\left(\dfrac{\rho U_\infty^{2}}{L} \right)$ and $\rho g = O\left(\dfrac{\rho U_\infty^{2}}{L} \right)$ exist in the same order as described in the Bernoulli equation (Darus, 1994; Ishak, 2008) where the pressure in the boundary layer is equal to the pressure at the boundary. Every terms are multiplied with $\dfrac{L}{U_\infty^{2}}$. Since the last two terms represent the viscosity, one of the terms will be eliminated due to the size being smaller than the others. The comparison can be done as follows:

$$\frac{\partial^{2} u}{\partial y^{2}} \bigg/ \frac{\partial^{2} u}{\partial x^{2}} = O\left(\frac{L}{\delta} \right)^{2} \geq 1. \qquad 2.13$$

21

Therefore, the term $\nu \dfrac{\partial^2 u}{\partial x^2}$ in the x component of the momentum Equation 2.8 can be ignored, but not the term $\nu \dfrac{\partial^2 u}{\partial y^2}$. If both terms are eliminated, Equation 2.8 will become the momentum equation for the inviscid flow. As the remaining terms in the momentum equations becomes $O(1)$, then

$$O\left(\frac{\nu}{U_\infty L}\left(\frac{L}{\delta}\right)^2 \right) = O(1), \qquad\qquad 2.14$$

where δ can be defined as

$$\delta = \left(\frac{\nu L}{U_\infty} \right)^{1/2}. \qquad\qquad 2.15$$

Next, the order of magnitude analysis for the y component of the momentum Equation 2.9 is conducted in Table 2.2.

Table 2.2   Order of magnitude analysis for y component of the momentum equation

Terms of equation	Used Equation 2.9	Magnitude Order $\times \dfrac{\delta}{U_\infty^2}$	Decision $\delta \le L$
$u\dfrac{\partial v}{\partial x}$	$U_\infty \dfrac{U_\infty \delta}{L^2}$	$O\left(\dfrac{\delta^2}{L^2}\right)$	can be negligible (≈ 0)
$v\dfrac{\partial v}{\partial y}$	$\left(\dfrac{U_\infty \delta}{L}\right)^2 \dfrac{1}{\delta}$	$O\left(\dfrac{\delta^2}{L^2}\right)$	can be negligible (≈ 0)
$\dfrac{1}{\rho}\dfrac{\partial p}{\partial y}$	$\dfrac{1}{\rho}\dfrac{\rho U_\infty^2}{\delta}$	$O(1)$	remain
$\nu\left(\dfrac{\partial^2 v}{\partial x^2}\right)$	$\nu \dfrac{U_\infty \delta}{L}\dfrac{1}{L^2}$	$O\left(\dfrac{\nu \delta^2}{U_\infty L^3}\right)$	can be negligible (≈ 0)
$\nu\left(\dfrac{\partial^2 v}{\partial y^2}\right)$	$\nu \dfrac{U_\infty \delta}{L}\dfrac{1}{\delta^2}$	$O\left(\dfrac{\nu}{U_\infty L}\right)$	can be negligible (≈ 0)

22

From Table 2.2, each terms is multiplied with $\dfrac{\delta}{U_\infty^2}$, and followed with a similar

process as in Table 2.1. Since $\delta \leq L$ and Reynolds number $Re = \dfrac{U_\infty L}{\nu}$ tends to

become infinity $Re \to \infty$, (note that the boundary layer approximation is only valid

when $Re \to \infty$), all of the terms except the pressure term, can be neglected due to very

small values compared to the pressure term (stated as $O(1)$ in the above equation).

Presently, the process of the order of magnitude analysis for energy Equation
2.10 is completed out as in Tables 2.3.

Table 2.3   Order of magnitude analysis for the energy equation

Terms of equation	Used Equation 2.10	Magnitude Order $\times \dfrac{L}{U_\infty T_\infty}$	Decision $\delta \leq L$
$u\dfrac{\partial T}{\partial x}$	$U_\infty \dfrac{T_\infty}{L}$	$O(1)$	remain
$v\dfrac{\partial T}{\partial y}$	$\dfrac{U_\infty \delta}{L}\dfrac{T_\infty}{\delta}$	$O(1)$	remain
$\dfrac{k}{\rho C_p}\left(\dfrac{\partial^2 T}{\partial x^2}\right)$	$\dfrac{T_\infty}{L^2}$	$O\left(\dfrac{1}{U_\infty L}\right)$	can be negligible (≈ 0)
$\dfrac{k}{\rho C_p}\left(\dfrac{\partial^2 T}{\partial y^2}\right)$	$\dfrac{T_\infty}{\delta^2}$	$O\left(\dfrac{1}{U_\infty \delta^2}\right)$	remain
$\dfrac{\partial u}{\partial x}$	$\dfrac{U_\infty}{L}$	$O\left(\dfrac{1}{T_\infty}\right)$	can be negligible (≈ 0)
$\dfrac{\partial v}{\partial y}$	$\dfrac{U_\infty}{L}$	$O\left(\dfrac{1}{T_\infty}\right)$	can be negligible (≈ 0)
$\dfrac{\partial u}{\partial y}$	$\dfrac{U_\infty}{\delta}$	$O\left(\dfrac{1}{T_\infty}\dfrac{L}{\delta}\right)$	remain
$\dfrac{\partial v}{\partial x}$	$\dfrac{U_\infty \delta}{L^2}$	$O\left(\dfrac{1}{T_\infty}\dfrac{\delta}{L}\right)$	can be negligible (≈ 0)

23

From Table 2.3, all terms are multiplied with $\dfrac{L}{U_\infty T_\infty}$. Similar to the previous, each term on the right-hand side of the energy Equation 2.10 will be eliminated due to its small size compared to the other terms. The comparison can be made as follows:

$$\frac{\partial^2 T}{\partial y^2}\bigg/\frac{\partial^2 T}{\partial x^2}=O\left(\frac{L}{\delta}\right)T_\infty\geq 1,$$

$$\frac{\partial u}{\partial y}\bigg/\frac{\partial v}{\partial x}=O\left(\frac{L}{\delta}\right)^2\geq 1,$$

$$\frac{\partial u}{\partial y}\bigg/\frac{\partial u}{\partial x}=O\left(\frac{L}{\delta}\right)\geq 1,$$

$$\frac{\partial u}{\partial y}\bigg/\frac{\partial v}{\partial y}=O\left(\frac{L}{\delta}\right)\geq 1.$$

Therefore, the term $\dfrac{k}{\rho C_p}\dfrac{\partial^2 T}{\partial x^2},\dfrac{\partial u}{\partial x},\dfrac{\partial v}{\partial y}$ and $\dfrac{\partial v}{\partial x}$ in the energy Equation 2.10 will be neglected, but not the term $\dfrac{k}{\rho C_p}\dfrac{\partial^2 T}{\partial y^2}$ and $\dfrac{\partial u}{\partial y}$.

By this boundary layer approximation, Equations 2.7 to 2.10 can now be written as

$$\frac{\partial u}{\partial x}+\frac{\partial v}{\partial y}=0,$$

$$u\frac{\partial u}{\partial x}+v\frac{\partial u}{\partial y}=-\frac{1}{\rho}\frac{\partial p}{\partial x}+\nu\frac{\partial^2 u}{\partial y^2}, \qquad\qquad 2.16$$

$$0=-\frac{1}{\rho}\frac{\partial p}{\partial y}, \qquad\qquad 2.17$$

$$u\frac{\partial T}{\partial x}+v\frac{\partial T}{\partial y}=\frac{k}{\rho C_p}\frac{\partial^2 T}{\partial y^2}+\frac{\mu}{\rho C_p}\left(\frac{\partial u}{\partial y}\right)^2. \qquad\qquad 2.18$$

24

The discussions on the derivation of boundary layer equations can be found in many books related to boundary layer, convection heat transfer or fluid dynamic such as Schlichting (1979), Bejan (1984), Baehr and Stephen (2006), Lienhard IV and Lienhard V (2011), Kreith et al. (2010), Rathore (2011) and Favre-Marinet and Tardu (2013) and Mohamed (2017).

From Equation 2.17 it is clear that the pressure p is constant in $y-$direction. p is only varied with x which is $p = p(x)$. Since p is constant in $y-$direction, the pressure distribution in the boundary layer is equal to the outside of the boundary layer for the same values of x. Hence, the term $\dfrac{\partial p}{\partial x}$ in Equation 2.16 can be written in the ordinary differential form and becomes

$$u\frac{\partial u}{\partial x} + v\frac{\partial u}{\partial y} = -\frac{1}{p}\frac{\partial p}{\partial x} + v\frac{\partial^2 u}{\partial y^2}. \qquad 2.19$$

As pressure p does not depend on y in the boundary layer as shown in Equation 2.17, the pressure distribution along the boundary layer is similar to the outside of the boundary layer, then in this case, the Bernoulli equation is considered

$$\frac{p}{\rho} + \frac{1}{2}U^2 = 0. \qquad 2.20$$

The Equation 2.20 is obtained by differentiating with respect to x which becomes,

$$\frac{1}{\rho}\frac{\partial p}{\partial x} + U\frac{\partial u}{\partial x} = 0, \qquad 2.21$$

and can be written as

$$-\frac{1}{\rho}\frac{\partial p}{\partial x} = U\frac{\partial u}{\partial x}. \qquad 2.22$$

By substituting Equation 2.22 into Equation 2.19, it becomes

$$u\frac{\partial u}{\partial x}+v\frac{\partial u}{\partial y}=U\frac{\partial u}{\partial x}+v\frac{\partial^2 u}{\partial y^2}. \qquad\qquad 2.23$$
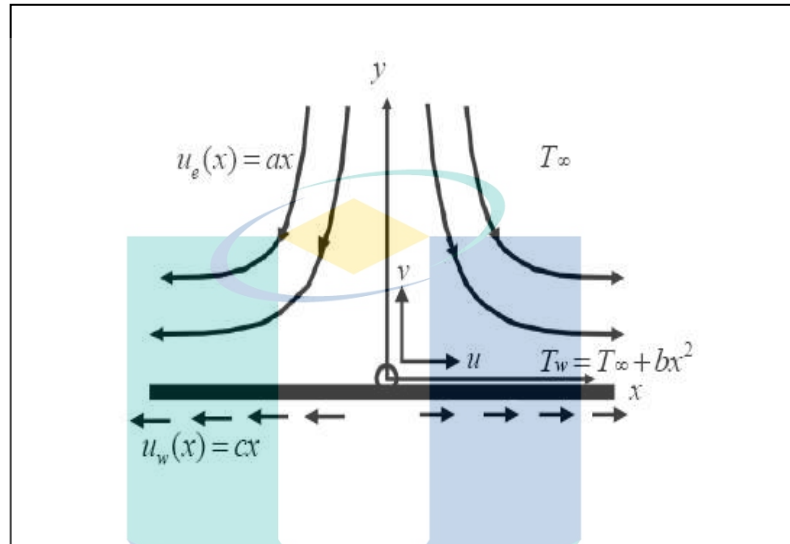
Figure 2.1   Schematic diagram for flow and heat transfer analysis of viscous fluid on the stagnation point over a stretching surface with viscous dissipation and slip conditions

The steady two-dimensional flow of a viscous fluid over a stretching plate is shown in Figure 2.1. It is assumed that the external and stretching velocities are $u_e(x)=ax$ and $u_w(x)=cx$, where a and c are constant. It is further assumed that the plate is subjected to obey the slip conditions. Recall the governing equation analyzing the two-dimensional boundary layer equation systems is rewritten as follows;

Continuity Equation

$$\frac{\partial u}{\partial x}+\frac{\partial v}{\partial y}=0$$

Momentum Equation

$$u\frac{\partial u}{\partial x}+v\frac{\partial u}{\partial y}=U\frac{\partial u}{\partial x}+v\frac{\partial^2 u}{\partial y^2}$$

26

Energy Equation

$$u\frac{\partial T}{\partial x}+v\frac{\partial T}{\partial y}=\frac{k}{\rho C_p}\frac{\partial^2 T}{\partial y^2}+\frac{\mu}{\rho C_p}\left(\frac{\partial u}{\partial y}\right)^2$$

subject to the boundary conditions (Salleh et al., 2009; Aziz, 2010) are as follows:

$$u=u_w(x)+\gamma^*\mu\frac{\partial u}{\partial y},\ v=0,\ T=T_w+\beta^*\frac{\partial T}{\partial y}\ \text{at}\ y=0 \qquad 2.24$$

$$u\to u_e(x),\ T\to T_\infty\ \text{as}\quad y\to\infty$$

where u and v are the velocity in the $x-$ and $y-$ axes, respectively, $T_w(x)=T_\infty+bx^2$ is the wall temperature (b is a positive constant), v is the kinematic viscosity, T is the fluid temperature, $\gamma*$ is the dimensional velocity slip parameter, β^* is the dimensional thermal slip parameter, k is the thermal conductivity, ρ is the fluid density, C_p is the specific heat and μ is the dynamic viscosity.

2.2.4 Similarity Transformation

A dimensional governing equation contains many dependent/independent variables which make the equation difficult to solve. In order to reduce the number of dependent/independent variables, the similarity transformation is applied.

The similarity transformation was first introduced by Blasius (1908). The main idea of this transformation is to eliminate at least one independent variable in the governing equation hence transform the governing partial differential equation to an ordinary differential equation. The similarity transformation is not applicable to all. The similarity variable is different for different types of geometry and boundary conditions.

The similarity transformation for Equations 2.7, 2.23 and 2.18 subjected to the boundary condition 2.24 can be written as follows (Merkin, 1994; Lesnic et al., 1999; Salleh et al., 2010; Yacob and Ishak, 2011; Mohamed 2017)

$$\eta = \left(\frac{c}{v}\right)^{1/2} y, \ \theta(\eta) = \frac{T - T_\infty}{T_w - T_\infty}, \ \psi = (cv)^{1/2} x f(\eta), \qquad 2.25$$

where η and $\theta(\eta)$ are dimensionless variables, while ψ is the stream function. Then, u and v can be defined as

$$u = \frac{\partial \psi}{\partial y}, \ v = -\frac{\partial \psi}{\partial x}, \qquad 2.26$$

which satisfy the continuity Equation 2.7. Then, u and v can be derived as

$$v = -\frac{\partial \psi}{\partial x} = -\frac{\partial}{\partial x} \left[(cv)^{1/2} x f(\eta) \right] = -(cv)^{1/2} f(\eta), \qquad 2.27$$

$$u = \frac{\partial \psi}{\partial y} = \frac{\partial \psi}{\partial \eta} \cdot \frac{\partial \eta}{\partial y} = \frac{\partial}{\partial \eta} \left[(cv)^{1/2} x f(\eta) \right] \cdot \frac{\partial}{\partial y} \left[\left(\frac{c}{v}\right)^{1/2} y \right]$$
$$= \left[(cv)^{1/2} x f'(\eta) \right] \cdot \left(\frac{c}{v}\right)^{1/2} = c x f'(\eta), \qquad 2.28$$

with

$$\frac{\partial u}{\partial x} = \frac{\partial}{\partial x} \left[c x f'(\eta) \right]$$
$$= c f'(\eta), \qquad 2.29$$

$$\frac{\partial v}{\partial y} = \frac{\partial v}{\partial \eta} \cdot \frac{\partial \eta}{\partial y} = \frac{\partial}{\partial \eta} \left[-(cv)^{1/2} f(\eta) \right] \cdot \frac{\partial}{\partial y} \left[\left(\frac{c}{v}\right)^{1/2} y \right]$$
$$= \left[-(cv)^{1/2} f'(\eta) \right] \cdot \left(\frac{c}{v}\right)^{1/2} = -c f'(\eta). \qquad 2.30$$

By substituting Equations 2.25 to 2.30 into continuity Equation 2.7, we obtain

$$\frac{\partial u}{\partial x} + \frac{\partial v}{\partial y} = 0$$

28

$$\frac{\partial u}{\partial x} + \frac{\partial v}{\partial \eta} \cdot \frac{\partial \eta}{\partial y} = 0 \qquad\qquad 2.31$$

$$cf'(\eta) + \left[\left(-(cv)^{1/2} f'(\eta) \right) \cdot \left(\frac{c}{v} \right)^{1/2} \right] = 0 \qquad\qquad 2.32$$

$$cf'(\eta) - cf'(\eta) = 0 \qquad\qquad 2.33$$

and Equation 2.7 is identically satisfied.

The same procedure is repeated for the case of momentum equation and it is found that

$$\frac{\partial u}{\partial x} = c\, f'(\eta), \ \frac{\partial \eta}{\partial y} = \left(\frac{c}{v} \right)^{1/2}, \ \frac{\partial u}{\partial x} = a, \qquad\qquad 2.34$$

$$\frac{\partial u}{\partial y} = \frac{\partial u}{\partial \eta} \cdot \frac{\partial \eta}{\partial y} = cxf''(\eta) \left(\frac{c}{v} \right)^{1/2}, \qquad\qquad 2.35$$

$$\frac{\partial^2 u}{\partial y^2} = \frac{\partial \left[\frac{\partial u}{\partial y} \right]}{\partial \eta} \cdot \frac{\partial \eta}{\partial y} = \left[cxf'''(\eta) \left(\frac{c}{v} \right)^{1/2} \right] \cdot \left(\frac{c}{v} \right)^{1/2} = \frac{c^2}{v} xf'''(\eta). \qquad\qquad 2.36$$

By substituting Equations 2.34, 2.35 and 2.36 into momentum Equation 2.23, then

$$u \frac{\partial u}{\partial x} + v \frac{\partial u}{\partial y} = U \frac{\partial u}{\partial x} + v \frac{\partial^2 u}{\partial y^2}$$

$$\left[cxf'(\eta) \right] \cdot \left[cf'(\eta) \right] + \left[-(cv)^{1/2} f(\eta) \right] \cdot \left[cxf''(\eta) \left(\frac{c}{v} \right)^{1/2} \right] = \\ (ax)(a) + (v) \left[\frac{c^2}{v} xf'''(\eta) \right] \qquad\qquad 2.37$$

$$f'(\eta)^2 - f(\eta) f''(\eta) = \left(\frac{a}{c} \right)^2 + f'''(\eta) \qquad\qquad 2.38$$

29

$$f'^2 - ff'' = \varepsilon^2 + f'''$$

2.39

$$f''' + ff'' + \varepsilon^2 - f'^2 = 0$$

2.40

where $\varepsilon = \dfrac{a}{c}$ is the stretching parameter, Equation 2.40 is a dimensionless momentum equation.

Next, for energy equation,

$$T = T_\infty + \theta(\eta)bx^2, \quad \frac{\partial T}{\partial \eta} = \theta'(\eta)bx^2, \quad \frac{\partial \eta}{\partial y} = \left(\frac{c}{v}\right)^{1/2},$$

2.41

$$\frac{\partial T}{\partial x} = 2\theta(\eta)bx,$$

2.42

$$\frac{\partial T}{\partial y} = \frac{\partial T}{\partial \eta} \cdot \frac{\partial \eta}{\partial y} = \left(\theta'(\eta)bx^2\right) \cdot \left(\frac{c}{v}\right)^{1/2} = \left(\theta'(\eta)bx^2\right)\left(\frac{c}{v}\right)^{1/2},$$

2.43

$$\frac{\partial^2 T}{\partial y^2} = \frac{\partial\left[\frac{\partial T}{\partial y}\right]}{\partial \eta} \cdot \frac{\partial \eta}{\partial y} = \left[\left(\theta''(\eta)bx^2\right)\left(\frac{c}{v}\right)^{1/2}\right] \cdot \left(\frac{c}{v}\right)^{1/2} = \left(\theta''(\eta)bx^2\right)\left(\frac{c}{v}\right).$$

2.44

By substituting Equations 2.41, 2.42, 2.43 and 2.44 into energy Equation 2.18, then

$$u\frac{\partial T}{\partial x} + v\frac{\partial T}{\partial y} = \frac{k}{\rho C_p}\frac{\partial^2 T}{\partial y^2} + \frac{\mu}{\rho C_p}\left(\frac{\partial u}{\partial y}\right)^2$$

$$\left[cxf'(\eta) \right] \cdot \left[2\theta(\eta)bx \right] + \left[-(cv)^{1/2} f(\eta) \right] \cdot \left[\left(\theta'(\eta)bx^2 \right) \left(\frac{c}{v} \right)^{1/2} \right] =$$

$$\frac{k}{\rho C_p} \left[\left(\theta''(\eta)bx^2 \right) \left(\frac{c}{v} \right) \right] + \frac{\mu}{\rho C_p} \left[\left(cxf''(\eta) \right) \left(\frac{c}{v} \right)^{1/2} \right]^2 \qquad\qquad 2.45$$

$$2\theta f' bcx^2 - bcx^2 \theta' f = \frac{k}{\rho C_p} \theta'' bcx^2 + \frac{c^3 x^2 f''}{C_p} \qquad\qquad 2.46$$

$$2\theta f' - \theta' f = \frac{1}{\mathrm{Pr}} \theta'' + \frac{(U_w)^2}{C_p (T_w - T_\infty)} f''^2 \qquad\qquad 2.47$$

$$2\theta f' - \theta' f = \frac{1}{\mathrm{Pr}} \theta'' + Ec\, f''^2 \qquad\qquad 2.48$$

$$\theta'' - \mathrm{Pr} \left[2f'\theta - f\theta' \right] + \mathrm{Pr}\, Ec\, f''^2 = 0 \qquad\qquad 2.49$$

where $\mathrm{Pr} = \dfrac{v \rho C_p}{k}$ is the Prandtl number, $Ec = \dfrac{(U_w)^2}{C_p (T_w - T_\infty)}$ is the Eckert number which represents the viscous dissipation and Equation 2.49 is a dimensionless energy equation.

The boundary conditions 2.24 for the variables are carried out as follows when $y = 0$ and details are given in Table 2.4

31

Table 2.4   Formulation of boundary conditions

Boundary condition	Transformed Boundary Condition
$u = u_w(x) + \gamma^*\mu\dfrac{\partial u}{\partial y}$	$u = u_w(x) + \gamma^*\mu\dfrac{\partial u}{\partial y}$
	$cxf'(0) = cx + \gamma^*\mu\cdot cxf''\left(\dfrac{c}{v}\right)^{1/2}$
	$\left[cxf'(0) = cx + \gamma^*\mu\cdot cxf''\left(\dfrac{c}{v}\right)^{1/2}\right] \div cx$
	$f'(0) = 1 + \gamma^*\mu f''\left(\dfrac{c}{v}\right)^{1/2}$
	$f'(0) = 1 + \dfrac{\gamma}{\rho(cv)^{1/2}}v\rho f''\left(\dfrac{c}{v}\right)^{1/2}$
	$f'(0) = 1 + \gamma f''(0)$
$T = T_w(x) + \beta^*\mu\dfrac{\partial T}{\partial y}$	$\theta(0)bx^2 + T_\infty = T_\infty + bx^2 + \beta^*\theta'(0)bx^2\left(\dfrac{c}{v}\right)^{1/2}$
	$\theta(0)(T_w - T_\infty) + T_\infty = T_\infty + (T_w - T_\infty) + \beta^*\theta'(0)(T_w - T_\infty)\left(\dfrac{c}{v}\right)^{1/2}$
	$\theta(0)(T_w - T_\infty) + T_\infty - T_\infty = (T_w - T_\infty) + \beta^*\theta'(0)(T_w - T_\infty)\left(\dfrac{c}{v}\right)^{1/2}$
	$\begin{pmatrix}\theta(0)(T_w - T_\infty) = (T_w - T_\infty) + \\ \beta^*\theta'(0)(T_w - T_\infty)\left(\dfrac{c}{v}\right)^{1/2}\end{pmatrix} \div (T_w - T_\infty)$
	$\theta(0) = 1 + \dfrac{\beta}{\left(\dfrac{c}{v}\right)^{1/2}}\theta'(0)\left(\dfrac{c}{v}\right)^{1/2}$
	$\theta(0) = 1 + \beta\theta'(0)$

32

Table 2.4 (continued)

Boundary condition	Transformed Boundary Condition
$v = 0$	$v = 0$
	$-(cv)^{1/2} f(0) = 0$
	$f(0) = \dfrac{0}{-(cv)^{1/2}}$
	$f(0) = 0$
$u \to u_e(x)$	$u \to u_e(x)$
	$cxf'(\infty) \to ax$
	$f'(\infty) \to \dfrac{a}{c}$
	$f'(\infty) \to \varepsilon$
$T \to T_\infty$	$T \to T_\infty(x)$
	$\theta(\infty)bx^2 + T_\infty \to T_\infty$
	$\theta(\infty)T_\infty bx^2 \to T_\infty - T_\infty$
	$\theta(\infty)(T_w - T_\infty) \to 0$
	$\theta(\infty) \to \dfrac{0}{(T_w - T_\infty)}$
	$\theta(\infty) \to 0$

In summary, Equations 2.23 and 2.18 which formulate to ordinary differentiation Equations 2.40 and 2.49 are subject to boundary conditions 2.50 as follows:

$$f(0) = 0,\ f'(0) = 1 + \gamma f''(0),\ \theta(0) = 1 + \beta \theta'(0) \qquad 2.50$$
$$f'(\eta) \to \varepsilon,\ \theta(\eta) \to 0 \ \text{ as } \ \eta \to \infty$$

33

The boundary layer equation described in this chapter will be solved numerically by using the shooting method. The numerical solution procedures are discussed in details in Section 2.3, while the numerical results will be discussed completely in Chapter 3.

2.3   Numerical Method: Shooting Method

In this thesis, we used the shooting method as numerical method to overcome the fluid mechanics problem from partial differential equation reduces to the non-linear ordinary differential equations. In addition, with this method, we have to determine the initial values that satisfied the boundary conditions at the endpoint. Furthermore, this method was applied in Maple programming language based on "dsolve" command and "shoot" implementation. The reasons for using this method were that; it could attempt to diagnose the applicable initial conditions for a related initial value problem (IVP) which brought the accurate solution to boundary value problem (BVP), easier to apply, reliable result could be obtained as well as very helpful when solving the boundary layer problems.

The researchers who used the shooting method to solve the boundary layer problems include Aman et al. (2013), Ibrahim et al. (2013), Dessie and Kishan (2014), Abbas et al. (2015), Paland Mandal (2015), Bhatti et al. (2016b), Dash et al. (2016), Raju and Sandeep (2017), Agbaje et al. (2018), Bilal et al. (2018) and many more.

The shooting method takes advantage of the speed and adaptivity for initial value problems. However, it is not as robust as collocation or finite difference methods. For example, even though the boundary value problem may look quite well-posed and stable but the growing modes of initial value problems may inherently be unstable and unnoticed. Therefore, the comparison of works was necessary.

According to the literature review, it could be seen that the shooting method has been used frequently to determine the numerical solutions for Newtonian or non-Newtonian flows problems, especially in science and engineering fields to solve the differential equations. Thus, in this thesis, we 'shoot' out trajectories in different direction until we managed to set a trajectory that has appropriate boundary value.

34

Shooting method is a method to overcome a boundary value problem by reducing it to the initial value problem solution. Linear problems can be described as follows

$$
\begin{aligned}
& X_c'(t) = J(t) X_c(t) + F_0(t); X_c(t_0) = c \\
& G\big(X_c(t_1), X_c(t_2), ..., X_c(t_n)\big) = G_0 + G_1 X_c(t_1) + G_2 X_c(t_2) \\
& + ... + G_N X_c(t_n)
\end{aligned}
\qquad 2.51
$$

where $J(t)$ is represented as a matrix, $F_0(t)$ is defined as vector possibly depending on t, G_0 is a constant vector and $G_1, G_2, ..., G_n$ are constant matrices. Let $Y = \dfrac{\partial X_c(t)}{\partial_c}$, then differentiating both the initial value problem (IVP) and boundary conditions with respect to c gives

$$
\begin{aligned}
& Y'(t) = J(t) Y(t); Y(t_0) = I \\
& \frac{\partial G}{\partial c} = G_1 Y(t_1) + G_2 Y(t_2) + ... + G_n Y(t_n) = 0.
\end{aligned}
\qquad 2.52
$$

Since G is linear and a function of c, we also have $G_c = G(c_0) + \dfrac{\partial G}{\partial c}(c - c_0)$, hence the value of c for which $G(c) = 0$ is satisfied is

$$
c = c_0 + \left(\frac{\partial G}{\partial c}\right)^{-1} G(c_0)
\qquad 2.53
$$

for any particular initial condition of c_0.

On the other hand, for a non-linear problem, by assuming $J(t)$ as the Jacobian for the non-linear ordinary differential equation system and let G_i be the Jacobian of the ith boundary condition, the computation of $\dfrac{\partial G}{\partial c}$ for the linearized system with a

35

particular initial condition given by Jacobian for the non-linear system leads to a Newton iteration,

$$c_{n+1} = c_n + \left(\frac{\partial G}{\partial c}(c_n) \right)^{-1} G(c_n) \qquad 2.54$$

The solutions are written in the form of a partial differential equation and then transformed into an ordinary differential equation. Besides, the solutions do not calculate the complicated integrals either analytically or numerically. Furthermore, these solutions are obtained by the shooting method which satisfies all the imposed boundaries and initial conditions as well as governing equations.

The procedure of shooting method for case flow and heat transfer analysis of viscous fluid on the stagnation point over a stretching surface with viscous dissipation and slip conditions is given below. The result analysis is discussed in Chapter 3.

The first step is to reduce the third-order system for the momentum equation to a first-order system,

$$\begin{aligned} f &= f_0 \\ f' &= f_1 \\ f'' &= f_2 \\ f''' &= f_3 \end{aligned} \qquad 2.55$$

Next, reduce the second-order system to a first-order system for the respective energy equation,

$$\begin{aligned} \theta &= \theta_0 \\ \theta' &= \theta_1 \\ \theta'' &= \theta_2 \end{aligned} \qquad 2.56$$

where prime is referred to the derivative with respect to η. Therefore, the new equation of momentum and energy is formed and illustrated as below:

$$\frac{df_0}{d\eta} = f_1,$$

$$\frac{df_1}{d\eta} = f_2,$$

$$\frac{df_2}{d\eta} = (f_1)^2 - f_0 f_2 - \varepsilon^2, \qquad\qquad 2.57$$

$$\frac{d\theta_0}{d\eta} = \theta_1,$$

$$\frac{d\theta_1}{d\eta} = \Pr[2f_1\theta_0 - f_0\theta_1] - \Pr Ec(f_2)^2$$

the new boundary conditions for the above three equations are given as follow:

$$f_0(0) = 0,\ f_1(0) = 1 + \gamma f_2(0),\ \theta_0(0) = 1 + \beta \theta_1(0) \qquad\qquad 2.58$$

$$f_1(\eta) \to \varepsilon,\ \theta_0(\eta) \to 0 \ \text{ as } \ \eta \to \infty$$

By using trial and error and the fourth-order Runge-Kutta method (RKF45), the solutions $f_2(0)$ and $\theta_1(0)$ are obtained. The initial value problem (IVP) result is obtained by using the shooting method on a set of parameters appearing in the governing equations with a known value of $f_2(0)$ and $\theta_1(0)$. The convergence criterion largely depends on good guesses of the initial conditions in the shooting method. The iterative process is terminated until the relative difference between the current iterative values of $f_2(0)$ matches with the previous iterative value of $f_2(0)$ up to a tolerance of 10^{-5}.

From the obtained solution, we see either the solution satisfies the boundary condition at the endpoints or by checking the velocity and temperature profiles graph. If the profiles have satisfied the boundary conditions at the endpoints asymptotically, it means the solution obtained is valid and very useful for the current study. The same procedure is repeated for another guessing value for the same values of parameters used. The programming works are shown in Appendix B by using Maple software.

CHAPTER 3

FLOW AND HEAT TRANSFER ANALYSIS OF VISCOUS FLUID ON THE STAGNATION POINT OVER A STRETCHING SURFACE WITH VISCOUS DISSIPATION AND SLIP CONDITIONS

3.1 Introduction

The boundary layer stagnation-point flow is the most interesting topic to explore due to its numerous applications in industries and engineering areas such as cooling, nuclear reactor, electronic, many hydrodynamics processes (Abu Bakar et al., 2019), melt-spinning processes, glass blowing and paper production (Nasir et al., 2019).

Hiemenz (1911) was the first to propose the problem that involved stagnation point and solve the exact value for Navier-Stokes equations. Next, Chao and Jeng (1965) investigated the unsteady stagnation point heat transfer. Chiam (1994) examined stagnation-point flow towards a stretching plate. Recent studies on this problem are by Abu Bakar et al. (2019), who investigated a stability analysis of boundary layer stagnation-point flow over a stretching/shrinking cylinder in a nanofluid and Nasir et al. (2019) investigated stagnation point flow and heat transfer past a permeable stretching/shrinking Riga plate with velocity slip and radiation effects. Both problems have been solved numerically using the shooting method in Maple software and a bvp4c in MATLAB software. Abu Bakar et al. (2019) found that dual solution exists for shrinking cylinder cases and a unique solution exists for stretching cylinder cases but Nasir et al. (2019) found a dual solution for both stretching and shrinking cases.

Furthermore, the stagnation point heat transfer flow over a stretching sheet in the presence of viscous dissipation and slip conditions are considered in this chapter. The

main idea for specific cases in this problem is from Mahapatra and Gupta (2002), Mohamed et al. (2012) and Mohamed et al. (2017). Mahapatra and Gupta (2002) have shown that, the rate of heat transfer at the stretching surface gives the best quality for the end product and for a fluid of small kinematic viscosity, a boundary layer is formed when the stretching velocity exceeds the free stream velocity. While Mohamed et al. (2012) have used the shooting method technique to solved the boundary layer problems generated by Newtonian heating in which the heat transfer from the surface is proportional to the local surface temperature. Mohamed et al.(2017) considered slip effect on stagnation point flow past a stretching surface with the presence of heat generation/absorption and Newtonian heating for boundary conditions. They used Runge-Kutta-Fehlberg method in Maple software to analyze the numerical solution.

Motivated from related studies, the aim of the present work is to investigate the stagnation point heat transfer flow over a stretching sheet in the presence of viscous dissipation and slip conditions. The solvable model of this problem is presented in Section 3.2, with the introduction of similarity transformations to governing equations which has been formulate in Chapter 2 before the shooting method is used numerically. Numerical results for the local Nusselt number and skin friction coefficient as well as the temperature and velocity field are elucidated through tables and graphs. The influence of Prandtl number, stretching parameter, Eckert number, thermal and velocity slip parameters on the flow and heat transfer characteristics are analyzed and discussed.

3.2   Mathematical Formulation

Consider the steady two-dimensional flow of a viscous fluid over a stretching plate as shown in the previous chapter in Figure 2.1. The external and stretching velocities are $u_e(x) = ax$ and $u_w(x) = cx$, where a and c are constants. It is further assumed that the plate is subjected to obey the slip conditions.

After substituting transformations, the systems equations in ordinary differential equations term are in the form of 3.1 and 3.2 subject to the boundary conditions 3.3, which have been discussed in detail in the previous chapter under Section 2.2.4.

$$f''' + ff'' + \varepsilon^2 - f'^2 = 0 \qquad\qquad 3.1$$

$$\theta'' - \Pr\left[2f'\theta - f\theta'\right] + \Pr Ec\, f''^2 = 0 \qquad\qquad 3.2$$

The boundary conditions

$$f(0)=0,\ f'(0)=1+\gamma\, f''(0),\ \theta(0)=1+\beta\theta'(0) \qquad\qquad 3.3$$

$$f'(\eta)\to\varepsilon,\ \theta(\eta)\to 0 \text{ as } \eta\to\infty$$

In Equations 3.1 and 3.2, the parameters of Prandtl number, $\Pr$, Eckert number (represent the viscous dissipation parameter) Ec, stretching parameter ε, dimensionless velocity parameter γ and thermal slip parameter β, can be defined as

$$\Pr = \frac{\nu\rho C_p}{k},\ Ec = \frac{\left(U_w\right)^2}{C_p\left(T_w - T_\infty\right)},\ \varepsilon = \frac{a}{c},\ \gamma = \gamma^*\rho\left(cv\right)^{1/2},\ \beta = \beta^*\left(\frac{c}{v}\right)^{1/2} \qquad 3.4$$

It is noticed that $\beta = 0$ is when the wall temperature remains constant (CWT). The skin friction coefficient C_f and the local Nusselt number Nu_x are given as

$$C_f = \frac{\tau_w}{\rho u_w^2}, \qquad\qquad 3.5$$

$$Nu_x = \frac{xq_w}{k\left(T_w - T_\infty\right)}, \qquad\qquad 3.6$$

The surface shear stress τ_w and heat flux q_w are defined as

$$\tau_w = \mu\left(\frac{\partial u}{\partial y}\right)_{y=0}, \qquad\qquad 3.7$$

40

$$q_w = -k \left(\frac{\partial T}{\partial y} \right)_{y=0}, \qquad\qquad 3.8$$

Using the similarity variables in Equations 3.9 to 3.11,

$$\eta = \left(\frac{c}{v} \right)^{1/2} y, \qquad\qquad 3.9$$

$$\psi = (cv)^{1/2} xf(\eta), \qquad\qquad 3.10$$

$$\theta(\eta) = \frac{T - T_\infty}{T_w - T_\infty}, \qquad\qquad 3.11$$

the outcomes are

$$C_f \, \mathrm{Re}_x^{1/2} = f''(0), \qquad\qquad 3.12$$

$$Nu_x \, \mathrm{Re}_x^{-1/2} = -\theta'(0), \qquad\qquad 3.13$$

where $\mathrm{Re}_x = \dfrac{u_w x}{v}$ is the local Reynolds number.

3.3   Results and Discussion

Equations 3.1 and 3.2 with corresponding boundary conditions 3.3 were solved numerically with the aid of the shooting method using Maple software. To study the flow behavior, we considered different parameters, namely the Prandtl number, Pr, the dimensionless velocity slip parameter, γ, the stretching parameter, ε, the dimensionless thermal slip parameter, β and the Eckert number, Ec. In order to validate the efficiency of the method used, the comparison values of reduced skin friction coefficient $C_f \, \mathrm{Re}_x^{1/2}$ have been made with previously published paper.

Table 3.1 shows the comparison of the present results to those obtained in previous works by Ishak et al. (2006) for different values of ε. In addition, the results from Ishak et al. (2006) are generated from Keller-box method with the aid of MATLAB software. The result obtained were in accordance with previous studies, therefore, the method that was used work efficiently in this problem.

Table 3.2 presents the various values of the viscous dissipation parameter Ec when $\Pr = \beta = \gamma = 1$ and $\varepsilon = 3$. It is found that as Ec increases the $Nu_x \operatorname{Re}_x^{-1/2}$ decreases which implies the reducing in ability of the convective heat transfer. Next, from the numerical calculation, there exist only unique solution for the skin friction coefficient, that is $f''(0) = 1.45373$.

Table 3.3 presents the values of $\theta(0)$ and $Nu_x \operatorname{Re}_x^{-1/2}$ for the various values of $\Pr$ when $Ec = \gamma = 1, \varepsilon = 3$ and $\beta = 0, 1, 7$. It is observed that when the dimensionless thermal slip parameter is not considered $(\beta = 0)$, an increased $\Pr$ makes value of $\theta(0)$ remains constant (CWT) by referring to the boundary conditions in Equation 3.3 while $Nu_x \operatorname{Re}_x^{-1/2}$ increases. For the case of $\beta = 1$ and $\beta = 7$ an increase of $\Pr$ makes $\theta(0)$ decreases while $Nu_x \operatorname{Re}_x^{-1/2}$ increases. When $\Pr$ is fixed and β increases, then $\theta(0)$ and $Nu_x \operatorname{Re}_x^{-1/2}$ decreases.

Table 3.4 presents the values of $C_f \operatorname{Re}_x^{1/2}$ for the various values of ε when $\Pr = Ec = \beta = 1$ and $\gamma = 0, 1, 7$. It is observed that when the dimensionless velocity slip parameter is not considered $(\gamma = 0)$, an increased ε makes $C_f \operatorname{Re}_x^{1/2}$ increases as well as for the case of $\gamma = 1$ and $\gamma = 7$. When ε is fixed with an increase of γ, $C_f \operatorname{Re}_x^{1/2}$ decreases.

Figure 3.1 points the temperature profiles for various values of $\Pr$. The value of $\Pr$ rises, but the value of the wall temperature and the thickness of the thermal

boundary layer drop. Physically, its means when we increase Pr, the thermal diffusivity decreases and these phenomena lead to the decrease in the ability of the energy and finally decreases the thermal boundary layer.

Figure 3.2 demonstrates the temperature profiles for various values of ε. The data found that when ε rises, the temperature profile increase, but the value of the thickness of thermal boundary layer drop. Figure 3.3 shows the velocity profiles for various values of ε which produce $f'(\eta)=\varepsilon$ as $\eta \to \infty$. The data found the thickness of the boundary layer increases with the increase of ε.

Figure 3.4 presents the temperature distribution for different values of Ec. Note that $Ec = 0$ refers to the case when viscous dissipation is not present. From Figure 3.4, the temperature profiles increases as Ec increases. This is due to large viscous resistance, there is more accumulation of heat energy in the fluid particles near the boundary. Also, it is noticed that Ec only gives a small effect for boundary layer thickness.

Next, Figures 3.5 and 3.6 elucidate the temperature profile for various values of β and γ, respectively. Similar trends occurred between both figures where the temperature profiles and boundary layer thickness decrease as β or γ increases. Physically, we can conclude that the presence of both velocity and thermal slip parameter reduce the temperature and the boundary layer thickness. In addition, it is noticed that the velocity gradient is not affected by various values of β, and the excuse for this phenomena can be seen from the boundary conditions in Equation 3.3.

Figure 3.7 illustrates the velocity profile and skin friction coefficient for several of the velocity slip parameter γ. From Figure 3.7, it is found that the velocity gradient decreases as γ increases.

43

Table 3.1   Comparison between the present results of the $C_f \, \mathrm{Re}_x^{1/2}$ or a different values of ε when $Ec = \gamma = \beta = 0$ and $\mathrm{Pr} = 1$

ε	Ishak et al. (2006)	Present
	$C_f \, \mathrm{Re}_x^{1/2}$	$C_f \, \mathrm{Re}_x^{1/2}$
0.1	- 0.9694	- 0.96945
0.2	- 0.9181	- 0.91811
0.5	- 0.6673	- 0.66726
2	2.0175	2.017502
3	4.7294	4.729282

Table 3.2   Values of $Nu_x \, \mathrm{Re}_x^{-1/2}$ for the various values of Ec when $\mathrm{Pr} = \beta = \gamma = 1$ and $\varepsilon = 3$

Ec	$Nu_x \, \mathrm{Re}_x^{-1/2}$
0.1	0.71353
1	0.63887
2	0.55591
3	0.47296
5	0.30705

Table 3.3   Values of $\theta(0)$ and $Nu_x \, \mathrm{Re}_x^{-1/2}$ for the various values of Pr when $Ec = \gamma = 1$, $\varepsilon = 3$ and $\beta = 0, 1, 7$

Pr	$\beta = 0$		$\beta = 1$		$\beta = 7$	
	$\theta(0)$	$Nu_x \, \mathrm{Re}_x^{-1/2}$	$\theta(0)$	$Nu_x \, \mathrm{Re}_x^{-1/2}$	$\theta(0)$	$Nu_x \, \mathrm{Re}_x^{-1/2}$
0.1	1	0.50464	0.66461	0.33539	0.22063	0.11134
1	1	1.59577	0.38524	0.61476	0.08217	0.13112
3	1	2.76395	0.26568	0.73432	0.04915	0.13584
5	1	3.56824	0.21890	0.78110	0.03850	0.13736
7	1	4.22208	0.19150	0.80850	0.03273	0.13818

Table 3.4   Values of $C_f \, \mathrm{Re}_x^{1/2}$ for the various values of ε when $\mathrm{Pr} = Ec = \beta = 1$ and $\gamma = 0, 1, 7$

ε	$\gamma = 0$	$\gamma = 1$	$\gamma = 7$
	$C_f \, \mathrm{Re}_x^{1/2}$	$C_f \, \mathrm{Re}_x^{1/2}$	$C_f \, \mathrm{Re}_x^{1/2}$
1.5	0.90953	0.32812	0.06654
2	2.01750	0.68599	0.13430
3	4.72928	1.45373	0.27158
5	11.75199	3.09847	0.54930
7	20.49788	4.81812	0.82894
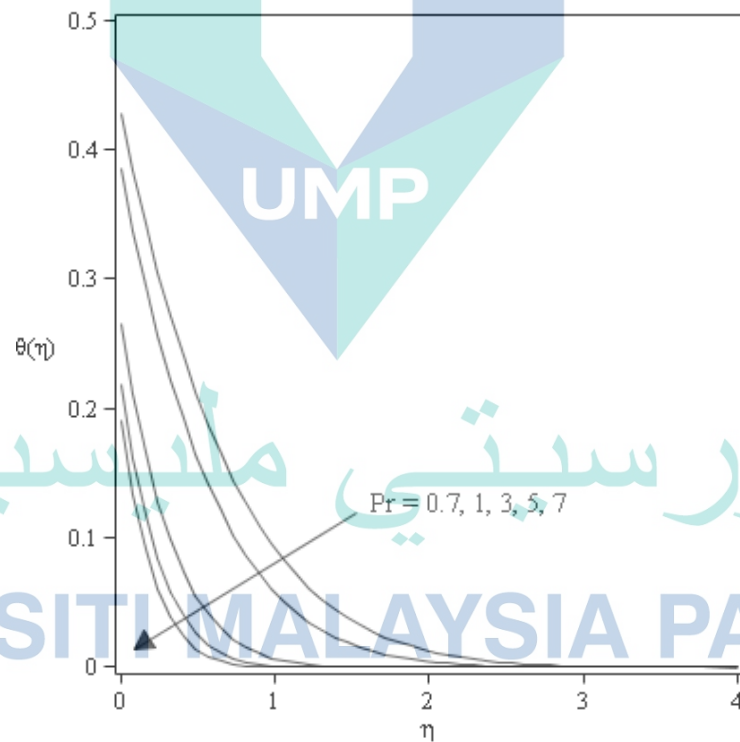
Figure 3.1   Temperature profiles $\theta(0)$ for various values of Pr when $\beta = \varepsilon = Ec = \gamma = 1$

45
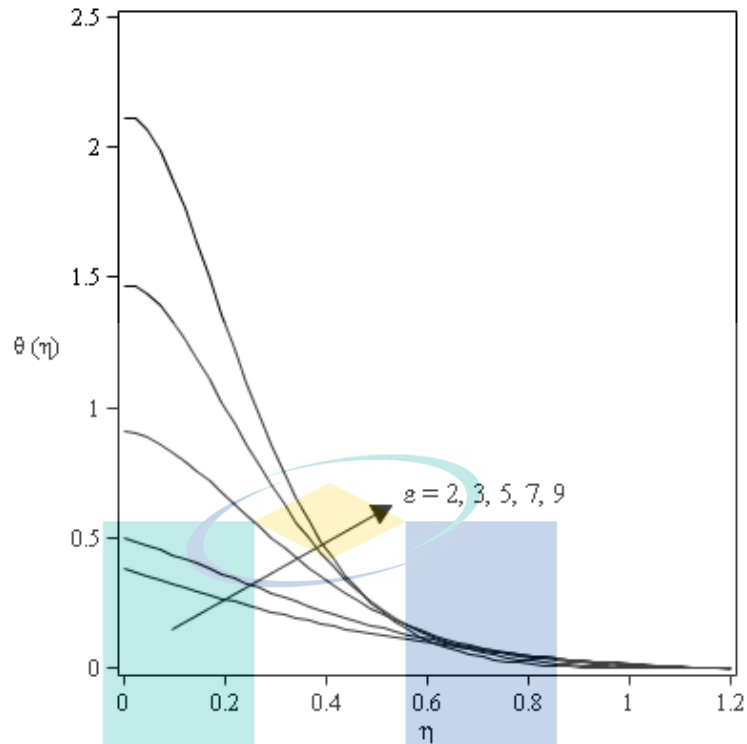
Figure 3.2   Temperature   profiles $\theta(0)$ for   various   values   of ε when $\beta = \text{Pr} = Ec = 1$ and $\gamma = 0.1$
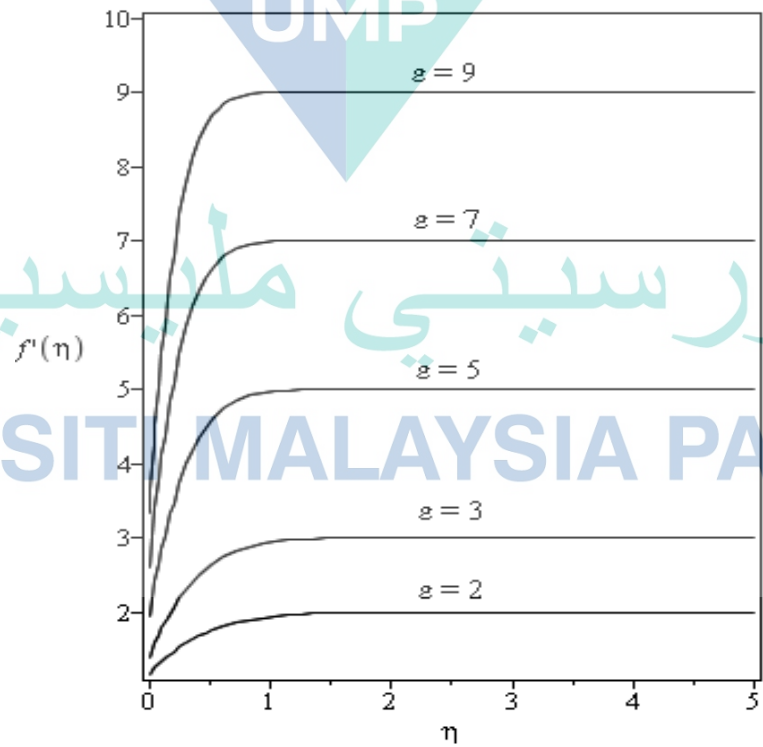
Figure 3.3   Velocity profiles $f'(\eta)$ for various values of ε when $\beta = \text{Pr} = Ec = 1$ and $\gamma = 0.1$

46
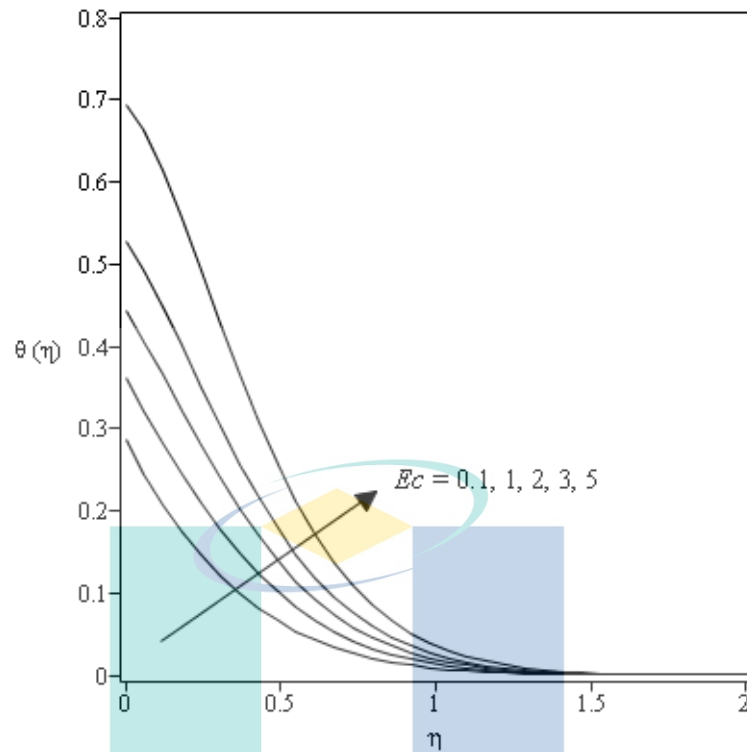
Figure 3.4   Temperature   profiles $\theta(0)$ for   various   values   of Ec when $\beta = \Pr = \varepsilon = \gamma = 1$
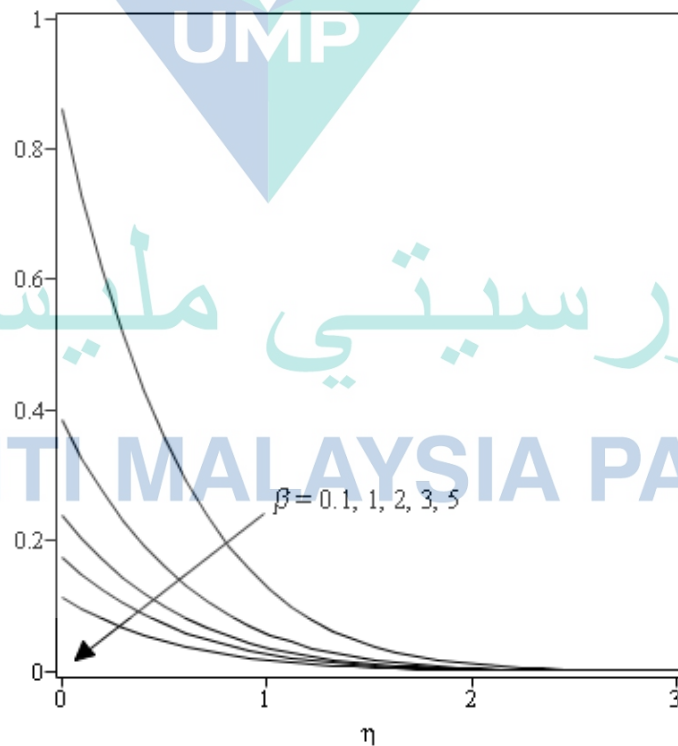
Figure 3.5   Temperature   profiles $\theta(0)$ for   various   values   of β when $Ec = \Pr = \varepsilon = \gamma = 1$
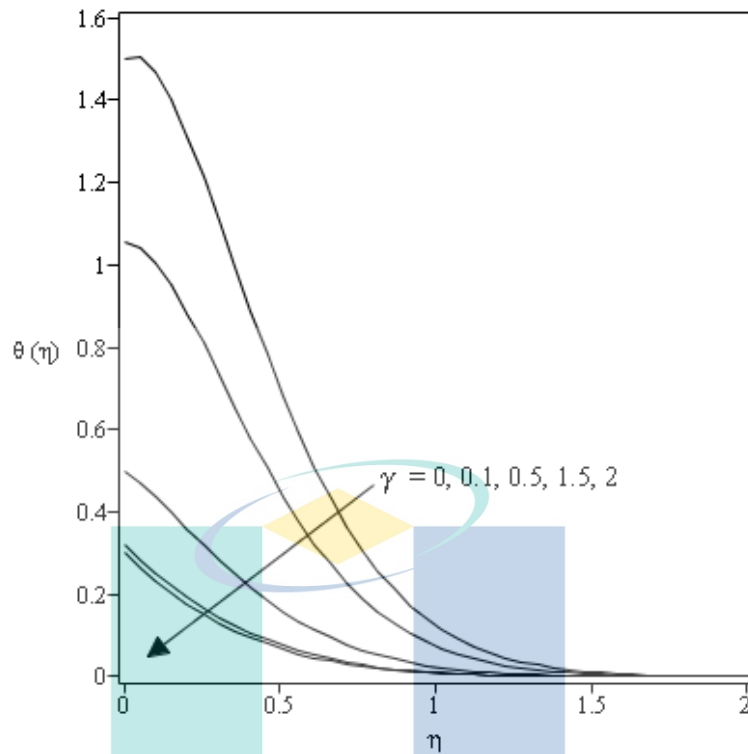
Figure 3.6   Temperature   profiles $\theta(0)$ for   various   values   of γ when $\beta = \Pr = Ec = 1$ and $\varepsilon = 3$
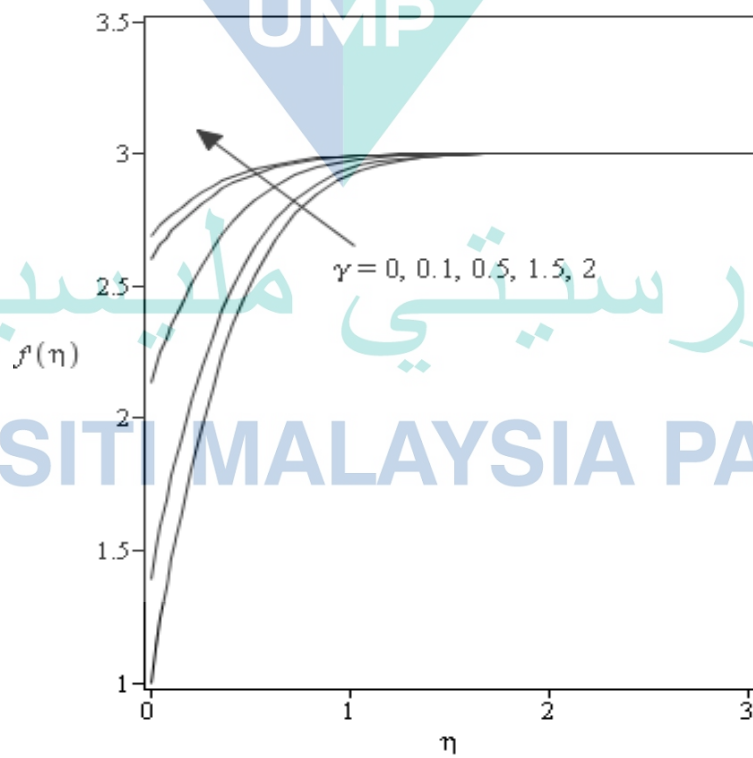
Figure 3.7   Velocity profiles $f'(\eta)$ for various values of γ when $\beta = \Pr = Ec = 1$ and $\varepsilon = 3$

3.4   Summary

In this study, the flow and heat transfer analysis of viscous fluid on the stagnation point towards a stretching sheet with viscous dissipation and slip conditions are numerically studied. The presented analysis leads to the following main results:

i. the increase of Prandtl number, dimensionless thermal and velocity slip parameter result in the decreasing in the wall temperature and also thermal boundary layer thickness.

ii. the presence of viscous dissipation and stretching parameter results in the increase of the wall temperature.

iii. the presence of velocity slip parameter is decreased by the skin friction coefficient while the Prandtl number, the stretching parameter, the thermal slip parameter and Eckert number have no effect on the skin friction coefficient.

Table 3.5 show the summarized mathematical formulations in this problem. The governing equations are first transformed into ordinary differential equations via similarity analysis and then, these resulting equations are solved using the transformed boundary conditions.

Table 3.5   Solution procedure for mathematical formulation flow and heat transfer of viscous fluid on stagnation point over stretching surface with viscous   dissipation and slip conditions

Steps	Equations
	$\dfrac{\partial u}{\partial x} + \dfrac{\partial v}{\partial y} = 0$
Governing Equations	$u\dfrac{\partial u}{\partial x} + v\dfrac{\partial u}{\partial y} = U\dfrac{\partial u}{\partial x} + v\dfrac{\partial^2 u}{\partial y^2}$
	$u\dfrac{\partial T}{\partial x} + v\dfrac{\partial T}{\partial y} = \dfrac{k}{\rho C_p}\dfrac{\partial^2 T}{\partial y^2} + \dfrac{\mu}{\rho C_p}\left(\dfrac{\partial u}{\partial y}\right)^2$

Table 3.5 Continued

Steps	Equations
Boundary conditions	$u = u_w(x) + \gamma^* \mu \dfrac{\partial u}{\partial y},\ v = 0,\ T = T_w + \beta^* \dfrac{\partial T}{\partial y}$ at $y = 0$ $u \to u_e(x),\ T \to T_\infty$ as $y \to \infty$
Similarity transformation	$\eta = \left(\dfrac{c}{\nu}\right)^{1/2} y,\ \theta(\eta) = \dfrac{T - T_\infty}{T_w - T_\infty},\ \psi = (c\nu)^{1/2} x f(\eta)$
Ordinary differential equations	$f''' + ff'' + \varepsilon^2 - f'^2 = 0$ $\theta'' - \Pr\left[2f'\theta - f\theta'\right] + \Pr Ec\, f''^2 = 0$
Transformed boundary conditions	$f(0) = 0,\ f'(0) = 1 + \gamma f''(0),\ \theta(0) = 1 + \beta\theta'(0),$ $f'(\eta) \to \varepsilon,\ \theta(\eta) \to 0$ as $\eta \to \infty$

50
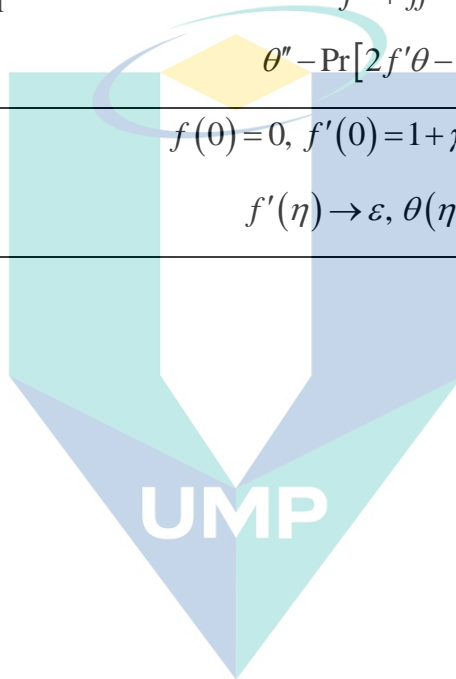
CHAPTER 4

FLOW AND HEAT TRANSFER ANALYSIS OF WILLIAMSON FLUID ON THE STAGNATION POINT OVER A STRETCHING SURFACE WITH VISCOUS DISSIPATION AND SLIP CONDITIONS

4.1 Introduction

In recent years, the study of non-Newtonian fluids has attracted the attention of many researchers. There are many theoretical and technical applications in both the industries and engineering processes such as in the aerodynamic extrusion of plastic sheets, glass fiber, paper production, manufacturing of polymer sheets (Nadeem et al., 2009), oil recovering and food processing (Das et al., 2015). In view of their difference with Newtonian fluids, many models of non-Newtonian fluid have been proposed such as the second-grade fluid (Nadeem et al., 2010), the micropolar fluid (Borrelli et al., 2012), the Williamson fluid (Nadeem et al., 2013), the Jeffrey fluid (Das et al., 2015) and the Casson fluid (Ramesh and Devakar, 2015).

Williamson (1929) proposed the flow of pseudoplastic materials and developed a model equation to illustrate the flow of pseudoplastic fluid. Next, Nadeem et al. (2013) investigated the flow of a Williamson fluid over a stretching sheet. The homotopy analysis is used to solve the non-linear differential equation. After that, Khan et al. (2014) and Nadeem and Hussain (2014) investigated the boundary layer flow and heat transfer of Williamson fluid with chemically reactive species using scaling transformation approaches. It is found that the Williamson fluid model is very much similar to blood and almost completely describes the blood flow.

Current studies with Williamson fluid such as Salahuddin et al. (2016) considered MHD flow of Cattaneo–Christov heat flux model for Williamson fluid over a stretching sheet with variable thickness using a numerical approach. Numerical solution of Williamson fluid flow past a stretching cylinder and heat transfer with variable thermal conductivity and heat generation/absorption was studied by Malik et al. (2016). They were using the shooting method in conjuction with Runge-Kutta- Fehlberg (RKF45) to find the solution of the problem. Kumaran and Sandeep (2017) presented thermophoresis and Brownian moment effects on the parabolic flow of MHD Casson and Williamson fluids with cross-diffusion. The results show that the heat and mass transfer performance of Casson fluid is comparatively higher than Williamson fluid. Shah et al. (2018) addressed the radiative MHD thin film flow of Williamson fluid over an unsteady permeable stretching sheet. The unsteady stagnation-point flow of Williamson fluid generated by stretching/shrinking sheet with Ohmic heating was reported by Hamid et al. (2018a). Simultaneous solutions for MHD flow of Williamson fluid over a curved sheet with nonuniform heat source/sink were explored by Kumar et al. (2019). They found that the curvature parameter enhances the velocity field while the reverse trend is detected due to the Williamson fluid and magnetic field parameters. Bhuvaneswari et al. (2019) described cross-diffusion effects on MHD convection of Casson-Williamson fluid over a stretching surface with radiation and chemical reaction. Arifin et al. (2019) computed and analyzed the two-phase mixed convection flow of dusty Williamson fluid with the aligned magnetic field over a vertical stretching sheet. Their study suggests that dust particle influencing the Williamson fluid flow which resulted to decrease the velocity of fluid.

The aim of the present work is to investigate the flow and heat transfer analysis of Williamson fluid on the stagnation point past a stretching surface in the presence of viscous dissipation and slip conditions. A similar transformation is first used to transform the governing non linear partial differential equations into an ordinary differential equations system before the shooting method is used numerically. The present problem has not been studied before, and then the results reported here are new.

4.2   Mathematical Formulation

For this part of the study, a steady two-dimensional flow of Williamson fluid over a stretching plate has been carried out. The physical flow of this study can be viewed in the Cartesian coordinate system as shown in Figure 4.1. The axes of x and y are directed in the same direction of the plate and perpendicular to it. The flow is originated from the stretched sheet which is produced by the two equal forces along the $x-$ axes. Keeping the origin fixed, the sheet is stretched with a velocity of $u_w(x) = cx$ (c is a positive constant) and is subjected to obey the slip conditions. Furthermore, for external velocities is $u_e(x) = ax$ (a is a positive constant) and boundary layer equations are (Salleh et al. 2009) are as follows
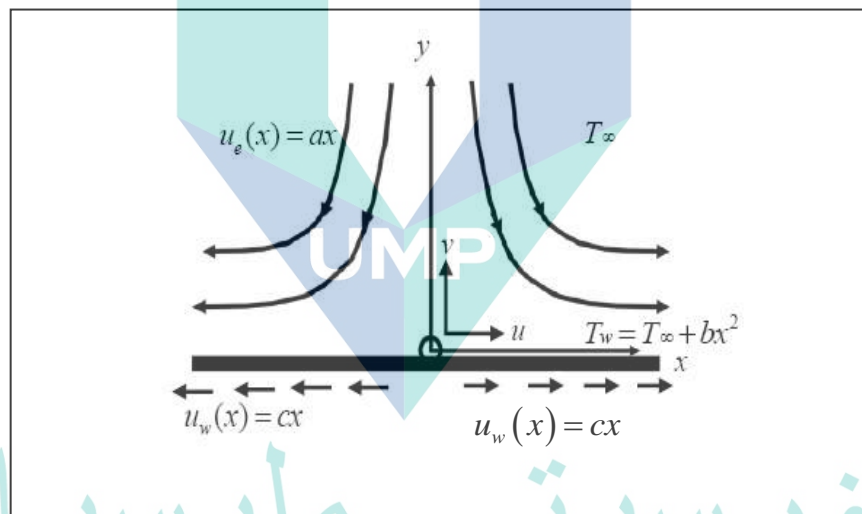
Figure 4.1   Schematic diagram for flow and heat transfer analysis of Williamson fluid on the stagnation point over a stretching surface with viscous dissipation and slip conditions

$$\frac{\partial u}{\partial x} + \frac{\partial v}{\partial y} = 0 \qquad\qquad 4.1$$

$$u\frac{\partial u}{\partial x} + v\frac{\partial u}{\partial y} = u_e\frac{\partial u_e}{\partial x} + v\frac{\partial^2 u}{\partial y^2} + \sqrt{2}\, v\, \Gamma\, \frac{\partial u}{\partial y}\frac{\partial^2 u}{\partial y^2} \qquad\qquad 4.2$$

53

$$u\frac{\partial T}{\partial x} + v\frac{\partial T}{\partial y} = \frac{k}{\rho C_p}\frac{\partial^2 T}{\partial y^2} + \frac{\mu}{\rho C_p}\left[\left(\frac{\partial u}{\partial y}\right)^2 + \frac{1}{\sqrt{2}}\Gamma\left(\frac{\partial u}{\partial y}\right)^3\right] \qquad 4.3$$

corresponds to the following conditions

$$u = u_w(x) + \gamma^*\mu\frac{\partial u}{\partial y},\ v = 0,\ T = T_w + \beta^*\frac{\partial T}{\partial y}\ \text{ at }\ y = 0 \qquad 4.4$$

$$u \to u_e(x),\ T \to T_\infty\ \text{ as }\ y \to \infty$$

where u and v are the velocities in the x and $y-$ axes, respectively, $T_w(x) = T_\infty + bx^2$ is the wall temperature (b is equal to positive constant), ν is the kinematic viscosity, T is the fluid temperature, γ^* is the dimensional velocity slip parameter, β^* is the dimensional thermal slip parameter, k is the thermal conductivity, ρ is the fluid density, C_p is the specific heat, Γ is the time constant and μ is the dynamic viscosity.

Now, we introduce the following similarity variables (Salleh et al. 2010) as follows

$$\eta = \left(\frac{c}{\nu}\right)^{1/2} y, \qquad 4.5$$

$$\theta(\eta) = \frac{T - T_\infty}{T_w - T_\infty}, \qquad 4.6$$

$$\psi = (c\nu)^{1/2} x f(\eta), \qquad 4.7$$

where η and $\theta(\eta)$ are dimensionless variables, while ψ is the stream function. Then, u and v can be defined as

$$u = \frac{\partial \psi}{\partial y}\ \text{ and }\ v = -\frac{\partial \psi}{\partial x}. \qquad 4.8$$

By using the above functions, Equation 4.1 is identically satisfied.

Thus, we obtain

$$u = cxf'(\eta), \quad v = -(c\nu)^{1/2} f(\eta),$$ 4.9

where prime represents differentiation with respect to η. By using Equations 4.5 to 4.7 and 4.9, Equations 4.2 and 4.3 are transformed and becomes

$$f''' + ff'' + \varepsilon^2 - f'^2 + \lambda f'' f''' = 0,$$ 4.10

$$\theta'' - \Pr\left[2f'\theta - f\theta'\right] + \Pr Ec\left[f''^2 + \frac{1}{2}\lambda f'''\right] = 0,$$ 4.11

where $\Pr = \dfrac{\nu \rho C_p}{k}$ is the Prandtl number, $Ec = \dfrac{c^2}{C_p b}$ is the Eckert number which represent the viscous dissipation parameter, $\lambda = x\Gamma\sqrt{\dfrac{2c^3}{\nu}}$ is the non-Newtonian Williamson fluid parameter and $\varepsilon = \dfrac{a}{c}$ is the stretching parameter.

Based on derivative by using Equations 4.5 to 4.7 and 4.9 into boundary conditions 4.4 become

$$f(0) = 0, \quad f'(0) = 1 + \gamma f''(0), \quad \theta(0) = 1 + \beta\theta'(0)$$ 4.12

$$f'(\eta) \to \varepsilon, \quad \theta(\eta) \to 0 \text{ as } \eta \to \infty$$

Furthermore, $\gamma = \gamma^* \rho(c\nu)^{1/2}$ and $\beta = \beta^*\left(\dfrac{c}{\nu}\right)^{1/2}$ are the dimensionless velocity and thermal slip parameter, respectively and it is noticed that $\beta = 0$ when the wall temperature remains constant (CWT).

The skin friction coefficient C_f and the local Nusselt number Nu are given as

$$C_f = \frac{\tau_w}{\rho u_w^2},$$ 4.13

$$Nu = \frac{-x}{T_w - T_\infty} \left.\frac{\partial T}{\partial y}\right|_{y=0}.$$ 4.14

The surface shear stress τ_w is defined as

$$\tau_w = \mu \frac{\partial u}{\partial y}\left[1 + \Gamma\sqrt{\frac{1}{2}}\frac{\partial u}{\partial y}\right].$$ 4.15

Using the similarity variables in Equations 4.5 to 4.7 give

$$C_f \operatorname{Re}^{1/2} = f''(0) + \frac{\lambda}{2}\left(f''(0)\right)^2,$$ 4.16

$$Nu_x \operatorname{Re}_x^{-1/2} = -\theta'(0),$$ 4.17

where $\operatorname{Re}_x = \frac{cx^2}{v}$ is the local Reynolds number.

4.3   Results and Discussion

The system of ordinary Equations 4.10 and 4.11 under the boundary conditions 4.12 are solved numerically with the help of the shooting method and the computation is performed in the Maple software. To study the influence on velocity, as well as temperature of fluid, we considered different parameters, namely the Prandtl number $\Pr$, the dimensionless velocity slip parameter γ, the dimensionless thermal slip parameter β, the stretching parameter ε, the non-Newtonian Williamson fluid parameter λ and the Eckert number Ec. The maximum finite boundary layer

56

thickness $\eta_\infty = 1.3$ and 5 is computed to statisfy the boundary conditions asymptotically.

To determine the correctness of the findings, comparison values of $f''(0)$ have been made. Table 4.1 shows the comparison with Nadeem et al. (2013) and Nadeem and Hussain (2014). Both solved analytically with the aid from the Homotopy Analysis technique (HAM) and it is found to be in good agreement, therefore we are confident with the accuracy of the results in this problem.

Table 4.2 presents the values of $Nu_x \operatorname{Re}_x^{-1/2}$ and $C_f \operatorname{Re}_x^{1/2}$ for various values of non-Newtonian Williamson fluid parameter λ when $\operatorname{Pr} = 7, \varepsilon = 3$ and $\beta = Ec = \gamma = 1$. It can be seen that, the increase of λ make $Nu_x \operatorname{Re}_x^{-1/2}$ decreases while $C_f \operatorname{Re}_x^{1/2}$ increases.

Table 4.3 shows the values of $\theta(0)$ and $Nu_x \operatorname{Re}_x^{-1/2}$ for various values of the dimensionless thermal slip parameter β when $\operatorname{Pr} = 7$, $\varepsilon = 3$, $Ec = \gamma = 1$ and $\lambda = 0,1$. It is noted that when the non-Newtonian Williamson fluid parameter λ is not considered $\lambda = 0$ (viscous fluid), an increase of β results in the decreases of $\theta(0)$ and $Nu_x \operatorname{Re}_x^{-1/2}$ as well as when $\lambda = 1$ (Williamson fluid). When β is fixed and λ increases, this result in the increases of $\theta(0)$ while $Nu_x \operatorname{Re}_x^{-1/2}$ decreases.

Table 4.4 presents the values of $\theta(0)$, $Nu_x \operatorname{Re}_x^{-1/2}$ and $C_f \operatorname{Re}_x^{1/2}$ for various values of dimensionless velocity slip parameter γ, when $\operatorname{Pr} = 7, \varepsilon = 3$, $Ec = \beta = 1$ and $\lambda = 0,1$. It can been seen that, when the non-Newtonian Williamson fluid parameter λ is not considered $\lambda = 0$ (viscous fluid), an increase of γ makes the values of $\theta(0)$ and $C_f \operatorname{Re}_x^{1/2}$ decreases while $Nu_x \operatorname{Re}_x^{-1/2}$ increases. The same trend occurs when $\lambda = 1$ (Williamson fluid). When γ is fixed, an increase of λ result in the increases of $\theta(0)$ and $C_f \operatorname{Re}_x^{1/2}$ while $Nu_x \operatorname{Re}_x^{-1/2}$ decreases.

Figure 4.2 illustrates the temperature profiles for various values of $\Pr$. It can be observed that the temperature profile decreases with the increases of $\Pr$. The cause of this phenomenon due to the reduction of thermal boundary layer thickness indicated by the increase of Prandtl number which leads to the decreases of the energy ability.

Figures 4.3 and 4.4 demonstrate the temperature $\theta(0)$ profiles for various values of ε and γ respectively. As ε increase, the value of the wall temperature increases, but the value of thickness of thermal boundary layer decreases, while as γ increase, the value of the wall temperature decreases.

Figure 4.5 presents the temperature $\theta(0)$ profiles for various values of the viscous dissipation parameter Ec. It is observed that the values of Ec increases as the temperature profiles increases. Ec is defined as the connection between the kinetic energy and the enthalpy of a fluid. The fluid viscosity receives energy from fluid motion (kinetic energy) and converts it into the fluid internal energy, which heats up the fluid. In addition, the temperature gradient is not only the main source of change in temperature, but with the dissipative effects emerging from the internal friction of the fluid leads to this phenomenon. Next, Figures 4.6 and 4.7 illustrate the temperature $\theta(0)$ profiles for various values of β and λ. It is found that as β and λ increases, the temperature profiles and boundary layer thickness decrease for β in contras with λ the temperature profiles and boundary layer thickness increase.

Figure 4.8 presents the velocity profiles $f'(\eta)$ for various values of γ. It is observed that the velocity gradient decreases as γ increases. While Figure 4.9, illustrates the velocity profiles $f'(\eta)$ for various values of λ. It is found that as the velocity gradient increases, λ is decreases.

Figure 4.10 shows the variation of temperature $\theta(0)$ with λ for several values of Ec when $\Pr = 7, \varepsilon = 3$ and $\beta = \gamma = 1$. It is seen from this figure that the temperature profiles increases as Ec increase and temperature profiles also increases as

λ increase for a fixed values of Ec. Figure 4.11 illustrates the variation of temperature $\theta(0)$ with Pr for several values of λ when $Ec = \beta = \gamma = 1$ and $\varepsilon = 3$. The result found is similar to Figure 4.10 where it shows that the temperature profiles increases as λ increases while the temperature profiles increases with as Pr increases for a fixed value of λ.

Figure 4.12 shows the variation Nusselt number $Nu_x \, Re_x^{-1/2}$ with ε for several values of γ when $\beta = Ec = \lambda = 1$ and Pr $= 7$. It is seen from this figure that the Nusselt number increases as γ increases but when $\gamma = 1$ the value of Nusselt number decrease as ε increases and when $\gamma = 7$ the Nusselt number increases as ε increases. Figure 4.13 shows the variation of Nusselt number $Nu_x \, Re_x^{-1/2}$ with λ for several values of Ec when Pr $= 7, \varepsilon = 3$ and $\beta = \gamma = 1$. From this figure, it is found that the Nusselt number increases as Ec decreases, the Nusselt number decreases as λ increases for a fixed values of Ec. Similar result is obtained in Figure 4.14 where the Nusselt number increases as λ decreases, while Nusselt number decreases as Pr increases for a fixed values of λ.

Figure 4.15 shows the variation of temperature profiles $\theta(0)$ with Ec for several values of γ when Pr $= 7, \varepsilon = 3$ and $\beta = \lambda = 1$. The result observed from this figure is the temperature profiles increases as γ decreases, while temperature profiles increases as Ec increases for a fixed values of γ. The same result is obtained in Figure 4.16 where the temperature profiles increase as γ decreases, while temperature profiles increase as ε increases for a fixed values of γ.

Figure 4.17 shows the variation of skin friction coefficient number $C_f \, Re_x^{1/2}$ with ε for severalvalues of γ when $\beta = Ec = \lambda = 1$ and Pr $= 7$. The result observed form this figure is the skin friction coefficient number increases as γ decreases, while temperature profiles increases as ε increases for a fixed values of γ.

Table 4.1   Comparison between the present results of $f''(0)$ for a different values of Williamson fluid parameter, λ when $Ec = \gamma = \varepsilon = \beta = 0$ and $\Pr = 3$

λ	Nadeem et al. (2013)	Nadeem and Hussain (2014)	Present
	$f''(0)$	$f''(0)$	$f''(0)$
0.1	-1.03446		-1.034981
0.2		-1.076	-1.076786

Table 4.2   Values of $Nu_x \operatorname{Re}_x^{-1/2}$ and $C_f \operatorname{Re}_x^{1/2}$ for the various values of λ when $\Pr = 7, \varepsilon = 3$ and $\beta = Ec = \gamma = 1$

λ	$Nu_x \operatorname{Re}_x^{-1/2}$	$C_f \operatorname{Re}_x^{1/2}$
0.1	0.67705	1.53831
1	0.57429	2.18834
3	0.40741	3.26958
5	0.28130	4.11212
7	0.17789	4.82299

Table 4.3   Values of $\theta(0)$ and $Nu_x \operatorname{Re}_x^{-1/2}$ for the various values of β when $\Pr = 7, \varepsilon = 3, Ec = \gamma = 1$ and $\lambda = 0,1$

β	Viscous fluid $\lambda = 0$		Williamson fluid $\lambda = 1$	
	$\theta(0)$	$Nu_x \operatorname{Re}_x^{-1/2}$	$\theta(0)$	$Nu_x \operatorname{Re}_x^{-1/2}$
0.1	0.68081	3.19190	0.73799	2.62008
1	0.30939	0.69061	0.42571	0.57429
3	0.24425	0.25192	0.37010	0.20997
5	0.22972	0.15406	0.35766	0.12847
7	0.22332	0.11095	0.35218	0.09255

Table 4.4   Values of $\theta(0)$, $Nu_x \, \text{Re}_x^{-1/2}$ and $C_f \, \text{Re}_x^{1/2}$ for the various values of γ when $\text{Pr} = 7, \varepsilon = 3, Ec = \beta = 1$ and $\lambda = 0,1$

γ	Viscous fluid $\lambda = 0$			Williamson fluid $\lambda = 1$		
	$\theta(0)$	$Nu_x \, \text{Re}_x^{-1/2}$	$C_f \, \text{Re}_x^{1/2}$	$\theta(0)$	$Nu_x \, \text{Re}_x^{-1/2}$	$C_f \, \text{Re}_x^{1/2}$
0.7	0.43634	0.56366	1.85165	0.64236	0.35764	2.88171
1	0.30939	0.69061	1.45373	0.42571	0.57429	2.18834
3	0.15146	0.84854	0.59397	0.16180	0.83820	0.75257
5	0.13311	0.86689	0.37278	0.13585	0.86415	0.43831
7	0.12745	0.87255	0.27158	0.12856	0.87144	0.30702
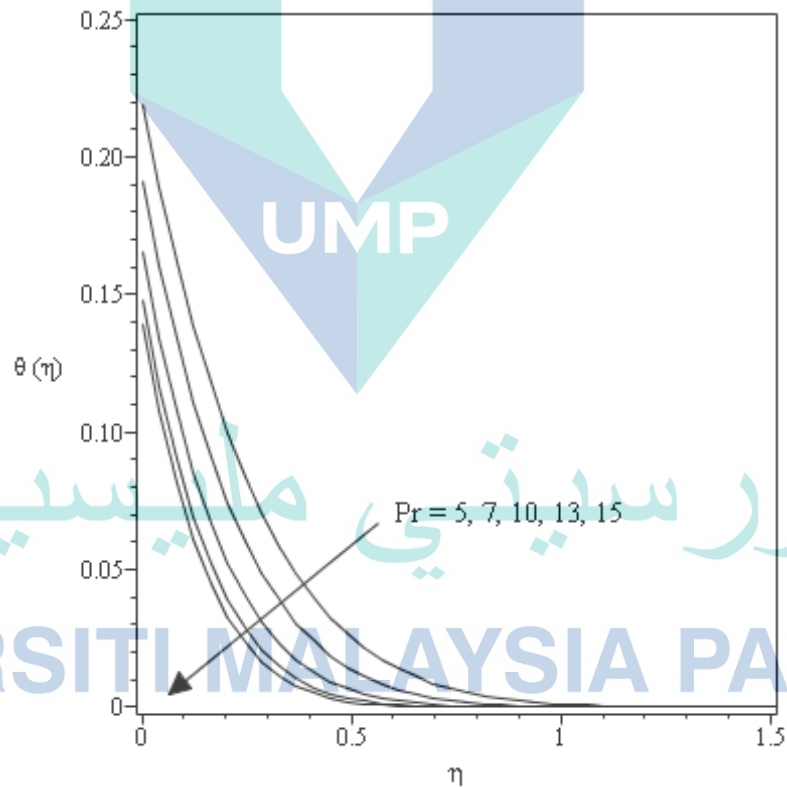
Figure 4.2   Temperature   profiles $\theta(0)$ for   various   values   of   Pr when $\beta = \varepsilon = Ec = \lambda = \gamma = 1$
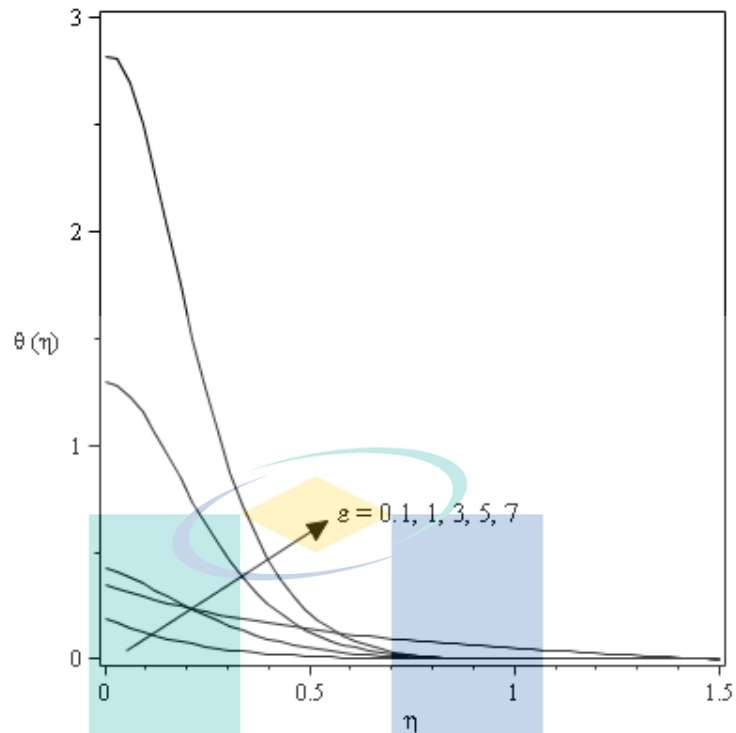
Figure 4.3   Temperature   profiles $\theta(0)$ for   various   values   of ε when $\beta = Ec = \lambda = \gamma = 1$ and $\mathrm{Pr} = 7$
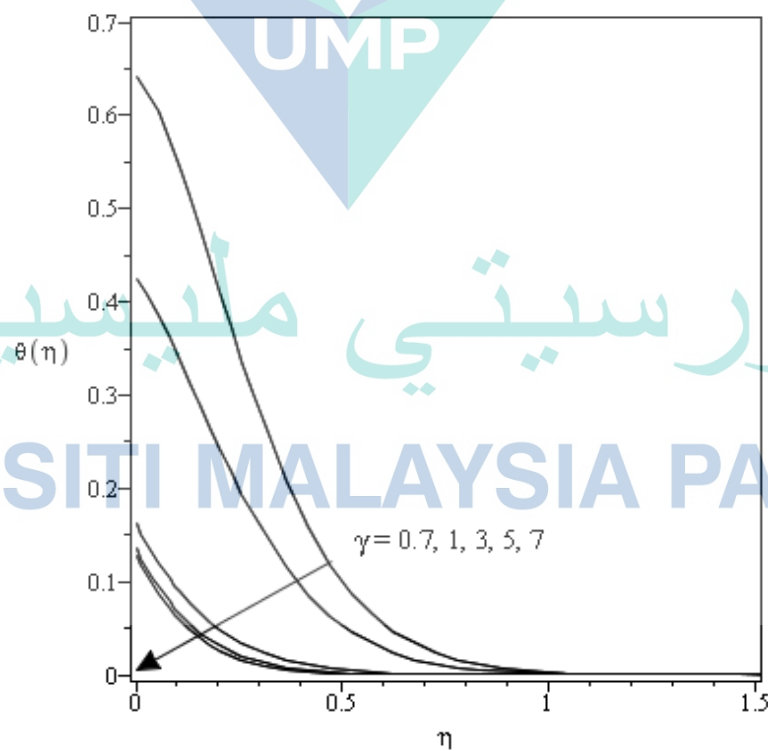
Figure 4.4   Temperature profiles $\theta(0)$ for various values of γ when $\mathrm{Pr} = 7, \varepsilon = 3$ and $\beta = Ec = \lambda = 1$
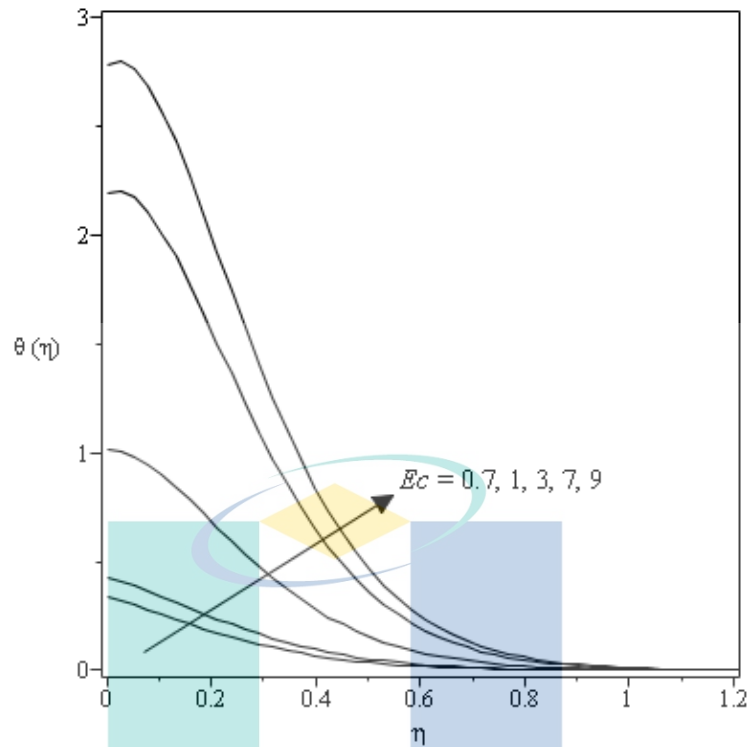
Figure 4.5   Temperature profiles $\theta(0)$ for various values of Ec when $\mathrm{Pr}=7, \varepsilon=3$ and $\beta=\lambda=\gamma=1$
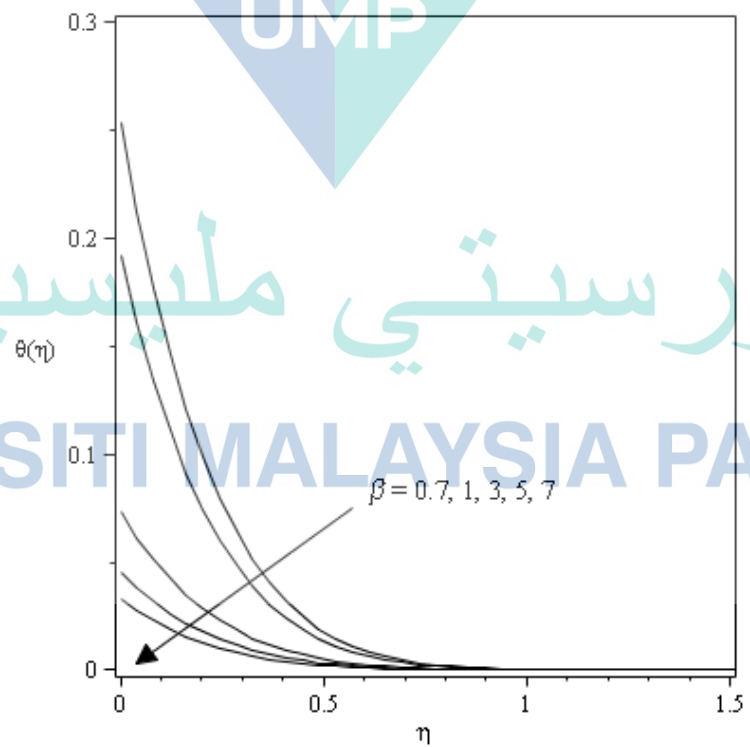
Figure 4.6   Temperature profiles $\theta(0)$ for various values of β when $\lambda=\varepsilon=Ec=\gamma=1$ and $\mathrm{Pr}=7$
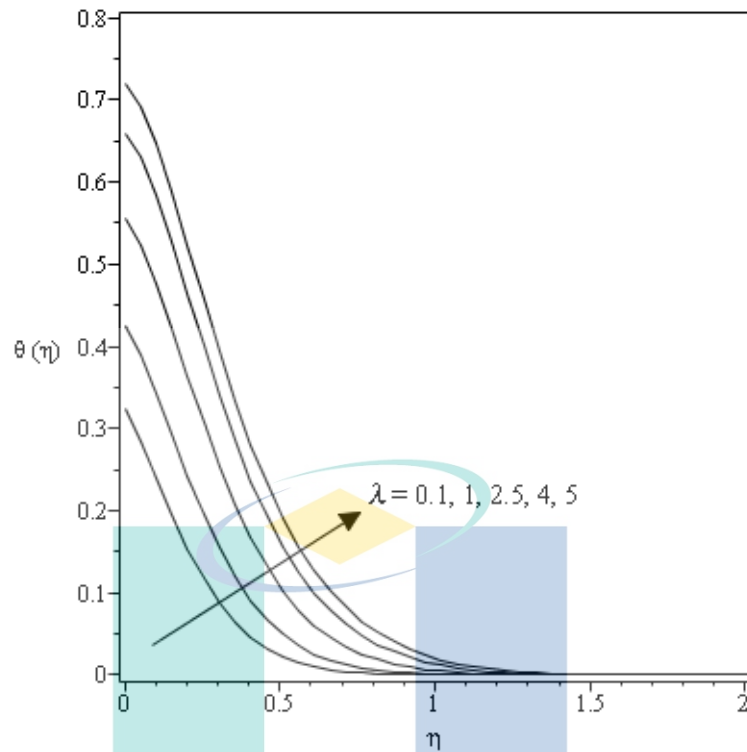
Figure 4.7   Temperature profiles $\theta(0)$ for various values of λ when $Pr = 7, \varepsilon = 3$ and $\gamma = Ec = \beta = 1$
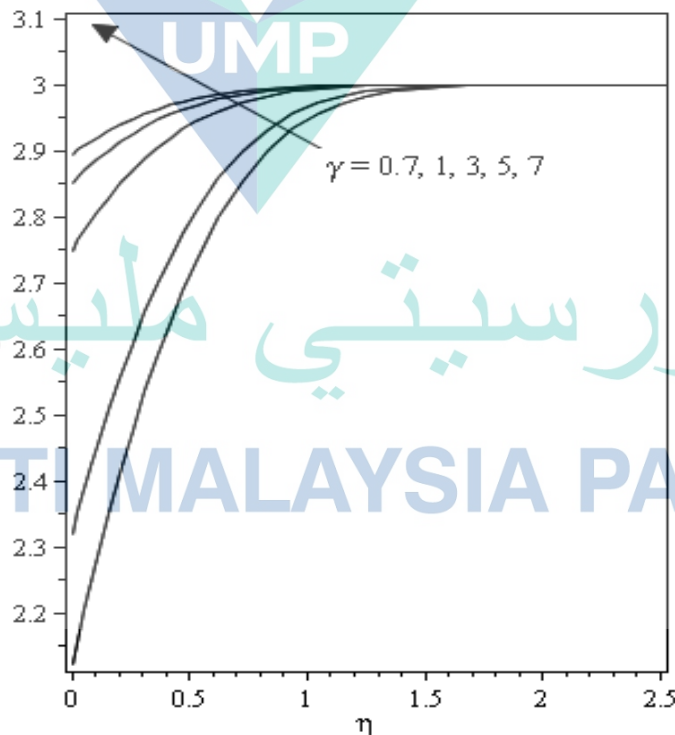
Figure 4.8   Velocity profiles $f'(\eta)$ for various values of γ when $Pr = 7, \varepsilon = 3$ and $\lambda = Ec = \beta = 1$
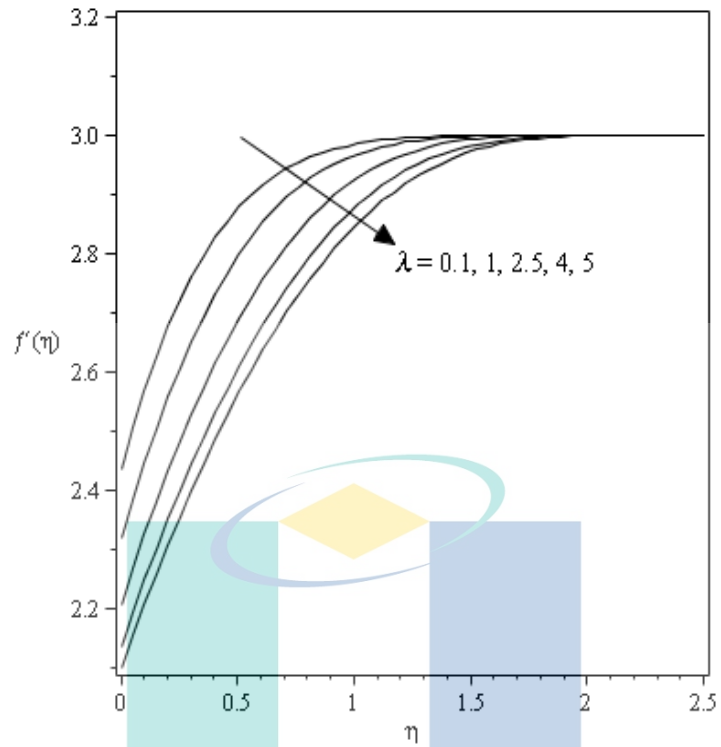
Figure 4.9   Velocity profiles $f'(\eta)$ for various values of λ when $\mathrm{Pr} = 7, \varepsilon = 3$ and $\gamma = Ec = \beta = 1$
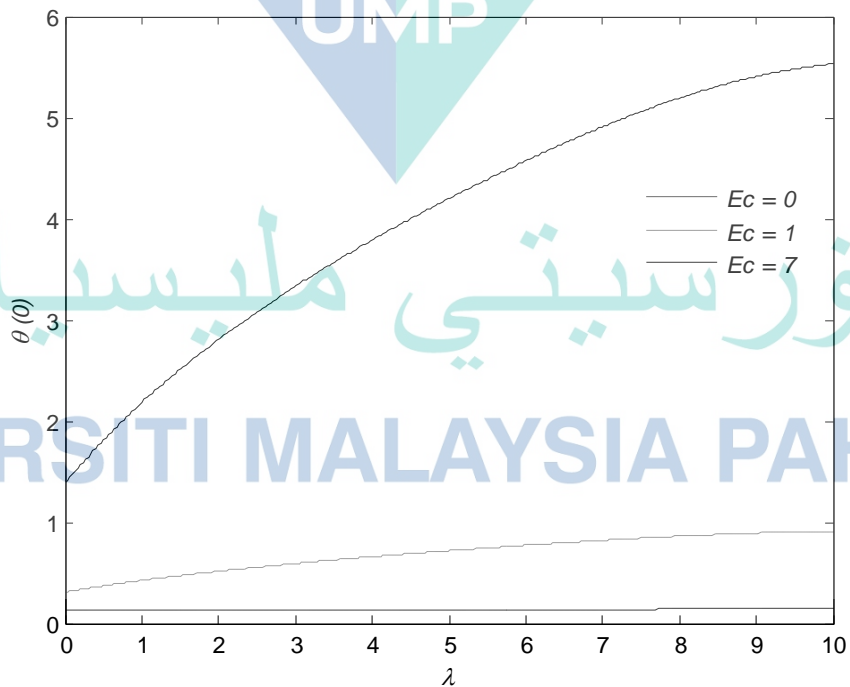
Figure 4.10   Variation of temperature $\theta(0)$ with λ for several values of Ec when $\mathrm{Pr} = 7, \varepsilon = 3$ and $\beta = \gamma = 1$
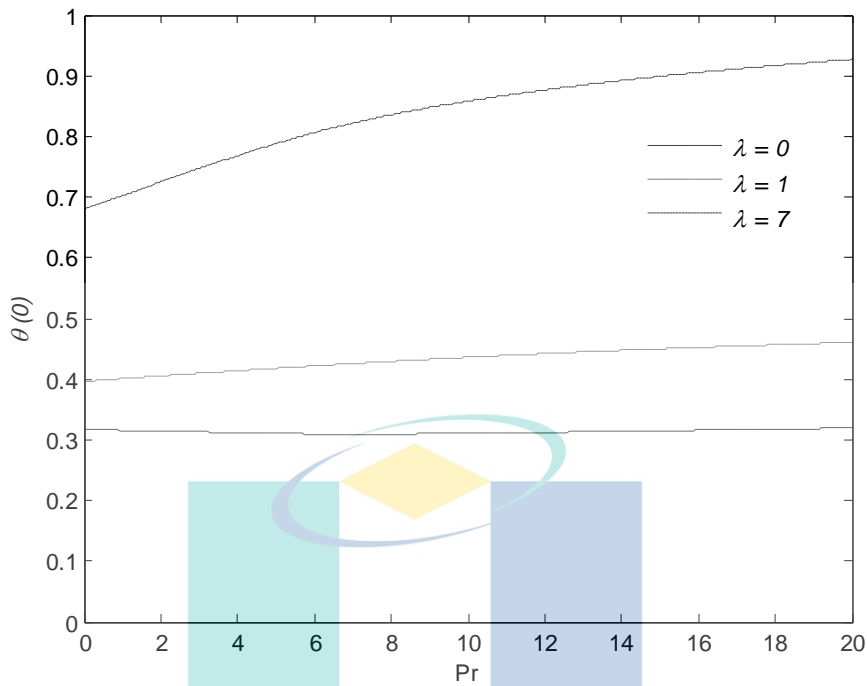
Figure 4.11   Variation of temperature $\theta(0)$ with Pr for several values of λ when $Ec = \beta = \gamma = 1$ and $\varepsilon = 3$
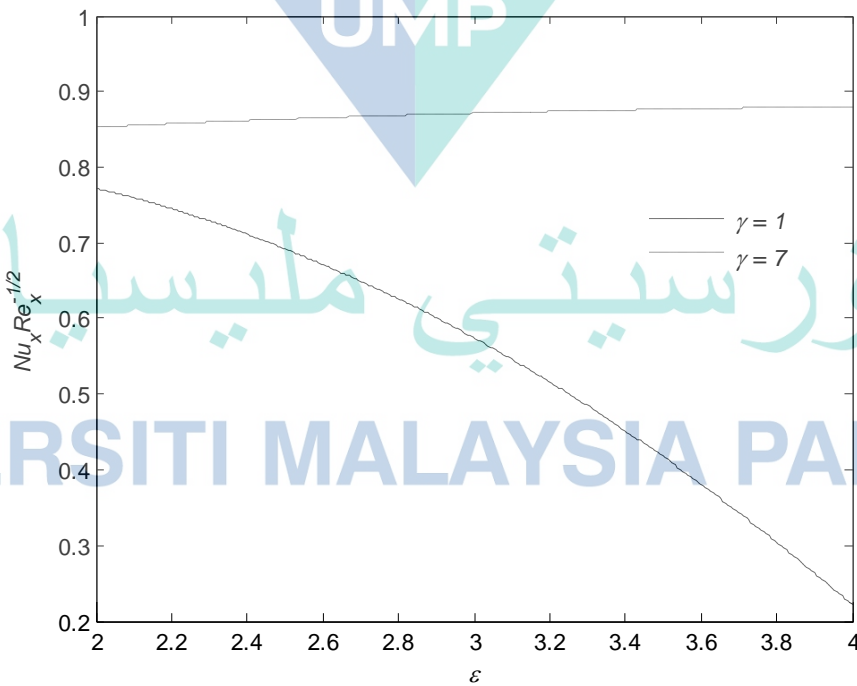
Figure 4.12   Variation of Nusselt number $Nu_x \operatorname{Re}_x^{-1/2}$ with ε for several values of γ when $\beta = Ec = \lambda = 1$ and Pr $= 7$

Figure 4.13   Variation of Nusselt number $Nu_x \operatorname{Re}_x^{-1/2}$ with λ for several values of Ec when $\Pr = 7, \varepsilon = 3$ and $\beta = \gamma = 1$

Figure 4.14   Variation of Nusselt number $Nu_x \operatorname{Re}_x^{-1/2}$ with $\Pr$ for several values of λ when $Ec = \beta = \gamma = 1$ and $\varepsilon = 3$

67
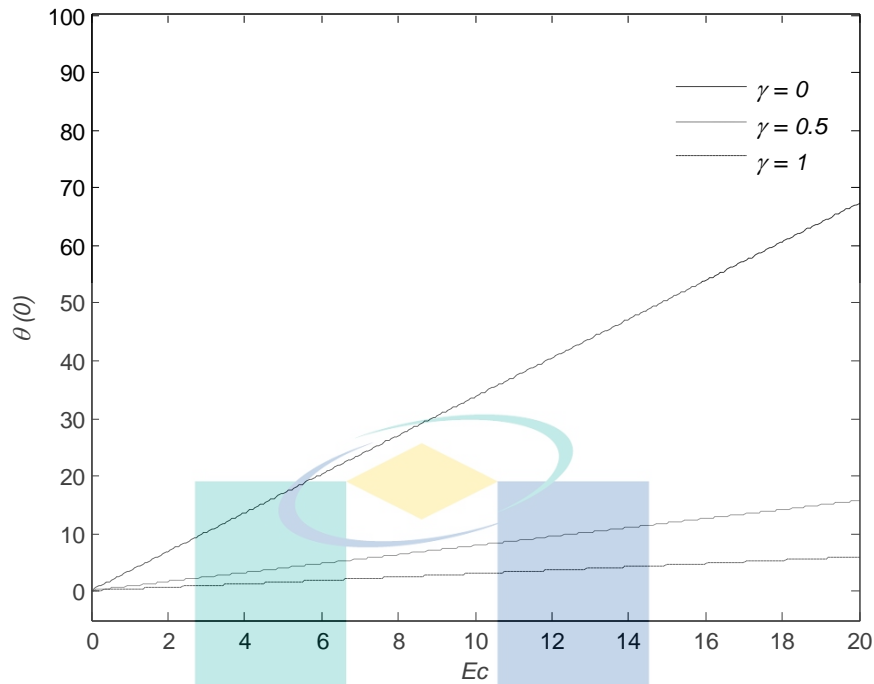
Figure 4.15   Variation of temperature profiles $\theta(0)$ with Ec for several values of γ when $\mathrm{Pr} = 7, \varepsilon = 3$ and $\beta = \lambda = 1$
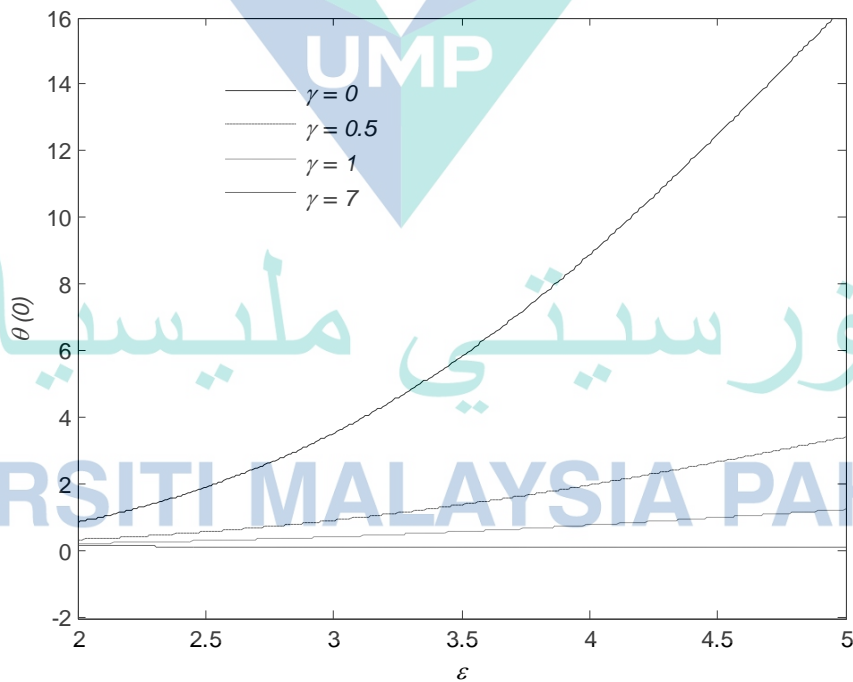
Figure 4.16   Variation of temperature profile $\theta(0)$ with ε for several values of γ when $\beta = Ec = \lambda = 1$ and $\mathrm{Pr} = 7$
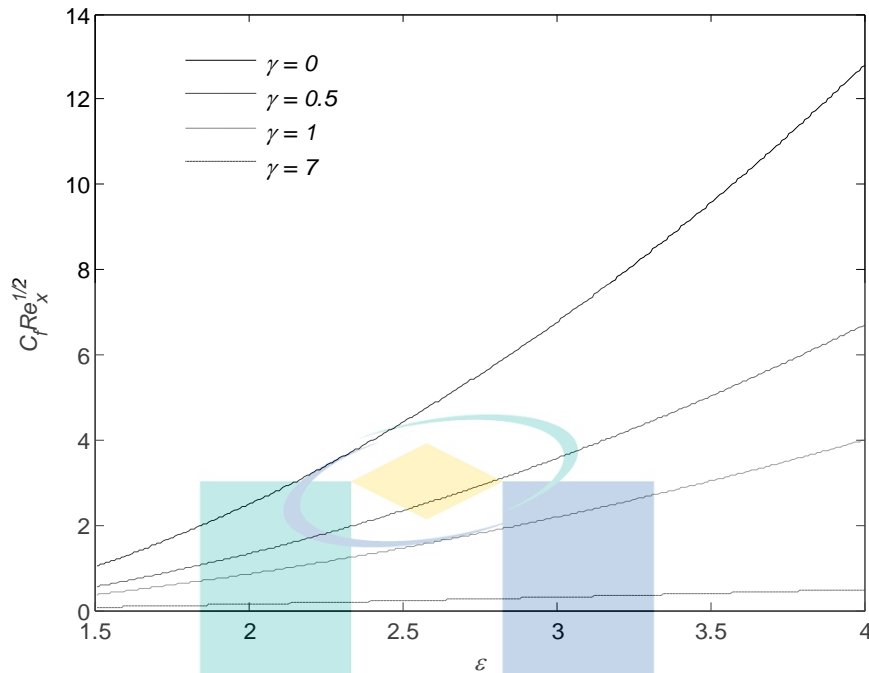
Figure 4.17   Variation of skin friction coefficient number $C_f \operatorname{Re}_x^{1/2}$ with ε for several values of γ when $\beta = Ec = \lambda = 1$ and $\operatorname{Pr} = 7$

4.4   Summary

This study solved the flow and heat transfer analysis of Williamson fluid on the stagnation point towards a stretching surface with slip conditions and viscous dissipation and Table 4.5 show the summarized mathematical formulation in this problem. The presented analysis leads to the following main results:

i.   the increase of Prandtl number, dimensionless thermal and velocity slip parameter result in the decrease in the wall temperature and thermal boundary layer thickness. While, the presence of stretching parameter, viscous dissipation and non-Newtonian Williamson fluid parameter increase the wall temperature.

ii.   the increase of Ec results in the increase in wall temperature and heat transfer coefficient as well as the increase in the range of λ for which the solutions exists.

69

iii. The Nusselt number increases as velocity slip parameter γ increases while the trend is observed for Eckert number and non-Newtonian Williamson fluid parameter. The increase in skin friction coefficient leads to the decrease in velocity slip parameter, while the stretching, while stretching parameter ε increases.

Table 4.5   Solution procedure for the mathematical formulation flow and heat transfer of Williamson fluid on stagnation point over a stretching surface with   viscous dissipation and slip conditions

Steps	Equations
Governing equations	$$\frac{\partial u}{\partial x} + \frac{\partial v}{\partial y} = 0$$ $$u\frac{\partial u}{\partial x} + v\frac{\partial u}{\partial y} = u_e\frac{\partial u_e}{\partial x} + v\frac{\partial^2 u}{\partial y^2} + \sqrt{2}\,v\,\Gamma\frac{\partial u}{\partial y}\frac{\partial^2 u}{\partial y^2}$$ $$u\frac{\partial T}{\partial x} + v\frac{\partial T}{\partial y} = \frac{k}{\rho C_p}\frac{\partial^2 T}{\partial y^2} + \frac{\mu}{\rho C_p}\left[\left(\frac{\partial u}{\partial y}\right)^2 + \frac{1}{\sqrt{2}}\Gamma\left(\frac{\partial u}{\partial y}\right)^3\right]$$
Boundary conditions	$$u = u_w(x) + \gamma^*\mu\frac{\partial u}{\partial y},\ v = 0,\ T = T_w + \beta^*\frac{\partial T}{\partial y}\ \text{at}\ y = 0$$ $$u \to u_e(x),\ T \to T_\infty\ \text{as}\quad y \to \infty$$
Similarity transformation	$$\eta = \left(\frac{c}{v}\right)^{1/2} y,\ \theta(\eta) = \frac{T - T_\infty}{T_w - T_\infty},\ \psi = (cv)^{1/2} x f(\eta)$$
Ordinary differential equations	$$f''' + ff'' + \varepsilon^2 - f'^2 + \lambda f'' f''' = 0$$ $$\theta'' - \Pr\left[2f'\theta - f\theta'\right] + \Pr\,Ec\left[f''^2 + \frac{1}{2}\lambda f'''\right] = 0$$
Transformed boundary conditions	$$f(0) = 0,\ f'(0) = 1 + \gamma f''(0),\ \theta(0) = 1 + \beta\theta'(0)$$ $$f'(\eta) \to \varepsilon,\ \theta(\eta) \to 0\ \text{as}\quad \eta \to \infty$$

CHAPTER 5

FLOW AND HEAT TRANSFER ANALYSIS OF WILLIAMSON FLUID ON MHD STAGNATION POINT OVER A STRETCHING SURFACE WITH THERMAL RADIATION EFFECTS

5.1   Introduction

The electrical components specifically deal with magnetic effects. The interaction of the fluid motion and the dynamics of fluids as good conductors of electricity with any ambient magnetic field coin as magnetohydrodynamic (MHD) effects (Batchelor et al., 2002). Meanwhile, the thermal radiation effects play an important role in engineering applications such as high-temperature plasmas, cooling of nuclear reactors and liquid metal fluids. Furthermore, the radiation heat transfer flow effects are also applied in space technology and processes involving high temperatures (Ali et al., 2013). Bataller (2008) and Mukhopadhyay (2009) studied the effects of radiation in both Blasius and Sakiadis flows and unsteady mixed convection flow and heat transfer over a porous stretching surface in a porous medium. Other researchers who considered the MHD and thermal radiation effects are Chen (2010), Hayat et al. (2010), Salleh et al. (2012), Anwar et al. (2012) and Elbashbeshy et al. (2012). Also, Makinde and Olanrewaju (2010), Makinde and Aziz (2010) and Olanrewaju et al. (2011) considered MHD and thermal radiation effects in heat and mass transfer, mixed convection over a vertical plate in a porous medium and viscous dissipation effects for Blasius and Sakiadis flow with convective boundary conditions. Thermal radiation and slip effects on magnetohydrodynamic (MHD) stagnation point flow of Casson fluid over a convective stretching sheet were examined by Raza (2019). It was found out that, there was an inverse relationship between magnetic parameter and stream wise velocity. Narayana and Babu (2016) analyzed the numerical study of MHD heat and mass

transfer of a Jeffrey fluid over a stretching sheet with chemical reaction and thermal radiation. The result shows the effects of thermal radiation have caused an increase in the temperature of the thermal boundary layer and the reverse effect is seen by increasing the Prandtl number. Hayat et al. (2017) addressed the simultaneous effects of heat generation/absorption and thermal radiation in magnetohydrodynamics (MHD) flow of Maxwell nanofluid towards a stretched surface. It was seen that, the thermal radiation parameter enhanced the temperature field and heat transfer rate. Gupta et al. (2018) observed MHD mixed convection stagnation point flow and heat transfer of an incompressible nanofluid over an inclined stretching sheet with chemical reaction and radiation.

The aim of this study is to investigate the flow and heat transfer analysis of Williamson fluid on MHD stagnation point flow over a stretching surface with thermal radiation effects. With the help of similarity transformation, the governing equations are converted to nonlinear ordinary differential equations and then solved numerically by the shooting method technique. Numerical results for the reduced Nusselt number and reduced skin friction coefficient as well as the temperature and velocity profiles are elucidated through tables and graphs. The influence of Prandtl number, stretching parameter, Williamson fluid parameter, thermal radiation parameter and magnetic parameter are analysed and discussed. From the literature studies, this problem has not been considered before, therefore, the results reported here are new.

5.2   Mathematical Formulation

The steady two-dimensional flow of a non-Newtonian Williamson fluid over a stretching plate, whose physical model is illustrated in Figure 5.1 is considered in this study. The external and stretching velocities are $u_e(x) = ax$ and $u_w(x) = cx$, respectively, where a and c are constants. The boundary layer equations are (Salleh et al., 2009; Nadeem et al., 2013) are as follows:

72
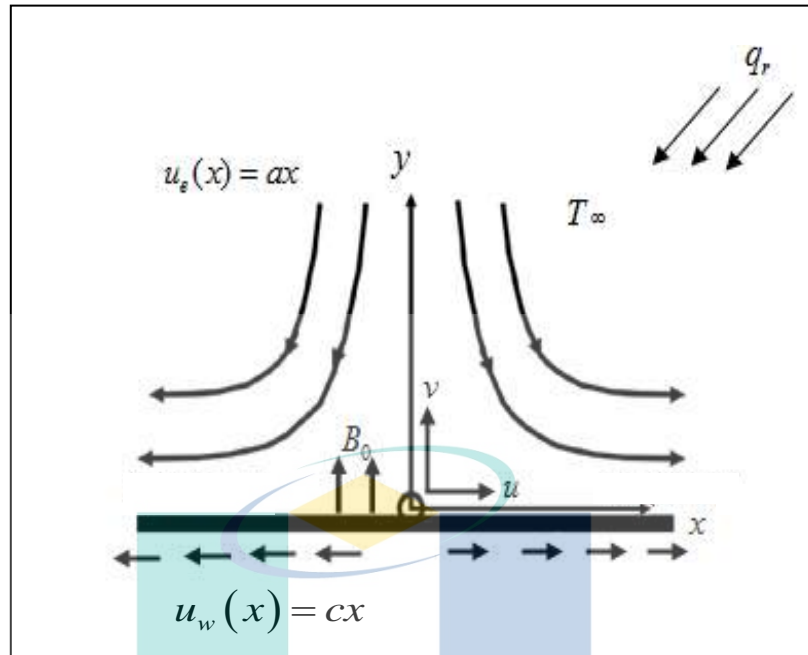
Figure 5.1   Schematic diagram flow and heat transfer analysis of Williamson fluid on MHD stagnation point over a stretching surface with thermal radiation effects

$$\frac{\partial u}{\partial x} + \frac{\partial v}{\partial y} = 0 \tag{5.1}$$

$$u\frac{\partial u}{\partial x} + v\frac{\partial u}{\partial y} = u_e\frac{\partial u_e}{\partial x} + v\frac{\partial^2 u}{\partial y^2} + \sqrt{2}\,v\,\Gamma\frac{\partial u}{\partial y}\frac{\partial^2 u}{\partial y^2} + \frac{\sigma B_o^2}{\rho}\left(u_e - u\right) \tag{5.2}$$

$$u\frac{\partial T}{\partial x} + v\frac{\partial T}{\partial y} = \frac{k}{\rho C_p}\frac{\partial^2 T}{\partial y^2} - \frac{\partial q_r}{\partial y} \tag{5.3}$$

corresponds to the following conditions

$$u = u_w\left(x\right),\ v = 0,\ T = T_w \quad \text{as} \quad y = 0 \tag{5.4}$$

$$u \to u_e\left(x\right), T \to T_\infty \quad \text{as} \quad y \to \infty$$

where u and v are the velocity in the x and $y-$ axes, respectively, $T_w\left(x\right) = T_\infty + bx^2$ is the wall temperature with b as constant, v is the kinematic viscosity, T is the fluid temperature, B_o is the uniform magnetic field strength, σ is

73

the electric conductivity, k is the thermal conductivity, ρ is the fluid density, C_p is the specific heat, Γ is the time constant and μ is the dynamic viscosity. Using Rosseland approximation for radiation (Bataller, 2008), the radiative heat flux q_r in Equation 5.3 may be simplified as

$$q_r = -\frac{4\sigma^*}{3k^*}\frac{\partial T^4}{\partial y},$$

5.5

where σ^* and k^* are the Stefan-Boltzmann constant and the mean absorption coefficient, respectively. We assume that the temperature differences within the flow region, namely, the term T^4 can be expressed as a linear function of temperature. Hence, expanding T^4 in a Taylor series about T_∞ and neglecting higher-order terms, we get

$$T^4 \cong 4T_\infty^3 T - 3T_\infty^4.$$

5.6

Using Equations 5.5 and 5.6, Equation 5.3 is reduced to

$$u\frac{\partial T}{\partial x} + v\frac{\partial T}{\partial y} = \left(\frac{k}{\rho C_p} + \frac{16\sigma^* T_\infty^3}{k^*}\right)\frac{\partial^2 T}{\partial y^2}$$

5.7

From the Equation 5.7 it is seen that the effect of radiation is to enhance the thermal diffusivity. If we take $Nr = \dfrac{4\sigma^* T_\infty^3 \rho C_p}{k^* k}$ as the radiation parameter, Equation 5.7 becomes

$$u\frac{\partial T}{\partial x} + v\frac{\partial T}{\partial y} = \frac{k}{\rho C_p}\left(1+\frac{4}{3}Nr\right)\frac{\partial^2 T}{\partial y^2}$$

5.8

Note that thermal radiation effects are absent when $Nr = 0$. Now, we introduce the following similarity variables

$$\eta = \left(\frac{c}{v}\right)^{1/2} y,$$

5.9

74

$$\theta(\eta) = \frac{T - T_\infty}{T_w - T_\infty}, \qquad\qquad 5.10$$

$$\psi = (cv)^{1/2} xf(\eta), \qquad\qquad 5.11$$

where η and $\theta(\eta)$ are dimensionless variables and ψ is the stream function defined by $u = \dfrac{\partial \psi}{\partial y}$ and $v = -\dfrac{\partial \psi}{\partial x}$, which satisfies the Equation 5.1. Furthermore, notice that

$$u = cxf'(\eta), \; v = -(cv)^{1/2} f(\eta), \qquad\qquad 5.12$$

where prime represents differentiation with respect to ψ. By substituting Equations 5.9 to 5.12, into Equations 5.2 and 5.8, the transformed ordinary differential equation is obtained as follows:

$$f''' + ff'' + \varepsilon^2 - f'^2 + \lambda f'' f''' + M(\varepsilon - f') = 0 \qquad\qquad 5.13$$

$$\left[1 + \frac{4}{3} Nr\right] \theta'' - \Pr\left[2f'\theta - f\theta'\right] = 0 \qquad\qquad 5.14$$

where $\Pr = \dfrac{v\rho C_p}{k}$ is the Prandtl number, $\lambda = x\Gamma\sqrt{\dfrac{2c^3}{v}}$ is the non-Newtonian Williamson fluid parameter, $M = \dfrac{\sigma B_o^2}{\rho c}$ is the magnetic parameter and $\varepsilon = \dfrac{a}{c}$ is the stretching parameter.

Based on derivative by using Equations 5.9 to 5.12 into boundary conditions 5.4, the outcomes are

$$f(0=)0, \; f'(0) = 1, \; \theta(0) = 1 \; \text{at} \; \eta = 0 \qquad\qquad 5.15$$

$$f'(\infty) \to \varepsilon, \; \theta(\infty) \to 0 \; \text{as} \; \eta \to \infty$$

The skin friction coefficient C_f and the local Nusselt number Nu_x are given as

$$C_f = \frac{\tau_w}{\rho\, u_w^2},$$

5.16

$$Nu_x = \frac{x q_w}{k\left(T_w - T_\infty\right)},$$

5.17

where, τ_w is the surface shear stress and q_w is the heat flux defined as

$$\tau_w = \mu \frac{\partial u}{\partial y}\left[1 + \Gamma\sqrt{\frac{1}{2}}\frac{\partial u}{\partial y}\right],$$

5.18

$$q_w = -k\frac{\partial T}{\partial y} + q_r,$$

5.19

Using the similarity variables in Equations 5.9 to 5.11, the outcomes are

$$C_f\,\mathrm{Re}_x^{1/2} = f''(0) + \frac{\lambda}{2}\left(f''(0)\right)^2,$$

5.20

$$Nu_x\,\mathrm{Re}_x^{-1/2} = -\left[1 + \frac{4}{3}Nr\right]\theta'(0),$$

5.21

where $\mathrm{Re}_x = \dfrac{c\,x^2}{v}$ is the local Reynolds number.

5.3 Results and Discussion

Equations 5.13 and 5.14 with boundary conditions 5.15 were solved numerically by the shooting method using the Maple software. In order to study the flow characteristic, pertinent parameters, namely the Prandtl number Pr, the stretching parameter ε, the magnetic parameter M, the non-Newtonian Williamson fluid

parameter λ and the thermal radiation parameter Nr are considered. The validation for the efficiency of the method used are shown in Tables 4.1 in the previous chapter. It is found that the results presented are in an excellent agreement, therefore, we are confident with the accuracy of the result in this problem.

Table 5.1 presents the values of the reduced Nusselt number $Nu_x \operatorname{Re}_x^{-1/2}$ and the reduced skin friction coefficient $C_f \operatorname{Re}_x^{1/2}$ for the various values of the non-Newtonian Williamson fluid parameter λ when $\operatorname{Pr} = 7, \varepsilon = 3, Nr = 1$ and $M = 0,1$. It is found that, when the MHD effect is not considered $M = 0$ an increase of λ leads to a decrease of $Nu_x \operatorname{Re}_x^{-1/2}$ while values of $C_f \operatorname{Re}_x^{1/2}$ increases the same trend occurs when $M = 1$. When λ is fixed, an increase of M leads to the increase of both $Nu_x \operatorname{Re}_x^{-1/2}$ and $C_f \operatorname{Re}_x^{1/2}$. It is found that the huge changes in λ has small effect on $Nu_x \operatorname{Re}_x^{-1/2}$ while it has huge effect on $C_f \operatorname{Re}_x^{1/2}$. Furthermore, the increase of λ promotes to a decrease in convection capabilities in Williamson fluid.

Table 5.2 presents the values of $Nu_x \operatorname{Re}_x^{-1/2}$ and $C_f \operatorname{Re}_x^{1/2}$ for various values of the stretching parameter ε when $Nr = M = \lambda = 1$ and $\operatorname{Pr} = 7,10,12$. It is observed that, when $\operatorname{Pr} = 7$, an increase of ε leads to the increase of $Nu_x \operatorname{Re}_x^{-1/2}$ and $C_f \operatorname{Re}_x^{1/2}$ for all values of Pr. Meanwhile, when ε is fixed, an increase of Pr results in the increase of $Nu_x \operatorname{Re}_x^{-1/2}$ and $C_f \operatorname{Re}_x^{1/2}$. Realistically, the increase of the stretching parameter increases the velocity difference between fluid and the plate surface, which therefore results in the increase in velocity gradient as well as the skin friction coefficient.

Table 5.3 presents the values of $Nu_x \operatorname{Re}_x^{-1/2}$ and $C_f \operatorname{Re}_x^{1/2}$ for various values of the magnetic parameter M when $\operatorname{Pr} = 7, \varepsilon = 3, \lambda = 1$ and $Nr = 0,1,7$. An increase of M lead to the increase of $Nu_x \operatorname{Re}_x^{-1/2}$ and $C_f \operatorname{Re}_x^{1/2}$. Meanwhile, it is noticed that the increase of Nr leads to the increase of $Nu_x \operatorname{Re}_x^{-1/2}$ and $C_f \operatorname{Re}_x^{1/2}$.

Figure 5.2 represents the temperature profiles for various values of $\Pr$. Since the value of $\Pr$ rises, it is found that the value of the wall temperature and the thickness of the thermal boundary layer drop. Physically, the Prandtl number indicates the ratio of momentum diffusivity to thermal diffusivity. Larger values of $\Pr$ have higher momentum diffusivity while smaller in thermal diffusivity. This higher momentum diffusivity corresponds to the thinning of thermal boundary layer thickness. Figure 5.3 presents the velocity profile and skin friction coefficient for several values of ε. It is found that the velocity gradient increases as ε increases which denotes the rise of the skin friction coefficient. Next, the velocity boundary layer thickness decreases as ε increases.

Figure 5.4 presents the temperature profile for various values of the non-Newtonian Williamson fluid parameter λ. It is observed that the changes of λ have a very small effect on the thermal boundary layer thickness. Figure 5.5 presents the temperature profile for various values of thermal radiation parameter Nr. From this figure, it is found that the temperature profiles and boundary layer thickness increase a Nr increases. The thermal radiation emits energy which raises the temperature, therefore, enhances the energy spreading far away from the plate surface. This increases the thickness of the thermal boundary layer.

Figure 5.6 illustrates the variation of Nusselt number $Nu_x \operatorname{Re}_x^{-1/2}$ with M for several values of ε when $\Pr = 7$ and $Nr = \lambda = 1$. It is observed that the Nusselt number increases with the increase values of ε, while the Nusselt number increases with the increase of M for a fixed values of ε. Similar result is obtained in Figure 5.7 in which the Nusselt number increases with the increase of Nr, while the Nusselt number increases with the increase of $\Pr$ for a fixed values of Nr.

Figure 5.8 presents the variation of skin friction coefficient number $C_f \operatorname{Re}_x^{1/2}$ with M for several values of ε when $\operatorname{Pr} = 7$ and $Nr = \lambda = 1$. It is found that the skin friction coefficient number increases with the increase of ε, while the skin friction coefficient number increases with the increase of M for a fixed values of ε.

Table 5.1   Values of $Nu_x \operatorname{Re}_x^{-1/2}$ and $C_f \operatorname{Re}_x^{1/2}$ for the various values of λ when $\operatorname{Pr} = 7$, $\varepsilon = 3$, $Nr = 1$ and $M = 0, 1$

λ	$M = 0$		$M = 1$	
	$Nu_x \operatorname{Re}_x^{-1/2}$	$C_f \operatorname{Re}_x^{1/2}$	$Nu_x \operatorname{Re}_x^{-1/2}$	$C_f \operatorname{Re}_x^{1/2}$
0.5	8.66127	5.98899	8.74162	6.71948
1	8.53415	6.76869	8.60367	7.62752
3	8.31837	8.70585	8.37247	9.86503
5	8.22098	9.97445	8.26885	11.32340
7	8.15969	10.96364	8.20378	12.45849

Table 5.2   Values of $Nu_x \operatorname{Re}_x^{-1/2}$ and $C_f \operatorname{Re}_x^{1/2}$ for the various values of ε when $Nr = M = \lambda = 1$ and $\operatorname{Pr} = 7, 10, 12$

ε	$\operatorname{Pr} = 7$		$\operatorname{Pr} = 10$		$\operatorname{Pr} = 12$	
	$Nu_x \operatorname{Re}_x^{-1/2}$	$C_f \operatorname{Re}_x^{1/2}$	$Nu_x \operatorname{Re}_x^{-1/2}$	$C_f \operatorname{Re}_x^{1/2}$	$Nu_x \operatorname{Re}_x^{-1/2}$	$C_f \operatorname{Re}_x^{1/2}$
0.5	7.47424	0.10496	8.94838	0.14244	9.80769	0.16188
1	7.69706	0.74641	9.16790	0.77580	10.02533	0.79023
3	8.60040	7.59112	10.10785	7.60808	10.98352	7.61564
5	9.32551	21.43984	10.88287	21.45303	11.78427	21.45875
7	9.92813	42.32314	11.53398	42.33457	12.46078	42.33945

Table 5.3   Values of $Nu_x \operatorname{Re}_x^{-1/2}$ and $C_f \operatorname{Re}_x^{1/2}$ for the various values of M when $\Pr = 7,\ \varepsilon = 3,\ \lambda = 1$ and $Nr = 0, 1, 7$

M	$Nr = 0$		$Nr = 1$		$Nr = 7$	
	$Nu_x \operatorname{Re}_x^{-1/2}$	$C_f \operatorname{Re}_x^{1/2}$	$Nu_x \operatorname{Re}_x^{-1/2}$	$C_f \operatorname{Re}_x^{1/2}$	$Nu_x \operatorname{Re}_x^{-1/2}$	$C_f \operatorname{Re}_x^{1/2}$
0.5	4.74218	7.17957	8.56787	7.17957	21.56548	7.18817
1	4.75753	7.59112	8.60040	7.59112	21.68010	7.60808
3	4.81422	9.24307	8.72026	9.24307	22.09911	9.29144
5	4.86480	10.90265	8.82683	10.90265	22.46765	10.97967
7	4.91061	12.56830	8.92309	12.56830	22.79763	12.67173
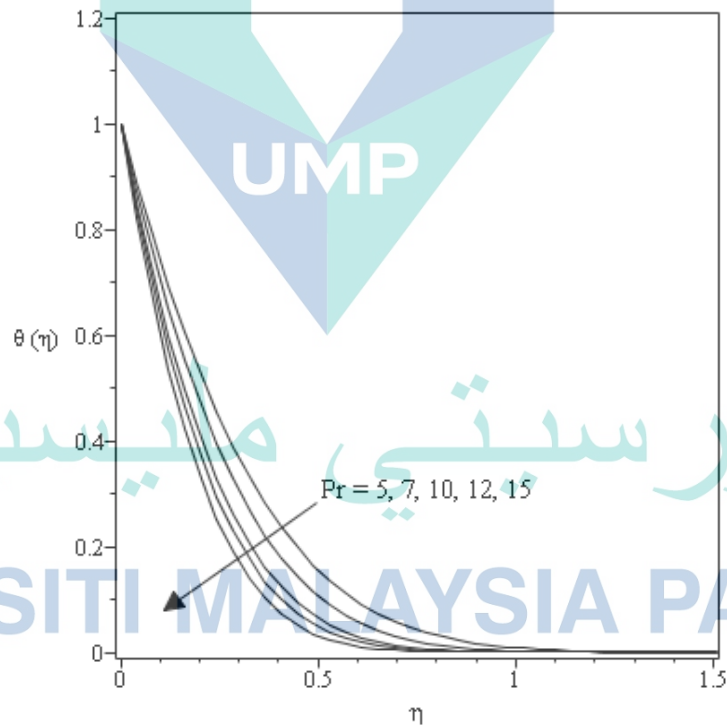
Figure 5.2   Temperature   profiles $\theta(0)$ for   various   values   of $\Pr$ when $Nr = M = \lambda = 1$ and $\varepsilon = 3$
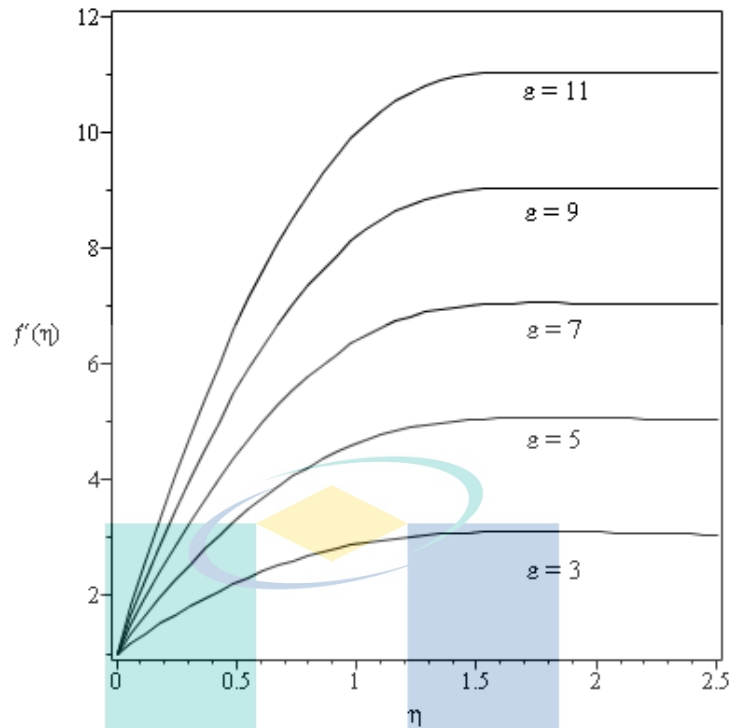
Figure 5.3: Velocity profiles $f'(\eta)$ for values of ε when $Nr = M = \lambda = 1$ and $\Pr = 7$
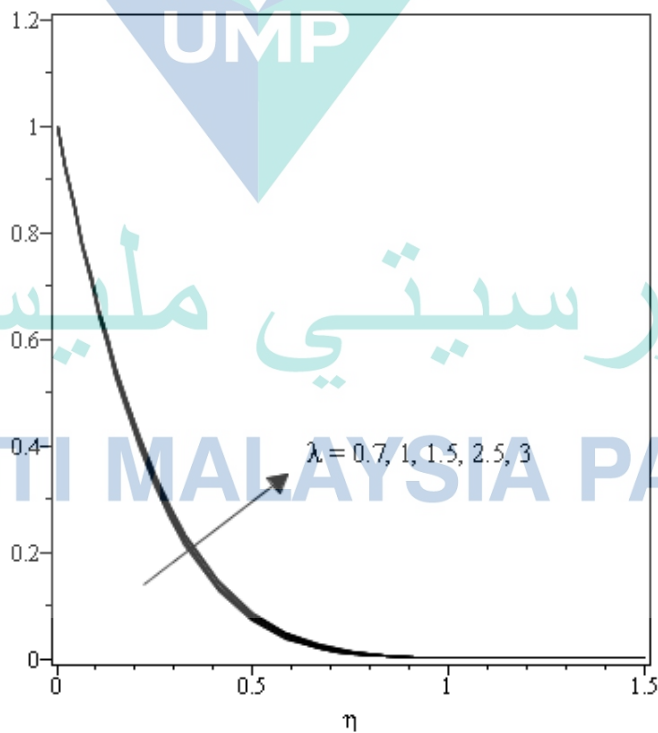
Figure 5.4   Temperature profiles $\theta(0)$ for various values of λ when $\Pr = 5$, $\varepsilon = 3$ and $Nr = M = 1$
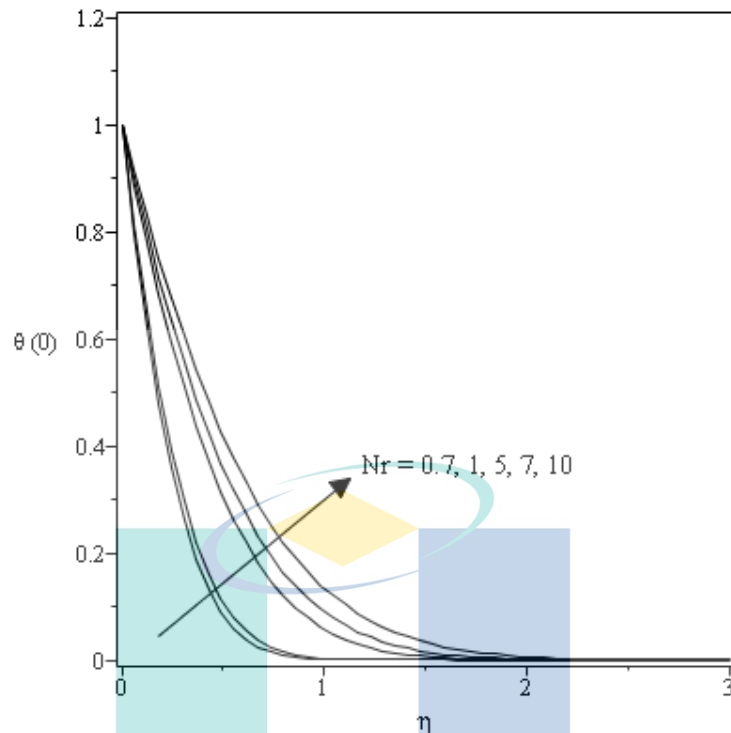
Figure 5.5   Temperature profiles $\theta(0)$ for several values of Nr when $\mathrm{Pr} = 7, \varepsilon = 3$ and $M = \lambda = 1$
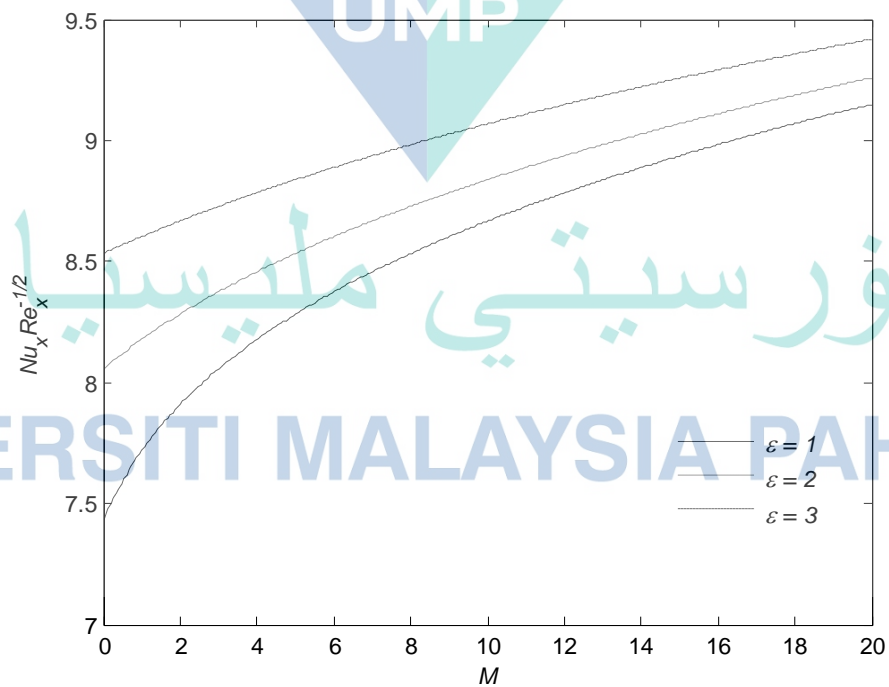
Figure 5.6   Variation of Nusselt number $Nu_x \, \mathrm{Re}_x^{-1/2}$ with M for several values of ε when $\mathrm{Pr} = 7$ and $Nr = \lambda = 1$
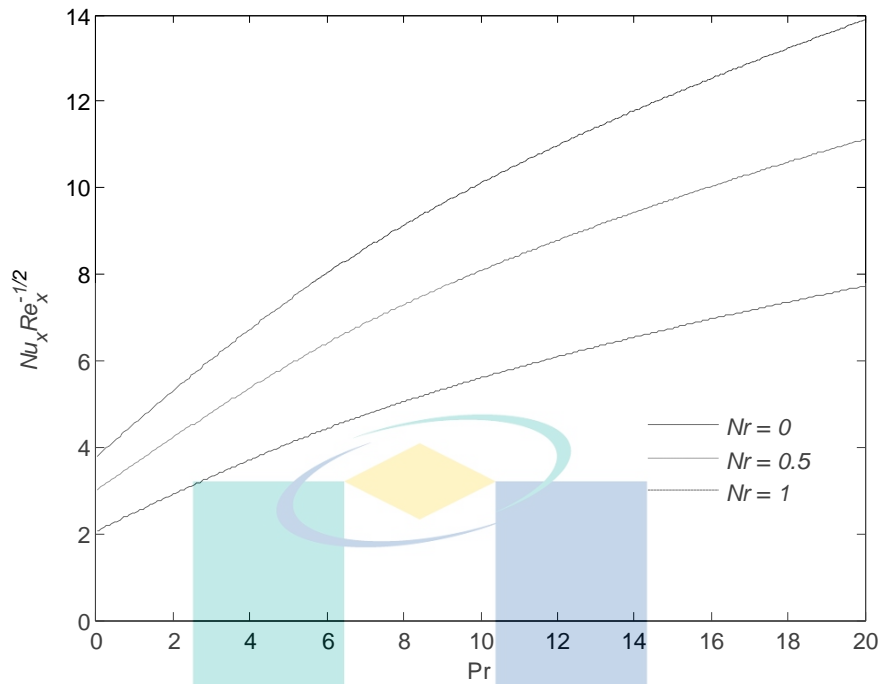
Figure 5.7   Variation of Nusselt number $Nu_x \, Re_x^{-1/2}$ with Pr for several values of *Nr* when $\varepsilon = 3$ and $M = \lambda = 1$
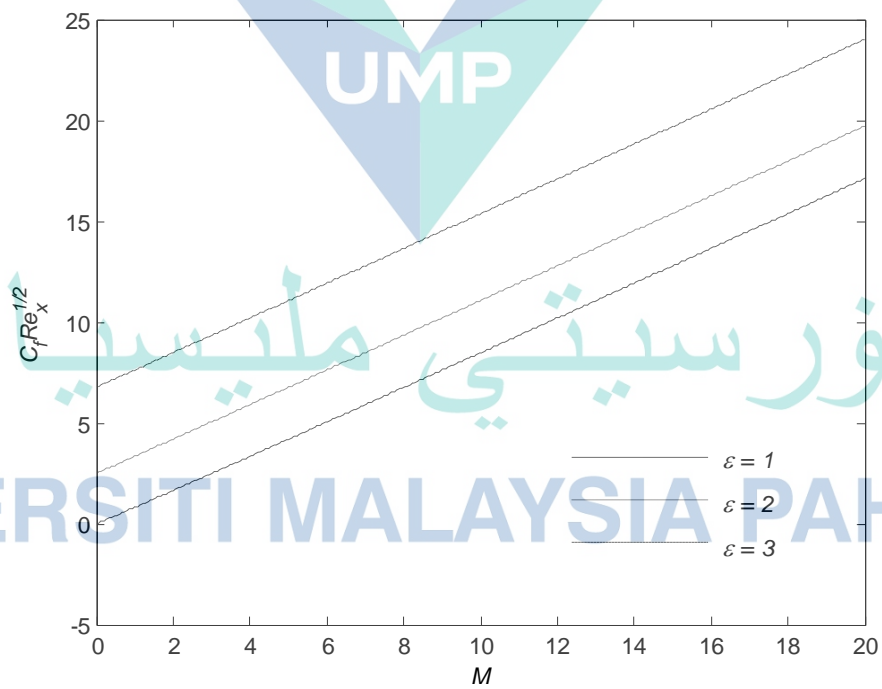
Figure 5.8   Variation of skin friction coefficient number $C_f \, Re_x^{1/2}$ with M for several values of ε when $Pr = 7$ and $Nr = \lambda = 1$

83

5.4   Summary

In this study, flow and heat transfer of Williamson fluid on MHD stagnation point over a stretching surface with thermal radiation effects are numerically studied and Table 5.4 show the summarized mathematical formulation in this problem.   The presented analysis leads to the following main results:

i.   The values of Nusselt number decrease and the skin friction coefficient increases, as a non-Newtonian Williamson fluid parameter λ increases.

ii.   The values of Nusselt number and skin friction coefficient increase, as the stretching parameter ε and magnetic parameter M increase.

iii.   The increase of Prandtl number $\Pr$ has resulted in a decrease of thermal boundary layer as well as skin friction coefficient.

iv.   As stretching parameter ε increases, the velocity profile increases while the velocity boundary layer thickness decreases.

v.   As a non-Newtonian Williamson fluid parameter λ and thermal radiation parameter Nr increase, the thermal boundary layer also increases. The energy obtained from the thermal radiation has raised the temperature and led to the increase in energy spreading far from the plate surface.

Table 5.4   Solution procedure for the mathematical formulation flow and heat transfer analysis of Williamson fluid on MHD stagnation point over a stretching surface with thermal radiation effects

Steps	Equations
Governing equations	$$\frac{\partial u}{\partial x}+\frac{\partial v}{\partial y}=0$$ $$u\frac{\partial u}{\partial x}+v\frac{\partial u}{\partial y}=u_e\frac{\partial u_e}{\partial x}+v\frac{\partial^2 u}{\partial y^2}+\sqrt{2}\,v\,\Gamma\frac{\partial u}{\partial y}\frac{\partial^2 u}{\partial y^2}+\frac{\sigma B_o^2}{\rho}\left(u_e-u\right)$$ $$u\frac{\partial T}{\partial x}+v\frac{\partial T}{\partial y}=\frac{k}{\rho C_p}\frac{\partial^2 T}{\partial y^2}-\frac{\partial q_r}{\partial y}$$
Boundary conditions	$$u=u_w(x),\;v=0,\;T=T_w\;\text{ as }\;y=0$$ $$u\to u_e(x),T\to T_\infty\;\text{ as }\;y\to\infty$$
Similarity transformation	$$\eta=\left(\frac{c}{v}\right)^{1/2}y,\;\theta(\eta)=\frac{T-T_\infty}{T_w-T_\infty},\;\psi=(cv)^{1/2}xf(\eta)$$
Ordinary differential equations	$$f'''+ff''+\varepsilon^2-f'^2+\lambda f''f'''+M(\varepsilon-f')=0$$ $$\left[1+\frac{4}{3}Nr\right]\theta''-\Pr\left[2f'\theta-f\theta'\right]=0$$
Transformed boundary conditions	$$f(0=)0,\;f'(0)=1,\;\theta(0)=1\;\text{ at }\;\eta=0$$ $$f'(\infty)\to\varepsilon,\;\theta(\infty)\to0\;\text{ as }\;\eta\to\infty$$

CHAPTER 6

CONCLUSION

6.1   Research Summary

The study was conducted to obtain the numerical solution to the stagnation point flow and heat transfer with several effects. All problems that considered the constant wall temperature and resulting nonlinear ordinary differential equations are successfully solved via the shooting method with the aid of Maple software. The whole thesis is assembled in Chapter 6 with a list of references in the last chapter.

Chapter 1 is an introductory chapter containing the general research background, research objectives, research scope, an overview with existing literature related to the problem in this study, research significance and thesis outline. The detailed governing equations and numerical method namely the shooting method are thoroughly discussed in Chapter 2.

In Chapter 3, the flow and heat transfer analysis of viscous fluid on the stagnation point over a stretching surface with viscous dissipation and slip conditions is studied which is the first problem. With the help of similarity transformation, the governing equations are converted to nonlinear ordinary differential equations and then solved numerically using the shooting method. Numerical results for the local Nusselt number and skin friction coefficient, as well as the temperature and velocity field, are elucidated through tables and graphs. The influence of Prandtl number, stretching parameter, Eckert number, thermal and velocity slip parameter on the flow and heat transfer characteristics are analyzed and discussed.

The flow and heat transfer analysis of Williamson fluid on the stagnation point over a stretching surface with viscous dissipation and slip conditions is studied in Chapter 4. With the help of similarity transformation, the governing equations are converted to nonlinear ordinary differential equations and then solved numerically by the shooting method. Numerical results of the local Nusselt number and skin friction coefficient, as well as the temperature and velocity field, are elucidated through tables and graphs. The influence of Prandtl number, stretching parameter, non-Newtonian Williamson fluid parameter, Eckert number, thermal and velocity slip parameter on the flow and heat transfer characteristics are analyzed and discussed.

Chapter 5 considers the flow and heat transfer analysis of Williamson fluid on MHD stagnation point over a stretching surface with thermal radiation effects which is the third problem. Like the previous problem, the governing equations are converted to nonlinear ordinary differential equations and then solved numerically by the shooting method. Numerical results for the reduced Nusselt number and reduced skin friction coefficient, as well as the temperature and velocity profiles, are elucidated through tables and graphs. The influence of Prandtl number, stretching parameter, Williamson fluid parameter, thermal radiation parameter and magnetic parameter are analyzed and discussed. It is found that, as Prandtl number and magnetic parameter increase, the temperature profiles decrease. Meanwhile, as Williamson fluid parameter and thermal radiation parameter decrease, the temperature profile increase.

Chapter 6 includes the research contributions and conclusion. The problems discussed in this thesis are new and the results are presented in the form of tables and figures. The numerical results obtained are very important as it can be used as a reference and for a comparison purpose in the future. Furthermore, some of the problems studied in this thesis have been published and the list of publications is presented in Appendix A.

6.2   Research Contribution

This thesis solved numerical solution of the stagnation point flow and heat transfer with several effects. Numerical results for the reduced Nusselt number and reduced skin friction coefficient, as well as the temperature and velocity profiles, are elucidated through tables and graphs. The influence of Prandtl number, stretching parameter, Williamson fluid parameter, thermal radiation parameter and magnetic parameter are analyzed and discussed. The present thesis has developed numerical algorithms for the computations for each problem considered. The authors acknowledge that there is no physical outcome or product resulted from this study, and this thesis built numerical algorithms or modeled the equations as well as made computations for every problem considered. The results of this study will also be used in providing theory predictions, numerical formulas and references to future experiments.

6.3   Research Future Studies

The present thesis only considered solved numerical solution on the flow and heat transfer on the stagnation point with several effects. All problems assumed a constant wall temperature. Therefore, there is a lot of study areas that may be considered in the future. The suggestions are as follows:

i.   The use of different types of fluids like Maxwell fluid, Walter's fluid, second-grade fluid, Casson fluid, Jeffrey's fluid and Burger's fluid.

ii. Include other physical effects like heat generation and absorption, chemical reaction as well as porosity effect.

iii. Other geometrices such as elliptic circular cylinder and solid sphere.

iv. Consider an unsteady boundary layer flow and stability analysis for dual solutions results usually occur on the stretching/shrinking geometries.

v.   Other boundary conditions such as Prescribed Heat Flux (PHF), Newtonian Heating (NH), Convective Boundary Condition (CBC) and Mixed thermal condition.

REFERENCES

Abbas, Z., Sheikh, M. and Pop, I. (2015). Stagnation-point flow of a hydromagnetic viscous fluid over stretching/shrinking sheet with generalized slip condition in the presence of homogeneous–heterogeneous reactions. Journal of the Taiwan Institute of Chemical Engineers, 55:69-75.

Abd El-Aziz, M. (2015). Dual solutions in hydromagnetic stagnation point flow and heat transfer towards a stretching/shrinking sheet with non-uniform heat source/sink and variable surface heat flux. Journal of the Egyptian Mathematical Society, 24(3):479-486.

Abu Bakar, N. A., Bachok, N. and Md Arifin, N. (2019). Boundary layer stagnation-point flow over a stretching/shrinking cylinder in a nanofluid: A stability analysis. Indian Journal of Pure and Applied Physics, 57(2):106-117.

Agbaje, T., Mondal, S., Makukula, Z., Motsa, S. and Sibanda, P. (2018). A new numerical approach to MHD stagnation point flow and heat transfer towards a stretching sheet. Ain Shams Engineering Journal, 9(2):233-243.

Ahmad, S. (2009). Convection boundary layer flows over needles and cylinders in viscous fluids. Ph.D Thesis. Universiti Putra Malaysia.

Alfvén, H. (1942). Existence of electromagnetic-hydrodynamic waves. Nature, 150(3805):405-406.

Ali, F. M., Nazar, R. and Arifin, N. M. (2013). Effect of thermal radiation on unsteady stagnation-point flow with mass transfer. In AIP Proceeding of Simposium Kebangsaan Sains Matematik ke-20, volume 1522, pages 80-85. AIP Publishing.

Alkanhal, T. A., Sheikholeslami, M., Usman, M., Haq, R.-u., Shafee, A., Al-Ahmadi, A. S. and Tlili, I. (2019). Thermal management of MHD nanofluid within the porous medium enclosed in a wavy shaped cavity with square obstacle in the presence of radiation heat source. International Journal of Heat and Mass Transfer, 139:87-94.

Aman, F., Ishak, A. and Pop, I. (2011). Mixed convection boundary layer flow near stagnation-point on vertical surface with slip. Applied Mathematics and Mechanics, 32(12):1599-1606.

Aman, F., Ishak, A. and Pop, I. (2013). Magnetohydrodynamic stagnation-point flow towards a stretching/shrinking sheet with slip effects. International Communications in Heat and Mass Transfer, 47:68-72.

Amanulla, C. H., Nagendra, N., Subba Rao, A., Anwar Bég, O. and Kadir, A. (2018). Numerical exploration of thermal radiation and Biot number effects on the flow of a non-Newtonian MHD Williamson fluid over a vertical convective surface. Heat Transfer Asian Research, 47(2):286-304.

89

Anderson, J. D. (2005). Ludwig Prandtl's Boundary Layer. Physics Today, 42-48.

Anwar, M. I., Shafie, S., Khan, I. and Salleh, M. Z. (2012). Conjugate effects of radiation flux on double diffusive MHD free convection flow of a nanofluid over a power law stretching sheet. International Scholarly Research Notices, 1-7.

Arifin, N. S., Zokri, S. M., Kasim, A. R. M., Salleh, M. Z. and Mohammad, N. F. (2019). Two-phase mixed convection flow of dusty Williamson fluid with aligned magnetic field over a vertical stretching sheet. Proceedings of the Third International Conference on Computing, Mathematics and Statistics, 209-216, Springer.

Aziz, A. (2009). A similarity solution for laminar thermal boundary layer over a flat plate with a convective surface boundary condition. Communications in Nonlinear Science and Numerical Simulation, 14(4):1064-1068.

Babu, D. H., Ajmath, K., Venkateswarlu, B. and Narayana, P. (2018). Thermal radiation and heat source effects on MHD non-Newtonian nanofluid flow over a stretching sheet. Journal of Nanofluids, 8(5):1085-1092.

Bachok, N., Ishak, A. and Pop, I. (2012). Boundary layer stagnation-point flow and heat transfer over an exponentially stretching/shrinking sheet in a nanofluid. International Journal of Heat and Mass Transfer, 55(25):8122-8128.

Baehr, H. D. and Stephen, K. (2006). Heat and Mass Transfer. Springer. Berlin, Heidelberg.

Bataller, R. C. (2008). Radiation effects for the Blasius and Sakiadis flows with a convective surface boundary condition. Applied Mathematics and Computation, 206(2):832-840.

Batchelor, G. K., Moffatt, H. K. and Worster, M. G. (2002). Perspectives in fluid dynamics. A Collective Introduction to Current Research, Cambridge University Press.

Bejan, A. (2013). Convection heat transfer. John Wiley & Sons. New York.

Besthapu, P., Haq, R. U., Bandari, S. and Al-Mdallal, Q. M. (2019). Thermal radiation and slip effects on MHD stagnation point flow of non-Newtonian nanofluid over a convective stretching surface. Neural Computing and Applications, 31(1):207-217.

Bhattacharyya, K., Mukhopadhyay, S. and Layek, G. C. (2011). Slip effects on boundary layer stagnation-point flow and heat transfer towards a shrinking sheet. International Journal of Heat and Mass Transfe, 54(1–3):308-313.

Bhatti, M., Abbas, T., Rashidi, M. and Ali, M. (2016a). Numerical simulation of entropy generation with thermal radiation on MHD Carreau nanofluid towards a shrinking sheet. Entropy, 18(6):200.

Bhatti, M., Shahid, A. and Rashidi, M. (2016b). Numerical simulation of fluid flow over a shrinking porous sheet by successive linearization method. Alexandria Engineering Journal, 55(1):51-56.

Bhuvaneswari, M., Sivasankaran, S., Niranjan, H. and Eswaramoorthi, S. (2019). Cross diffusion effects on MHD convection of Casson-Williamson fluid over a stretching surface with radiation and chemical reaction. Applied Mathematics and Scientific Computing, 139-146.

Bilal, M., Sagheer, M. and Hussain, S. (2018). Numerical study of magnetohydrodynamics and thermal radiation on Williamson nanofluid flow over a stretching cylinder with variable thermal conductivity. Alexandria Engineering Journal, 57(4):3281-3289.

Blasius, H. (1908). Boundary layers in fluids of small viscosity. Zeitschrift für Angewandte Mathematik und Physik ZAMP, 56(1): 1-37.

Borrelli, A., Giantesio, G. and Patria, M. C. (2012). MHD oblique stagnation-point flow of a micropolar fluid. Applied Mathematical Modelling, 36(9):3949-3970.

Chao, B. T. and Jeng, D. R. (1965). Unsteady stagnation point heat transfer. Journal of Heat Transfer, 87:221-230.

Chen, C. H. (2010). On the analytic solution of MHD flow and heat transfer for two types of viscoelastic fluid over a stretching sheet with energy dissipation, internal heat source and thermal radiation. International Journal of Heat and Mass Transfer, 53(19–20):4264-4273.

Chiam, T. C. (1994). Stagnation-point flow towards a stretching plate. Journal of the Physical Society of Japan, 63:2443-2444.

Crane, L. J. (1970). Flow Past a Stretching Plate. Zeitschrift für Angewandte Mathematik und Physik ZAMP, 21(4):645-647.

Daniel, Y. S., Aziz, Z. A., Ismail, Z. and Salah, F. (2018). Impact of thermal radiation on electrical MHD flow of nanofluid over nonlinear stretching sheet with variable thickness. Alexandria Engineering Journal, 57(3):2187-2197.

Darus, A. N. (1994). Dinamik aliran bendalir: Suatu penyelesaian. Dewan Bahasa dan Pustaka. Kuala Lumpur.

Das, K., Acharya, N. and Kundu, P. K. (2015). Radiative flow of MHD Jeffrey fluid past a stretching sheet with surface slip and melting heat transfer. Alexandria Engineering Journal, 54(4):815-821.

Dash, G., Tripathy, R., Rashidi, M. and Mishra, S. (2016). Numerical approach to boundary layer stagnation-point flow past a stretching/shrinking sheet. Journal of Molecular Liquids, 221:860-866.

Dessie, H. and Kishan, N. (2014). MHD effects on heat transfer over stretching sheet embedded in porous medium with variable viscosity, viscous dissipation and heat source/sink. Ain Shams Engineering Journal, 5(3):967-977.

Elbashbeshy, E. M. A., Emam, T. G. and Abdelgaber, K. M. (2012). Effects of thermal radiation and magnetic field on unsteady mixed convection flow and heat transfer over an exponentially stretching surface with suction in the presence of internal heat generation/absorption. Journal of the Egyptian Mathematical Society, 20(3):215-222.

Ellahi, R., Shivanian, E., Abbasbandy, S. and Hayat, T. (2016). Numerical study of magnetohydrodynamics generalized Couette flow of Eyring-Powell fluid with heat transfer and slip condition. International Journal of Numerical Methods for Heat and Fluid Flow, 26(5):1433-1445.

Favre-Marinet, M. and Tardu, S. (2013). Convective Heat Transfer. John Wiley & Sons. United States.

Gebhart, B. (1962). Effects of viscous dissipation in natural convection. Journal of Fluid Mechanics, 14(02):225-232.

Gupta, P. S. and Gupta, A. S. (1977). Heat and mass transfer on a stretching sheet with suction or blowing. The Canadian Journal of Chemical Engineering, 55(6):744-746.

Gupta, S., Kumar, D. and Singh, J. (2018). MHD mixed convective stagnation point flow and heat transfer of an incompressible nanofluid over an inclined stretching sheet with chemical reaction and radiation. International Journal of Heat and Mass Transfer, 118:378-387.

Hamid, A., Khan, M. and Hafeez, A. (2018a). Unsteady stagnation-point flow of Williamson fluid generated by stretching/shrinking sheet with ohmic heating. International Journal of Heat and Mass Transfer, 126: 933-940.

Hamid, A., Khan, M. and Khan, U. (2018b). Thermal radiation effects on Williamson fluid flow due to an expanding/contracting cylinder with nanomaterials: dual solutions. Physics Letters A, 382(30):1982-1991.

Hamid, M., Usman, M., Khan, Z., Haq, R. and Wang, W. (2018c). Numerical study of unsteady MHD flow of Williamson nanofluid in a permeable channel with heat source/sink and thermal radiation. The European Physical Journal Plus, 133(12):527.

Haq, R. U., Nadeem, S., Khan, Z. H. and Akbar, N. S. (2015). Thermal radiation and slip effects on MHD stagnation point flow of nanofluid over a stretching sheet. Physica E: Low-dimensional Systems and Nanostructures, 65:17-23.

Hayat, T., Abbas, Z., Pop, I. and Asghar, S. (2010). Effects of radiation and magnetic field on the mixed convection stagnation-point flow over a vertical stretching sheet in a porous medium. International Journal of Heat and Mass Transfer, 53(1–3):466-474.

Hayat, T., Bibi, S., Rafiq, M., Alsaedi, A. and Abbasi, F. (2016a). Effect of an inclined magnetic field on peristaltic flow of Williamson fluid in an inclined channel with convective conditions. Journal of Magnetism and Magnetic Materials, 401:733-745.

Hayat, T. and Qasim, M. (2010). Influence of thermal radiation and Joule heating on MHD flow of a Maxwell fluid in the presence of thermophoresis. International Journal of Heat and Mass Transfer, 53(21-22):4780-4788.

Hayat, T., Qayyum, S., Shehzad, S. A. and Alsaedi, A. (2017). Simultaneous effects of heat generation/absorption and thermal radiation in magnetohydrodynamics (MHD) flow of Maxwell nanofluid towards a stretched surface. Results in physics, 7:562-573.

Hayat, T., Shafiq, A. and Alsaedi, A. (2016b). Hydromagnetic boundary layer flow of Williamson fluid in the presence of thermal radiation and ohmic dissipation. Alexandria Engineering Journal, 55(3):2229-2240.

Hiemenz, K. (1911). DIe Grenzschicht an einem in den gleichformigen Flussigkeitsstrom eingetauchten ger-aden Kreiszylinder. Dingley's Polytechnic Journal, 32:321-410.

Ibrahim, W. and Shankar, B. (2013). MHD boundary layer flow and heat transfer of a nanofluid past a permeable stretching sheet with velocity, thermal and solutal slip boundary conditions. Computers and Fluids, 75:1-10.

Ibrahim, W., Shankar, B. and Nandeppanavar, M. M. (2013). MHD stagnation point flow and heat transfer due to nanofluid towards a stretching sheet. International Journal of Heat and Mass Transfer, 56(1–2):1-9.

Imran, M., Riaz, M., Shah, N. and Zafar, A. (2018). Boundary layer flow of MHD generalized Maxwell fluid over an exponentially accelerated infinite vertical surface with slip and Newtonian heating at the boundary. Results in physic, 8:1061-1067.

Incropera, F. (1996). DP deWitt. Fundamentals of heat and mass transfer. John Wiley & Sons. New York.

Ishak, A. (2008). Penyelesaian keserupaan bagi aliran sempadan olakan dalam bendalir likat. Ph.D Tesis. Universiti Kebangsaan Malaysia.

Ishak, A., Nazar, R. and Pop, I. (2006). Mixed convection boundary layers in the stagnation-point flow toward a stretching vertical sheet. Meccanica, 41(5):509-518.

Jain, S. and Parmar, A. (2018). Radiation effect on MHD williamson fluid flow over stretching cylinder through porous medium with heat source. In Applications of Fluid Dynamics, pages 61-78, Springer.

Kamal, F., Zaimi, K., Ishak, A. and Pop, I. (2019). Stability analysis of MHD stagnation-point flow towards a permeable stretching/shrinking sheet in a nanofluid with chemical reactions effect. Sains Malaysiana, 48(1):243-250.

Khan, M. S., Karim, I., Ali, L. E. and Islam, A. (2012). Unsteady MHD free convection boundary-layer flow of a nanofluid along a stretching sheet with thermal radiation and viscous dissipation effects. International Nano Letters, 2(1):24-32.

Khan, N. A., Khan, S. and Riaz, F. (2014). Boundary Layer Flow of Williamson Fluid with Chemically Reactive Species using Scaling Transformation and Homotopy Analysis Method. Mathematical Sciences Letters, 3(3):199-205.

Khan, W., Makinde, O. and Khan, Z. (2016). Non-aligned MHD stagnation point flow of variable viscosity nanofluids past a stretching sheet with radiative heat. International Journal of Heat and Mass Transfer, 96:525-534.

Kreith, F., Manglik, R. M. and Bohn, M. S. (2010). Principles of Heat Transfer: Stamford USA. Cengage Learning.

Krishnamurthy, M., Prasannakumara, B., Gireesha, B. and Gorla, R. S. R. (2016). Effect of chemical reaction on MHD boundary layer flow and melting heat transfer of Williamson nanofluid in porous medium. Engineering Science and Technology, An International Journal, 19(1):53-61.

Kumar, K. A., Reddy, J. R., Sugunamma, V. and Sandeep, N. (2019). Simultaneous solutions for MHD flow of williamson fluid over a curved sheet with nonuniform heat source/sink. Heat Transfer Research, 50(6):581-603.

Kumaran, G. and Sandeep, N. (2017). Thermophoresis and Brownian moment effects on parabolic flow of MHD Casson and Williamson fluids with cross diffusion. Journal of Molecular Liquids, 233:262-269.

Lesnic, D., Ingham, D. B. and Pop, I. (1999). Free convection boundary-layer flow along a vertical surface in a porous medium with Newtonian heating. International Journal of Heat and Mass Transfer, 42(14):2621-2627.

Lienhard IV, J. H. and Lienhard V, J. H. (2011). A heat transfer textbook. Phlogiston Press. Cambridge.

Lok, Y. Y. (2002). Nonisothermal free convection boundary layer over a vertical flat plate. Master Thesis. Universiti Teknologi Malaysia.

Mahapatra, T. R. and Gupta, A. S. (2002). Heat transfer in stagnation-point flow towards a stretching sheet. Heat and Mass Transfer, 38(6):517-521.

Mahmoud, M. A. A. and Waheed, S. E. (2012). MHD flow and heat transfer of a micropolar fluid over a stretching surface with heat generation (absorption) and slip velocity. Journal of the Egyptian Mathematical Society, 20(1):20-27.

Majeed, A., Zeeshan, A., Mahmood, T., Rahman, S. U. and Khan, I. (2019). Impact of magnetic field and second-order slip flow of Casson liquid with heat transfer subject to suction/injection and convective boundary condition. Journal of Magnetics, 24(1):81-89.

Makinde, O. D. and Aziz, A. (2010). MHD mixed convection from a vertical plate embedded in a porous medium with a convective boundary condition. International Journal of Thermal Sciences, 49(9):1813-1820.

Makinde, O. D., Khan, W. A. and Khan, Z. H. (2013). Buoyancy effects on MHD stagnation point flow and heat transfer of a nanofluid past a convectively heated stretching/shrinking sheet. International Journal of Heat and Mass Transfer, 62:526-533.

Makinde, O. and Olanrewaju, P. (2010). Buoyancy effects on thermal boundary layer over a vertical plate with a convective surface boundary condition. Journal of Fluids Engineering, 132(4):044502.

Malik, M., Bibi, M., Khan, F. and Salahuddin, T. (2016). Numerical solution of Williamson fluid flow past a stretching cylinder and heat transfer with variable thermal conductivity and heat generation/absorption. AIP Advances, 6(3):035101.

Mansur, S., Ishak, A. and Pop, I. (2015). The magnetohydrodynamic stagnation point flow of a nanofluid over a stretching/shrinking sheet with suction. Plos One, 10(3):e0117733.

Martin, M. J. and Boyd, I. D. (2006). Momentum and heat transfer in a laminar boundary layer with slip flow. Journal of Thermophysics and Heat Transfer, 20(4): 710-719.

Mehmood, R., Rana, S., Akbar, N. and Nadeem, S. (2018). Non-aligned stagnation point flow of radiating Casson fluid over a stretching surface. Alexandria Engineering Journal, 57(2):939-946.

Merkin, J. H. (1994). Natural-convection boundary-layer flow on a vertical surface with Newtonian heating. International Journal of Heat and Fluid Flow, 15(5):392-398.

Metzner, A. (1965). Heat transfer in non-Newtonian fluids. Advances in Heat Transfer, 2:357-397.

Mohamed, M. K. A. (2013). Mathematical modeling for convection boundary layer flow in a viscous fluid with Newtonian heating and convective boundary conditions. Master Thesis. Universiti Malaysia Pahang.

Mohamed, M. K. A. (2017). Steady convective boundary layer flow in a nanofluid past on a bluff body with the viscous dissipation effect. Ph.D Thesis. Universiti Malaysia Pahang.

Mohamed, M. K. A., Noar, N. A. Z. M., Ismail, Z., Kasim, A. R. M., Sarif, N. M., Salleh, M. Z. and Ishak, A. (2017). Slip effect on stagnation point flow past a stretching surface with the presence of heat generation/absorption and Newtonian heating. In AIP Conference Proceedings, Volume.1867, No.1, pages 020009.

Mohamed, M. K. A., Salleh, M. Z., Nazar, R. and Ishak, A. (2012). Stagnation point flow over a stretching sheet with newtonian heating. Sains Malaysiana, 41(11):1467-1473.

Mohamed, M. K. A., Salleh, M. Z., Nazar, R. and Ishak, A. (2013). Numerical investigation of stagnation point flow over a stretching sheet with convective boundary conditions. Boundary Value Problems, 2013(1):1-10.

Mukhopadhyay, S. (2009). Effect of thermal radiation on unsteady mixed convection flow and heat transfer over a porous stretching surface in porous medium. International Journal of Heat and Mass Transfer, 52(13–14):3261-3265.

Mukhopadhyay, S. (2013). Slip effects on MHD boundary layer flow over an exponentially stretching sheet with suction/blowing and thermal radiation. Ain Shams Engineering Journal, 4(3):485-491.

Nadeem, S., Hussain, A., Malik, M. and Hayat, T. (2009). Series solutions for the stagnation flow of a second-grade fluid over a shrinking sheet. Applied Mathematics and Mechanics, 30(10):1255-1262.

Nadeem, S., Hussain, A. and Vajravelu, K. (2010). Effects of heat transfer on the stagnation flow of a third-order fluid over a shrinking sheet. Zeitschrift für Naturforschung A, 65(11):969-994.

Nadeem, S. and Hussain, S. (2014). Flow and heat transfer analysis of Williamson nanofluid. Applied Nanoscience, 4(8):1005-1012.

Nadeem, S., Hussain, S. and Lee, C. (2013). Flow of a Williamson fluid over a stretching sheet. Brazilian Journal of Chemical Engineering, 30(3):619-625.

Nandy, S. K. and Mahapatra, T. R. (2013). Effects of slip and heat generation/absorption on MHD stagnation flow of nanofluid past a stretching/shrinking surface with convective boundary conditions. International Journal of Heat and Mass Transfer, 64:1091-1100.

Narayana, P. S. and Babu, D. H. (2016). Numerical study of MHD heat and mass transfer of a Jeffrey fluid over a stretching sheet with chemical reaction and thermal radiation. Journal of the Taiwan Institute of Chemical Engineers, 59:18-25.

Nasir, N. A. A. M., Ishak, A. and Pop, I. (2019). Stagnation point flow and heat transfer past a permeable stretching/shrinking Riga plate with velocity slip and radiation effects. Journal of Zhejiang University-SCIENCE A, 20(4):290-299.

Nayak, M. (2017). MHD 3D flow and heat transfer analysis of nanofluid by shrinking surface inspired by thermal radiation and viscous dissipation. International Journal of Mechanical Sciences, 124:185-193.

Nazar, R., Amin, N., Filip, D. and Pop, I. (2004a). Stagnation point flow of a micropolar fluid towards a stretching sheet. International Journal of Non-Linear Mechanics, 39(7):1227-1235.

Nazar, R., Amin, N., Filip, D. and Pop, I. (2004b). Unsteady boundary layer flow in the region of the stagnation point on a stretching sheet. International Journal of Engineering Science, 42(11):1241-1253.

Olanrewaju, P., Gbadeyan, J. and Abah, S. (2011). Radiation and viscous dissipation effects for the Blasius and Sakiadis flows with a convective surface boundary condition. International Journal of Advances in Science and Technology, 2(4):102-115.

Ozisik, M. N. (1985). Heat Transfer: A basic approach. McGraw-Hill.New York.

Pal, D. and Mandal, G. (2015). Mixed convection–radiation on stagnation-point flow of nanofluids over a stretching/shrinking sheet in a porous medium with heat generation and viscous dissipation. Journal of Petroleum Science and Engineering, 126:16-25.

Pal, D., Mandal, G. and Vajravelu, K. (2014). Flow and heat transfer of nanofluids at a stagnation point flow over a stretching/shrinking surface in a porous medium with thermal radiation. Applied Mathematics and Computation, 238:208-224.

Pop, I. and Ingham, D. B. (2001). Convective heat transfer: Mathematical and computational modelling of viscous fluids and porous media. Elsevier.

Prabhakara, S. and Deshpande, M. (2004). The no-slip boundary condition in fluid mechanics. Resonance, 9(5):61-71.

Raisi, A., Ghasemi, B. and Aminossadati, S. (2011). A numerical study on the forced convection of laminar nanofluid in a microchannel with both slip and no-slip conditions. Numerical Heat Transfer, Part A: Applications, 59(2):114-129.

Raju, C. and Sandeep, N. (2017). Unsteady Casson nanofluid flow over a rotating cone in a rotating frame filled with ferrous nanoparticles: a numerical study. Journal of Magnetism and Magnetic Materials, 421:216-224.

Raju, V. N., Hemalatha, K. and Babu, V. S. (2019). MHD viscoelastic fluid flow past an infinite vertical plate in the presence of radiation and chemical reaction. International Journal of Applied Engineering Research, 14(5):1062-1069.

Ramesh, K. and Devakar, M. (2015). Some analytical solutions for flows of Casson fluid with slip boundary conditions. Ain Shams Engineering Journal, 6(3):967-975.

Rashidi, M., Ganesh, N. V., Hakeem, A. A. and Ganga, B. (2014). Buoyancy effect on MHD flow of nanofluid over a stretching sheet in the presence of thermal radiation. Journal of Molecular Liquids, 198:234-238.

Rathore, M. M. (2011). Engineering Heat Transfer. Jones & Bartlett Learning. Canada.

Raza, J. (2019). Thermal radiation and slip effects on magnetohydrodynamic (MHD) stagnation point flow of Casson fluid over a convective stretching sheet. Propulsion and Power Research, 8(2):138-146.

Reddy, M. G., Padma, P. and Shankar, B. (2015). Effects of viscous dissipation and heat source on unsteady MHD flow over a stretching sheet. Ain Shams Engineering Journal, 6(4):1195-1201.

Rehman, F. U., Nadeem, S., Rehman, H. U. and Haq, R. U. (2018). Thermophysical analysis for three-dimensional MHD stagnation-point flow of nano-material influenced by an exponential stretching surface. Results in Physics, 8:316-323.

Roşca, N. C., Roşca, A. V. and Pop, I. (2014). Stagnation point flow and heat transfer over a non-linearly moving flat plate in a parallel free stream with slip. Communications in Nonlinear Science and Numerical Simulation, 19(6):1822-1835.

Sahoo, B. (2010). Flow and heat transfer of a non-Newtonian fluid past a stretching sheet with partial slip. Communications in Nonlinear Science and Numerical Simulation, 15(3):602-615.

Salahuddin, T., Malik, M. Y., Hussain, A., Bilal, S. and Awais, M. (2016). MHD flow of Cattanneo–Christov heat flux model for Williamson fluid over a stretching sheet with variable thickness: Using numerical approach. Journal of Magnetism and Magnetic Materials, 401:991-997.

Salleh, M. Z., Mohamed, N., Khairuddin, R., Khasi'ie, N. S., Nazar, R. and Pop, I. (2012). Free convection over a permeable horizontal flat plate embedded in a porous medium with radiation effects and mixed thermal boundary conditions. Journal of Mathematics and Statistics, 8(1):122-128.

Salleh, M. Z., Nazar, R. and Pop, I. (2009). Forced convection boundary layer flow at a forward stagnation point with newtonian heating. Chemical Engineering Communications, 196:987-996.

Salleh, M. Z., Nazar, R. and Pop, I. (2010). Boundary layer flow and heat transfer over a stretching sheet with Newtonian heating. Journal of the Taiwan Institute of Chemical Engineers, 41(6):651-655.

Sandeep, N., Sulochana, C. and Animasaun, I. L. (2016). Stagnation-point flow of a Jeffrey nanofluid over a stretching surface with induced magnetic field and chemical reaction. International Journal of Engineering Research in Africa, 20:93-111.

Schlichting, H. (1979). Boundary layer theory. McGraw-Hill. New York.

Shah, Z., Bonyah, E., Islam, S., Khan, W. and Ishaq, M. (2018). Radiative MHD thin film flow of Williamson fluid over an unsteady permeable stretching sheet. Heliyon, 4(10):e00825.

Sheikholeslami, M., Hayat, T. and Alsaedi, A. (2016). MHD free convection of Al_2O_3– water nanofluid considering thermal radiation: a numerical study. International Journal of Heat and Mass Transfer, 96:513-524.

Sheikholeslami, M. and Shehzad, S. (2017). Thermal radiation of ferrofluid in existence of Lorentz forces considering variable viscosity. International Journal of Heat and Mass Transfer, 109:82-92.

Sobamowo, M., Jayesimi, L. and Waheed, M. (2018). Magnetohydrodynamic squeezing flow analysis of nanofluid under the effect of slip boundary conditions using variation of parameter method. Karbala International Journal of Modern Science, 4(1):107-118.

Soundalgekar, V. M. (1972). Viscous dissipation effects on unsteady free convective flow past an infinite, vertical porous plate with constant suction. International Journal of Heat and Mass Transfer, 15(6):1253-1261.

Suali, M., Asri, N. M. and Ishak, A. (2012). Unsteady stagnation point flow and heat transfer over a stretching/shrinking sheet with prescribed surface heat flux. Appl. Math. Comput. Intell, 1: 1-11.

Tannehill, J. C., Anderson, D. A. and Pletcher, R. H. (1997). Computational fluid mechanics and heat transfer. Philadelphia: Hemisphere Publishing Corporation.

Weidman, P. D., Kubitschek, D. G. and Davis, A. M. J. (2006). The effect of transpiration on self-similar boundary layer flow over moving surfaces. International Journal of Engineering Science, 44(11–12):730-737.

Williamson, R. V. (1929). The flow of pseudoplastic materials. Industrial and Engineering Chemistry, 21(11):1108-1111.

Yacob, N. A. and Ishak, A. (2011). Stagnation point flow towards a stretching/shrinking sheet in a micropolar fluid with a convective surface boundary condition. The Canadian Journal of Chemical Engineering, 90(3):621-626.

APPENDIX A

Shooting method to obtain the solution for Chapter 3

```
        f''+ ff'+ ee^2-f'^2=0
        h"-Pr(2 fh-f h')+ Pr Ec f'^2=0
f(0)=0    f'(0)=1+ ga f''         h(0)=1+ be h'
        f'(infty)-->ee   h(infty)-->0
```

> *restart* ;
> *Shootlib* := "C:\\Program Files/Maple 13/Shoot9/";

$$Shootlib := \text{"C:\textbackslash Program Files/Maple 13/Shoot9/"} \tag{1}$$

> *libname* := *Shootlib*, *libname*;

$$libname := \text{"C:\textbackslash Program Files/Maple 13/Shoot9/"}, \text{"C:\textbackslash Program Files\textbackslash Maple 13/lib"} \tag{2}$$

> with(*Shoot*);

$$[shoot] \tag{3}$$

> with(*plots*);

[*animate, animate3d, animatecurve, arrow, changecoords, complexplot, complexplot3d,* (4)
conformal, conformal3d, contourplot, contourplot3d, coordplot, coordplot3d, densityplot,
display, dualaxisplot, fieldplot, fieldplot3d, gradplot, gradplot3d, graphplot3d, implicitplot,
implicitplot3d, inequal, interactive, interactiveparams, intersectplot, listcontplot,
listcontplot3d, listdensityplot, listplot, listplot3d, loglogplot, logplot, matrixplot, multiple,
odeplot, pareto, plotcompare, pointplot, pointplot3d, polarplot, polygonplot, polygonplot3d,
polyhedra_supported, polyhedraplot, rootlocus, semilogplot, setcolors, setoptions,
setoptions3d, spacecurve, sparsematrixplot, surfdata, textplot, textplot3d, tubeplot]

> *blt* := 5.5; *Ga* := 1; *ee* := 1; *Be* := 1; *Ec* := 1

$$blt := 5.5$$
$$Ga := 1$$
$$ee := 1$$
$$Be := 1$$
$$Ec := 1 \tag{5}$$

> *FNS* := { *F(Z)*, *Fp(Z)*, *Fpp(Z)*, *G(Z)*, *Gp(Z)* } :

> *ODE* := { *diff*(*F(Z)*, *Z*) = *Fp(Z)*, *diff*(*Fp(Z)*, *Z*) = *Fpp(Z)*, *diff*(*Fpp(Z)*, *Z*) = *Fp(Z)^2 − ee*
    *^2 −Fpp(Z) * F(Z)*, *diff*(*G(Z)*, *Z*) = *Gp(Z)*, *diff*(*Gp(Z)*, *Z*) = Pr·(2·*Fp(Z)·G(Z)−F(Z)*
    ·Gp(Z)) − *Pr·Ec·(Fpp(Z)^2)* };

$$ODE := \left\{ \frac{d}{dZ} F(Z) = Fp(Z),\ \frac{d}{dZ} Fp(Z) = Fpp(Z),\ \frac{d}{dZ} Fpp(Z) = Fp(Z)^2 - 1 \right. \tag{6}$$
$$- Fpp(Z)\, F(Z),\ \frac{d}{dZ} G(Z) = Gp(Z),\ \frac{d}{dZ} Gp(Z) = Pr\,(2\,Fp(Z)\,G(Z) - F(Z)\,Gp(Z))$$
$$\left. - Pr\, Fpp(Z)^2 \right\}$$

> *IC* := { *F*(0) = 0,   *Fp*(0) = 0,   *G*(0) = 1,   *Fpp*(0) = α,   *Gp*(0) = β };

$$IC := \{ F(0) = 0, Fp(0) = 0, Fpp(0) = \alpha, G(0) = 1, Gp(0) = \beta \} \tag{7}$$

> *IC1* := { *F*(0) = 0,   *Fp*(0) = 0,   *Gp*(0) = −1,   *Fpp*(0) = α,   *G*(0) = β } :

> *IC2* := { *F*(0) = 0,   *Fp*(0) = *ee*,   *G*(0) = −*Ga*·(1.00 + β),   *Fpp*(0) = α,   *Gp*(0) = β } :

> *IC3* := { *F*(0) = 0,   *Fp*(0) = 1 + *Ga*·α,   *G*(0) = 1 + *Be*·β,   *Fpp*(0) = α,   *Gp*(0) = β }

$$IC3 := \{ F(0) = 0, Fp(0) = 1 + \alpha, Fpp(0) = \alpha, G(0) = 1 + \beta, Gp(0) = \beta \} \tag{8}$$

> $BC := \{Fp(\text{blt}) = ee, G(\text{blt}) = 0\};$

$$BC := \{Fp(5.5) = 1, G(5.5) = 0\} \tag{9}$$

> $infolevel[shoot] := 1:$

> $Pr := 0.72; S1 := shoot(ODE, IC3, BC, FNS, [\alpha = -0, \beta = 0.575]): Pr := 1; S2$
  $:= shoot(ODE, IC3, BC, FNS, [\alpha = -0, \beta = 0.615]): Pr := 3; S3 := shoot(ODE, IC3,$
  $BC, FNS, [\alpha = -0, \beta = 0.734]): Pr := 5; S4 := shoot(ODE, IC3, BC, FNS, [\alpha = -0, \beta$
  $= 0.781]): Pr := 7; S5 := shoot(ODE, IC3, BC, FNS, [\alpha = -0, \beta = 0.809]):$

$$Pr := 0.72$$

```
shoot: Step #  1
shoot: Parameter values :   alpha = 0 beta = .575
shoot: Step #  2
shoot: Parameter values :   alpha = -0.482783236851197345e-17
beta = -.575201091224522898
```

$$Pr := 1$$

```
shoot: Step #  1
shoot: Parameter values :   alpha = 0 beta = .615
shoot: Step #  2
shoot: Parameter values :   alpha = 0.103914355612564965e-17 beta
= -.614757725085021800
```

$$Pr := 3$$

```
shoot: Step #  1
shoot: Parameter values :   alpha = 0 beta = .734
shoot: Step #  2
shoot: Parameter values :   alpha = -0.109020341856400502e-17
beta = -.734321881666163856
shoot: Step #  3
shoot: Parameter values :   alpha = -0.109020341856400502e-17
beta = -.734321881488766759
```

$$Pr := 5$$

```
shoot: Step #  1
shoot: Parameter values :   alpha = 0 beta = .781
shoot: Step #  2
shoot: Parameter values :   alpha = 0.162198316532156540e-17 beta
= -.781097709236407645
shoot: Step #  3
shoot: Parameter values :   alpha = 0.162198316532156540e-17 beta
= -.781097709108127258
```

$$Pr := 7$$

```
shoot: Step #  1
shoot: Parameter values :   alpha = 0 beta = .809
shoot: Step #  2
shoot: Parameter values :   alpha = -0.161953843181965100e-17
```

101

Maple (Shoot) Program for obtained Figure 3.2
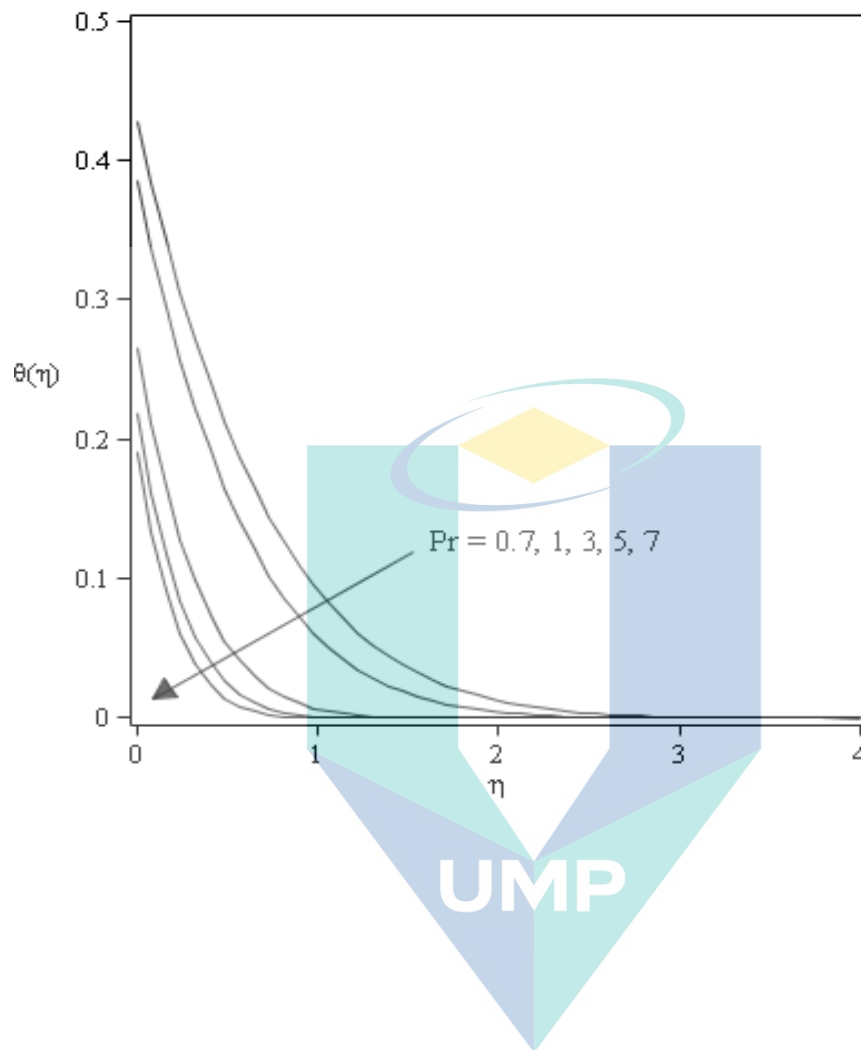
In this appendix, the transformation of Partial Differential Equations to Ordinary differential Equations in Chapter 4 will be discussed in detail by using a similarity transformation in exponential form. The governing equations are shown as below:

Continuity equation:

$$\frac{\partial u}{\partial x} + \frac{\partial v}{\partial y} = 0 \qquad \text{B.1}$$

Momentum equation:

$$u\frac{\partial u}{\partial x} + v\frac{\partial u}{\partial y} = u_e\frac{\partial u_e}{\partial x} + v\frac{\partial^2 u}{\partial y^2} + \sqrt{2}\, v\, \Gamma\, \frac{\partial u}{\partial y}\frac{\partial^2 u}{\partial y^2} \qquad \text{B.2}$$

Energy equation:

$$u\frac{\partial T}{\partial x} + v\frac{\partial T}{\partial y} = \frac{k}{\rho C_p}\frac{\partial^2 T}{\partial y^2} + \frac{\mu}{\rho C_p}\left[\left(\frac{\partial u}{\partial y}\right)^2 + \frac{\Gamma}{\sqrt{2}}\left(\frac{\partial u}{\partial y}\right)^3\right] \qquad \text{B.3}$$

corresponds to the following conditions

$$u = u_w(x) + \gamma^*\mu\frac{\partial u}{\partial y}, \quad v = 0, \quad T = T_w + \beta^*\frac{\partial T}{\partial y} \quad \text{at} \quad y = 0 \qquad \text{B.4}$$

$$u \to u_e(x), \quad T \to T_\infty \quad \text{as} \quad y \to \infty$$

The following Equations (B.1), (B.2), (B.3) and (B.4) are transformed to ODEs by using the similarity transformations in exponential form below

$$\eta = \left(\frac{c}{v}\right)^{1/2} y, \qquad \text{B.5}$$

$$\psi = (cv)^{1/2}\, xf(\eta), \qquad \text{B.6}$$

$$\theta(\eta) = \frac{T - T_\infty}{T_w - T_\infty}, \qquad \text{B.7}$$

where η and $\theta(\eta)$ are dimensionless variables, while ψ is the stream function. Then, u and v can be defined as

$$u = \frac{\partial \psi}{\partial y}, \qquad\qquad\qquad \text{B.8}$$

$$v = -\frac{\partial \psi}{\partial x}, \qquad\qquad\qquad \text{B.9}$$

Thus, we obtain

$$u = cxf'(\eta), \qquad\qquad\qquad \text{B.10}$$

$$v = -(c\nu)^{1/2} f(\eta). \qquad\qquad\qquad \text{B.11}$$

Then, u and v can be derived as

$$
\begin{aligned}
u &= cxf'(\eta) \\
u &= \frac{\partial \psi}{\partial y} \\
&= \frac{\partial \psi}{\partial \eta} \cdot \frac{\partial \eta}{\partial y} \\
&= \frac{\partial}{\partial \eta}\left[(c\nu)^{1/2} xf'(\eta) \right] \cdot \frac{\partial}{\partial y}\left[\left(\frac{c}{\nu}\right)^{1/2} y \right] \\
&= \left[(c\nu)^{1/2} xf'(\eta) \right] \cdot \left(\frac{c}{\nu}\right)^{1/2} \\
&= cxf'(\eta)
\end{aligned}
\qquad \text{B.12}
$$

$$
\begin{aligned}
v &= -\frac{\partial \psi}{\partial x} \\
&= -\frac{\partial}{\partial x}\left[(c\nu)^{1/2} xf'(\eta) \right], \\
&= -(c\nu)^{1/2} xf'(\eta)
\end{aligned}
\qquad \text{B.13}
$$

104

with

$$\frac{\partial u}{\partial x} = \frac{\partial}{\partial x}\left(cxf'(\eta)\right)$$
$$= cf'(\eta)$$

B.14

$$\frac{\partial v}{\partial y} = \frac{\partial v}{\partial \eta} \cdot \frac{\partial \eta}{\partial y}$$
$$= \frac{\partial}{\partial \eta}\left[-(cv)^{1/2} f'(\eta)\right] \cdot \frac{\partial}{\partial y}\left[\left(\frac{c}{v}\right)^{1/2} y\right]$$
$$= \left[-(cv)^{1/2} f'(\eta)\right] \cdot \left(\frac{c}{v}\right)^{1/2}$$
$$= -cf'(\eta)$$

B.15

Continuity Equation:

By substituting the above equations into Equation (B.1), then

$$\frac{\partial u}{\partial x} + \frac{\partial v}{\partial y} = 0,$$

B.16

$$\frac{\partial u}{\partial x} + \frac{\partial v}{\partial y} = cf'(\eta) + \left(-cf'(\eta)\right)$$
$$= 0$$

and Equation (B.1) is identically satisfied.

Momentum equation:

From the similarity Equations (B.5) to (B.7), it is found that

$$u = c x f'(\eta), \ \frac{\partial u}{\partial x} = cf'(\eta), \ v = -(cv)^{1/2} f'(\eta), \ u_e(x) = ax,$$

B.17

$$\frac{\partial u}{\partial x} = cf'(\eta), \ \frac{\partial \eta}{\partial y} = \left(\frac{c}{v}\right)^{1/2}, \ \frac{\partial u_e}{\partial x} = a \ ,$$

B.18

105

$$\frac{\partial u}{\partial y} = \frac{\partial u}{\partial \eta} \cdot \frac{\partial \eta}{\partial y} = cxf''(\eta)\left(\frac{c}{v}\right)^{1/2},$$

B.19

$$\frac{\partial^2 u}{\partial y^2} = \frac{\partial\left[\frac{\partial u}{\partial y}\right]}{\partial \eta} \cdot \frac{\partial \eta}{\partial y} = \left[cxf'''(\eta)\left(\frac{c}{v}\right)^{1/2}\right]\cdot\left(\frac{c}{v}\right)^{1/2} = \frac{c^2}{v}xf'''(\eta),$$

B.20

By substituting the above equation into momentum Equation (B.2), then

$$u\frac{\partial u}{\partial x} + v\frac{\partial u}{\partial y} = u_e\frac{\partial u_e}{\partial x} + v\frac{\partial^2 u}{\partial y^2} + \sqrt{2}\ v\ \Gamma\ \frac{\partial u}{\partial y}\frac{\partial^2 u}{\partial y^2}$$

$$\left[cxf'(\eta)\right]\left[c\,f'(\eta)\right] + \left[-(cv)^{1/2}\,f'(\eta)\right]\left[cxf''(\eta)\left(\frac{c}{v}\right)^{1/2}\right] = [ax][a] +$$
$$v\left[\frac{c^2xf'''(\eta)}{v}\right] + \sqrt{2}\ v\Gamma\left[cxf''(\eta)\left(\frac{c}{v}\right)^{1/2}\right]\left[cxf'''(\eta)\left(\frac{c}{v}\right)\right]$$

B.21

$$c^2\,x\,f'(\eta)^2 - c^2\,x\,f'(\eta)^2\,f''(\eta) = a^2\,x + c^2\,x\,f'''(\eta) +$$
$$\sqrt{2}\,v\,\Gamma\,c^3\,x^2\,f''(\eta)\,f'''(\eta)\left(\frac{c}{v}\right)^{1/2}$$

B.22

$$c^2\,x\,f'(\eta)^2 - c^2\,x\,f'(\eta)\,f''(\eta) = a^2\,x + c^2\,x\,f'''(\eta) +$$
$$\sqrt{2}v\,\Gamma\,c^{7/2}\,x^2\,v^{-1/2}\,f''(\eta)\,f'''(\eta)$$

B.23

$$\left[\begin{array}{l}c^2\,x\,f'(\eta)^2 - c^2\,x\,f'(\eta)\,f''(\eta) = a^2\,x + c^2\,x\,f'''(\eta) + \\ \sqrt{2}\,v\,\Gamma\,c^{7/2}\,x^2\,v^{-1/2}\,f''(\eta)\,f'''(\eta)\end{array}\right] \div c^2\,x$$

B.24

$$f'(\eta)^2 - f'(\eta)\,f''(\eta) = \frac{a^2}{c^2} + f'''(\eta) + \sqrt{2}\ c^{3/2}\ v^{-1/2}\ x\Gamma\,f''(\eta)\,f'''(\eta)$$

B.25

$$f'(\eta)^2 - f'(\eta)f''(\eta) = \left(\frac{a}{c}\right)^2 + f'''(\eta) + \left(x\Gamma\sqrt{\frac{2c^3}{\nu}}\right)f''(\eta)f'''(\eta) \qquad \text{B.26}$$

we assume

$$f'(\eta) = f' \qquad \text{B.27}$$

therefore we get,

$$f'^2 - f'f'' = \left(\frac{a}{c}\right)^2 + f''' + \left(x\Gamma\sqrt{\frac{2c^3}{\nu}}\right)f''f''' \qquad \text{B.28}$$

where,

$$\left(\frac{a}{c}\right)^2 = \varepsilon \text{ (stretching parameter)} \qquad \text{B.29}$$

$$\left(x\Gamma\sqrt{\frac{2c^3}{\nu}}\right) = \lambda \text{ (non-Newtonion Williamson fluid parameter)} \qquad \text{B.30}$$

now the momentum equation become

$$f'^2 - f'f'' = \varepsilon^2 + f''' + \lambda f''f''' \qquad \text{B.31}$$

therefore, the new momentum equation as below

$$f''' + f'f'' + \varepsilon^2 - f'^2 + \lambda f''f''' = 0 \qquad \text{B.32}$$

Energy equation:

From the similarity Equations (B.5) to (B.7), it is found that

$$T = T_\infty + \theta(\eta)bx^2, \ \frac{\partial T}{\partial \eta} = \theta'(\eta)bx^2, \ \frac{\partial \eta}{\partial y} = \left(\frac{c}{\nu}\right)^{1/2}, \qquad \text{B.33}$$

$$\frac{\partial T}{\partial x} = 2\theta(\eta)bx \qquad \text{B.34}$$

107

$$\frac{\partial T}{\partial y} = \frac{\partial T}{\partial \eta} \cdot \frac{\partial \eta}{\partial y} = \left[\left(\theta'(\eta) b x^2 \right) \right] \cdot \left(\frac{c}{\nu} \right)^{1/2} = \left(\theta'(\eta) b x^2 \right) \left(\frac{c}{\nu} \right)^{1/2} \qquad \text{B.35}$$

$$\frac{\partial^2 T}{\partial y^2} = \frac{\partial \left[\frac{\partial T}{\partial y} \right]}{\partial \eta} \cdot \frac{\partial \eta}{\partial y} = \left[\left(\theta''(\eta) b x^2 \right) \left(\frac{c}{\nu} \right)^{1/2} \right] \cdot \left(\frac{c}{\nu} \right)^{1/2} = \left(\theta''(\eta) b x^2 \right) \left(\frac{c}{\nu} \right) \qquad \text{B.36}$$

By substituting the above equation into energy Equation (B.3), then

$$u \frac{\partial T}{\partial x} + v \frac{\partial T}{\partial y} = \frac{k}{\rho C_p} \frac{\partial^2 T}{\partial y^2} + \frac{\mu}{\rho C_p} \left[\left(\frac{\partial u}{\partial y} \right)^2 + \frac{\Gamma}{\sqrt{2}} \left(\frac{\partial u}{\partial y} \right)^3 \right]$$

$$\left[c x f'(\eta) \right] \left[2 b x \theta(\eta) \right] + \left[-(c\nu)^{1/2} f'(\eta) \right] \left[\theta'(\eta) b x^2 \left(\frac{c}{\nu} \right)^{1/2} \right] = \frac{k}{\rho C_p}$$
$$\left[\theta''(\eta) b x^2 \left(\frac{c}{\nu} \right) \right] + \frac{\mu}{\rho C_p} \left[\left(c^2 x^2 f''^2(\eta) \left(\frac{c}{\nu} \right) \right) + \frac{\Gamma}{\sqrt{2}} \left(c^3 x^3 f''^3(\eta) \left(\frac{c}{\nu} \right)^{3/2} \right) \right] \qquad \text{B.37}$$

$$2 b c x^2 f'(\eta) \theta(\eta) - b c x^2 f(\eta) \theta'(0) = \frac{k}{\rho C_p} \theta''(\eta) b c x^2 + \frac{\mu}{\rho C_p}$$
$$\left(c^2 x^2 f''(\eta) \frac{c}{\nu} + \frac{\Gamma}{\sqrt{2}} c^3 x^3 f''^3(\eta) \left(\frac{c}{\nu} \right)^{3/2} \right) \qquad \text{B.38}$$

$$2 b c x^2 f'(\eta) \theta(\eta) - b c x^2 f(\eta) \theta'(0) = \frac{k}{\rho C_p} \theta''(\eta) b c x^2 + \frac{\mu}{\rho C_p}$$
$$\left(\frac{c^3 x^2}{\nu} f''^2(\eta) + \frac{1}{2} \Gamma x \sqrt{\frac{2 c^3}{\nu}} f''^3(\eta) \right) \qquad \text{B.39}$$

$$\lambda = x \Gamma \sqrt{\frac{2 c^3}{\nu}} \quad \text{(non-Newtonion Williamson fluid parameter)} \qquad \text{B.40}$$

$$2bcx^2 f'(\eta)\theta(\eta) - bcx^2 f(\eta)\theta'(\eta) = \frac{k}{\rho C_p}\theta''(\eta)bcx^2 + \frac{\mu}{\rho C_p}$$

$$\left(\frac{c^3 x^2}{\nu}f''^2(\eta) + \frac{1}{2}\lambda\frac{c^3 x^2}{\nu}f''^3(\eta)\right)$$

B.41

$$2bcx^2 f'(\eta)\theta(\eta) - bcx^2 f(\eta)\theta'(\eta) = \frac{k}{\rho C_p}\theta''(\eta)bcx^2 +$$

$$\frac{\mu}{\rho C_p}\frac{c^3 x^2}{\nu}\left(f''^2(\eta) + \frac{1}{2}\lambda f''^3(\eta)\right)$$

B.42

$$\left[\begin{array}{l}2bcx^2 f'(\eta)\theta(\eta) - bcx^2 f(\eta)\theta'(\eta) = \frac{k}{\rho C_p}\theta''(\eta)bcx^2 + \\ \frac{\mu}{\rho C_p}\frac{c^3 x^2}{\nu}\left(f''^2(\eta) + \frac{1}{2}\lambda f''^3(\eta)\right)\end{array}\right] \div bcx^2$$

B.43

$$\Pr = \frac{\nu\rho C_p}{k}, \text{ Prandtl number, where } \frac{1}{\Pr} = \frac{k}{\rho C_p}$$

B.44

$$2f'(\eta)\theta(\eta) - f(\eta)\theta'(\eta) = \frac{1}{\Pr}\theta''(\eta) + \frac{\nu\rho}{\rho C_p}\frac{c^2}{\nu b}\left(f''^2(\eta) + \frac{\lambda}{2}f''^3(\eta)\right)$$

B.45

$$2f'(\eta)\theta(\eta) - f(\eta)\theta'(\eta) = \frac{1}{\Pr}\theta''(\eta) + \frac{c^2}{C_p b}\left(f''^2(\eta) + \frac{\lambda}{2}f''^3(\eta)\right)$$

B.46

$$Ec = \frac{c^2}{C_p b} \text{ (Eckert number)}$$

B.47

$$2f'(\eta)\theta(\eta) - f(\eta)\theta'(\eta) = \frac{1}{\Pr}\theta''(\eta) + Ec\left(f''^2(\eta) + \frac{\lambda}{2}f''^3(\eta)\right)$$

B.48

we assume

$$f'(\eta) = f'$$
$$\theta'(\eta) = \theta'$$

B.49

$$2 f' \theta - f \theta' = \frac{1}{\text{Pr}} \theta'' + Ec \left(f''^2 + \frac{\lambda}{2} f''^3 \right) \qquad \text{B.50}$$

$$\text{Pr} \left(2 f' \theta - f \theta' \right) = \theta'' + \text{Pr} \, Ec \left(f''^2 + \frac{\lambda}{2} f''^3 \right) \qquad \text{B.51}$$

$$\theta'' - \text{Pr} \left(2 f' \theta - f \theta' \right) + \text{Pr} \, Ec \left(f''^2 + \frac{\lambda}{2} f''^3 \right) = 0 \qquad \text{B.52}$$

The boundary conditions (B.4) for the variables are carried out as follows when $y = 0$, is detailed out as in Table B.1.
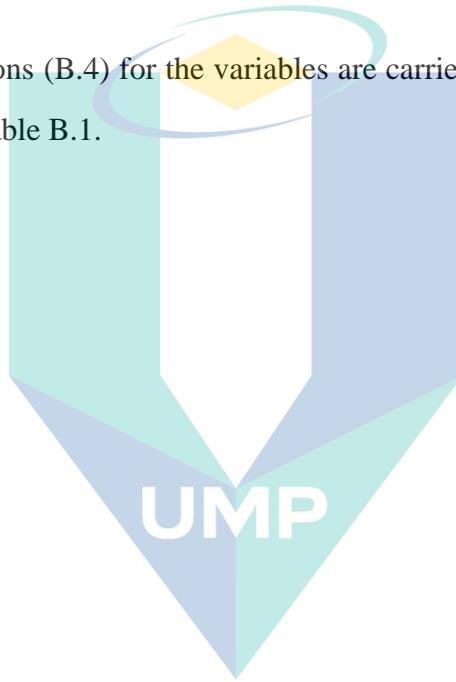
Table B.1   Formulation of Boundary Conditions

Boundary condition	Transformed Boundary Condition
$u = u_w(x) + \gamma^* \mu \dfrac{\partial u}{\partial y}$	$u = u_w(x) + \gamma^* \mu \dfrac{\partial u}{\partial y}$
	$cxf'(0) = cx + \gamma^* \mu \cdot cxf''\left(\dfrac{c}{\nu}\right)^{1/2}$
	$\left[cxf'(0) = cx + \gamma^* \mu \cdot cxf''\left(\dfrac{c}{\nu}\right)^{1/2} \right] \div cx$
	$f'(0) = 1 + \gamma^* \mu f''\left(\dfrac{c}{\nu}\right)^{1/2}$
	$f'(0) = 1 + \dfrac{\gamma}{\rho(c\nu)^{1/2}} \nu \rho f''\left(\dfrac{c}{\nu}\right)^{1/2}$
	$f'(0) = 1 + \gamma f''(0)$
$T = T_w(x) + \beta^* \mu \dfrac{\partial T}{\partial y}$	$\theta(0) b x^2 + T_\infty = T_\infty + b x^2 + \beta^* \theta'(0) b x^2 \left(\dfrac{c}{\nu}\right)^{1/2}$
	$\theta(0)(T_w - T_\infty) + T_\infty = T_\infty + (T_w - T_\infty) + \beta^* \theta'(0)(T_w - T_\infty)\left(\dfrac{c}{\nu}\right)^{1/2}$
	$\theta(0)(T_w - T_\infty) + T_\infty - T_\infty = (T_w - T_\infty) + \beta^* \theta'(0)(T_w - T_\infty)\left(\dfrac{c}{\nu}\right)^{1/2}$
	$\left(\begin{array}{l} \theta(0)(T_w - T_\infty) = (T_w - T_\infty) + \\ \beta^* \theta'(0)(T_w - T_\infty)\left(\dfrac{c}{\nu}\right)^{1/2} \end{array} \right) \div (T_w - T_\infty)$
	$\theta(0) = 1 + \dfrac{\beta}{\left(\dfrac{c}{\nu}\right)^{1/2}} \theta'(0)\left(\dfrac{c}{\nu}\right)^{1/2}$
	$\theta(0) = 1 + \beta \theta'(0)$

111

Table B.1 (continued)

Boundary condition	Transformed Boundary Condition
$v = 0$	$v = 0$
	$-(cv)^{1/2} f(0) = 0$
	$f(0) = \dfrac{0}{-(cv)^{1/2}}$
	$f(0) = 0$
$u \to u_e(x)$	$u \to u_e(x)$
	$cxf'(\infty) \to ax$
	$f'(\infty) \to \dfrac{a}{c}$
	$f'(\infty) \to \varepsilon$
$T \to T_\infty$	$T \to T_\infty(x)$
	$\theta(\infty)bx^2 + T_\infty \to T_\infty$
	$\theta(\infty)T_\infty bx^2 \to T_\infty - T_\infty$
	$\theta(\infty)(T_w - T_\infty) \to 0$
	$\theta(\infty) \to \dfrac{0}{(T_w - T_\infty)}$
	$\theta(\infty) \to 0$

Thus, the boundary conditions are obtained after the similarity transformations as follows:

$$f(0) = 0,\ f'(0) = 1 + \gamma f''(0),\ \theta(0) = 1 + \beta \theta'(0)$$

$$f'(\eta) \to \varepsilon,\ \theta(\eta) \to 0 \ \text{ as } \ \eta \to \infty$$

112

In this appendix, the transformation of Partial Differential Equations to Ordinary Differential Equationcs in Chapter 5 will be discussed in detail by using a similarity transformation in exponential form. The governing equations are shown as below:

Continuity equation:

$$\frac{\partial u}{\partial x} + \frac{\partial v}{\partial y} = 0 \qquad \text{C.1}$$

Momentum equation:

$$u\frac{\partial u}{\partial x} + v\frac{\partial u}{\partial y} = u_e\frac{\partial u_e}{\partial x} + v\frac{\partial^2 u}{\partial y^2} + \sqrt{2}\,v\,\Gamma\,\frac{\partial u}{\partial y}\frac{\partial^2 u}{\partial y^2} + \frac{\sigma B_o^2}{\rho}\left(u_e - u\right) \qquad \text{C.2}$$

Energy equation:

$$u\frac{\partial T}{\partial x} + v\frac{\partial T}{\partial y} = \frac{k}{\rho C_p}\frac{\partial^2 T}{\partial y^2} - \frac{\partial q_r}{\partial y} \qquad \text{C.3}$$

corresponds to the following conditions

$$u = u_w(x),\ v = 0,\ T = T_w \ \text{at}\ y = 0 \qquad \text{C.4}$$

$$u \to u_e(x),\ T \to T_\infty \ \text{as}\ y \to \infty$$

The following Equations (C.1), (C.2), (C.3) and (C.4) are transformed to ordinary differential equations by using the similarity transformations in exponential form below

$$\eta = \left(\frac{c}{v}\right)^{1/2} y, \qquad \text{C.5}$$

$$\psi = (cv)^{1/2} xf(\eta), \qquad \text{C.6}$$

$$\theta(\eta) = \frac{T - T_\infty}{T_w - T_\infty}, \qquad \text{C.7}$$

where η and $\theta(\eta)$ are dimensionless variables, while ψ is the stream function. Then, u and v can be defined as

$$u = \frac{\partial \psi}{\partial y}, \qquad\qquad \text{C.8}$$

$$v = -\frac{\partial \psi}{\partial x}, \qquad\qquad \text{C.9}$$

Thus, we obtain

$$u = c\, x\, f'(\eta), \qquad\qquad \text{C.10}$$

$$v = -(c\nu)^{1/2} f(\eta). \qquad\qquad \text{C.11}$$

Then, u and v can be derived as

$$
\begin{aligned}
u &= c\, x\, f'(\eta) \\
u &= \frac{\partial \psi}{\partial y} \\
&= \frac{\partial \psi}{\partial \eta} \cdot \frac{\partial \eta}{\partial y} \\
&= \frac{\partial}{\partial \eta}\Big[(c\nu)^{1/2} x\, f'(\eta) \Big] \cdot \frac{\partial}{\partial y}\left[\left(\frac{c}{\nu}\right)^{1/2} y \right] \\
&= \Big[(c\nu)^{1/2} x\, f'(\eta) \Big] \cdot \left(\frac{c}{\nu}\right)^{1/2} \\
&= c\, x\, f'(\eta)
\end{aligned}
\qquad \text{C.12}
$$

$$
\begin{aligned}
v &= -\frac{\partial \psi}{\partial x} \\
&= -\frac{\partial}{\partial x}\Big[(c\nu)^{1/2} x\, f'(\eta) \Big], \\
&= -(c\nu)^{1/2} x\, f'(\eta)
\end{aligned}
\qquad \text{C.13}
$$

with

$$\frac{\partial u}{\partial x} = \frac{\partial}{\partial x}\big(c\,x\,f'(\eta)\big),$$
$$= c\,f'(\eta)$$

C.14

$$\frac{\partial v}{\partial y} = \frac{\partial v}{\partial \eta}\cdot\frac{\partial \eta}{\partial y}$$
$$= \frac{\partial}{\partial \eta}\Big[-(c\nu)^{1/2}\,f'(\eta)\Big]\cdot\frac{\partial}{\partial y}\left[\left(\frac{c}{\nu}\right)^{1/2} y\right]$$
$$= -(c\nu)^{1/2}\,f'(\eta)\cdot\left(\frac{c}{\nu}\right)^{1/2}$$
$$= -c\,f'(\eta)$$

C.15

Continuity Equation:

By substituting the above equations into Equation (C.1), then

$$\frac{\partial u}{\partial x} + \frac{\partial v}{\partial y} = 0,$$
$$\frac{\partial u}{\partial x} + \frac{\partial v}{\partial y} = c\,f'(\eta) + \big(-c\,f'(\eta)\big)$$
$$= 0$$

C.16

and Equation (C.1) is identically satisfied.

Momentum equation:

From the similarity Equation (C.5) to (C.7), it is found that

$$u = c\,x\,f'(\eta),\ \ \frac{\partial u}{\partial x} = c\,f'(\eta),\ \ v = -(\nu c)^{1/2}\,f'(\eta),\ \ u_e(x) = a\,x,$$

C.17

115

$$\frac{\partial u}{\partial x} = c\, f'(\eta), \ \frac{\partial \eta}{\partial y} = \left(\frac{c}{v}\right)^{1/2}, \ \frac{\partial u_e}{\partial x} = a \,, \qquad \text{C.18}$$

$$\frac{\partial u}{\partial y} = \frac{\partial u}{\partial \eta} \cdot \frac{\partial \eta}{\partial y} = c\, x\, f''(\eta)\left(\frac{c}{v}\right)^{1/2}, \qquad \text{C.19}$$

$$\frac{\partial^2 u}{\partial y^2} = \frac{\partial \left[\frac{\partial u}{\partial y}\right]}{\partial \eta} \cdot \frac{\partial \eta}{\partial y} = c\, x\, f'''(\eta) \cdot \left(\frac{c}{v}\right)^{1/2} \cdot \left(\frac{c}{v}\right)^{1/2} = \frac{c^2}{v} x\, f'''(\eta), \qquad \text{C.20}$$

By substituting the above equation into momentum Equation (C.2), then

$$u\frac{\partial u}{\partial x} + v\frac{\partial u}{\partial y} = u_e \frac{\partial u_e}{\partial x} + v\frac{\partial^2 u}{\partial y^2} + \sqrt{2}\, v\, \Gamma\, \frac{\partial u}{\partial y}\frac{\partial^2 u}{\partial y^2} + \frac{\sigma B_o^2}{\rho}(u_e - u)$$

$$\left[c\, x\, f'(\eta)\right]\left[c\, f'(\eta)\right] + \left[-(c v)^{1/2}\, f(\eta)\right]\left[c\, x\, f''(\eta)\left(\frac{c}{v}\right)^{1/2}\right] =$$

$$(a\, x)(a) + v\left[\frac{c^2\, x\, f'''(\eta)}{v}\right] + \sqrt{2}\, v\, \Gamma\left[c\, x\, f''(\eta)\left(\frac{c}{v}\right)^{1/2}\right]\left[c\, x\, f'''(\eta)\left(\frac{c}{v}\right)\right] \quad \text{C.21}$$

$$+ \frac{\sigma B_o^2}{\rho}\left[a\, x - c\, x\, f'(\eta)\right]$$

$$c^2\, x\, f'^2(\eta) - c^2\, f(\eta)\, f''(\eta) = a^2\, x + c^2\, x\, f'''(\eta) +$$

$$v\, \Gamma \sqrt{2}\, c^2\, x^2\, f''(\eta)\, f'''(\eta)\left(\frac{c}{v}\right)^{1/2} + \frac{\sigma B_o^2}{\rho}\left(a\, x - c\, x\, f'(\eta)\right) \qquad \text{C.22}$$

$$\left[\begin{array}{l} c^2\, x\, f'^2(\eta) - c^2\, f(\eta)\, f''(\eta) = a^2\, x + c^2\, x\, f'''(\eta) + \\[2mm] v\, \Gamma \sqrt{2}\, c^2\, x^2\, f''(\eta)\, f'''(\eta)\left(\frac{c}{v}\right)^{1/2} + \frac{\sigma B_o^2}{\rho}\left(a\, x - c\, x\, f'(\eta)\right) \end{array}\right] \div c^2 x \qquad \text{C.23}$$

$$f'^2(\eta) - f(\eta)f''(\eta) = \left(\frac{a}{c}\right)^2 + f'''(\eta) + \nu\,\Gamma\sqrt{\frac{2c^3}{\nu}}\,f''(\eta)f'''(\eta)$$
$$+\frac{\sigma B_o^2}{\rho}\left(\frac{a - c\,f'(\eta)}{c}\right) \tag{C.24}$$

$$f'^2(\eta) - f(\eta)f''(\eta) = \left(\frac{a}{c}\right)^2 + f'''(\eta) + \nu\,\Gamma\sqrt{\frac{2c^3}{\nu}}\,f''(\eta)f'''(\eta)$$
$$+\frac{\sigma B_o^2}{\rho c}\left(\frac{a}{c} - f'(\eta)\right) \tag{C.25}$$

where,

$$\left(\frac{a}{c}\right)^2 = \varepsilon \quad \text{(stretching parameter)} \tag{C.26}$$

$$\left(x\,\Gamma\sqrt{\frac{2c^3}{\nu}}\right) = \lambda \quad \text{(non-Newtonion Williamson fluid parameter)} \tag{C.27}$$

$$\frac{\sigma B_o^2}{\rho c} = M \quad \text{(magnetic parameter)} \tag{C.28}$$

$$f'^2(\eta) - f(\eta)f''(\eta) = \varepsilon^2 + f'''(\eta) + \lambda\,f''(\eta)f'''(\eta) + M\big(\varepsilon - f'(\eta)\big) \tag{C.29}$$

we assume
$$f'(\eta) = f' \tag{C.30}$$

therefore we get,
$$f'^2 - f\,f'' = \varepsilon^2 + f''' + \lambda\,f''\,f''' + M\big(\varepsilon - f'\big) \tag{C.31}$$

now the equation become

$$f''' + f\,f'' + \varepsilon^2 - f'^2 + \lambda\,f''\,f''' + M\big(\varepsilon - f'\big) = 0 \tag{C.32}$$

117

Energy equation:

From the similarity Equation (C.5), it is found that

$$T = T_\infty + \theta(\eta)b\,x^2, \quad \frac{\partial T}{\partial \eta} = \theta'(\eta)b\,x^2, \quad \frac{\partial \eta}{\partial y} = \left(\frac{c}{v}\right)^{1/2}, \quad q_r = -\frac{4\sigma^*}{3k^*}\frac{\partial T^4}{\partial y} \qquad \text{C.33}$$

$$T^4 \cong 4T_\infty^3 T - 3T_\infty^4 \qquad \text{C.34}$$

$$\frac{\partial T}{\partial x} = 2\theta(\eta)b\,x \qquad \text{C.35}$$

$$\frac{\partial T}{\partial y} = \frac{\partial T}{\partial \eta} \cdot \frac{\partial \eta}{\partial y} = \left(\theta'(\eta)b\,x^2\right) \cdot \left(\frac{c}{v}\right)^{1/2} = \left(\theta'(\eta)b\,x^2\right)\left(\frac{c}{v}\right)^{1/2} \qquad \text{C.36}$$

$$\frac{\partial^2 T}{\partial y^2} = \frac{\partial\left[\frac{\partial T}{\partial y}\right]}{\partial \eta} \cdot \frac{\partial \eta}{\partial y} = \left(\theta''(\eta)b\,x^2\right)\left(\frac{c}{v}\right)^{1/2} \cdot \left(\frac{c}{v}\right)^{1/2} = \left(\theta''(\eta)b\,x^2\right)\left(\frac{c}{v}\right) \qquad \text{C.37}$$

$$\frac{\partial q_r}{\partial y} = -\frac{-16\sigma^* T_\infty^3}{3k^*}\frac{\partial^2 T}{\partial y^2} = -\frac{-16\sigma^* T_\infty^3}{3k^*}\left(\theta''(\eta)b\,x^2\left(\frac{c}{v}\right)\right) \qquad \text{C.38}$$

By substituting the above equation into energy Equation (C.3), then

$$u\frac{\partial T}{\partial x} + v\frac{\partial T}{\partial y} = \frac{k}{\rho C_p}\frac{\partial^2 T}{\partial y^2} - \frac{\partial q_r}{\partial y}$$

$$\begin{aligned}
&\left[c\,x\,f'(\eta)\right]\left[2b\,x\,\theta(\eta)\right] + \left[-(cv)^{1/2} f(\eta)\right]\left[\theta'(\eta)b\,x^2\left(\frac{c}{v}\right)^{1/2}\right] = \\
&\frac{k}{\rho C_p}\left[\theta''(\eta)b\,x^2\left(\frac{c}{v}\right)\right] - \left[\frac{-16\sigma^* T_\infty^3}{3k^*}\left(\theta''(\eta)b\,x^2\left(\frac{c}{v}\right)\right)\right]
\end{aligned} \qquad \text{C.39}$$

$$2bcx^2 f'(\eta)\theta(\eta) - bcx^2 f(\eta)\theta'(\eta) = \frac{k}{\rho C_p}\left[\theta''(\eta)bx^2\left(\frac{c}{v}\right)\right]$$
$$+\frac{16\sigma^* T_\infty^3}{3k^*}\left[\left(\theta''(\eta)bx^2\left(\frac{c}{v}\right)\right)\right] \tag{C.40}$$

$$2bcx^2 f'(\eta)\theta(\eta) - bcx^2 f(\eta)\theta'(\eta) = \theta''(\eta)bx^2\left(\frac{c}{v}\right)$$
$$\left(\frac{k}{\rho C_p}+\frac{16\sigma^* T_\infty^3}{3k^*}\right) \tag{C.41}$$

$$\left[\begin{array}{l}2bcx^2 f'(\eta)\theta(\eta) - bcx^2 f(\eta)\theta'(\eta) = \theta''(\eta)bx^2\left(\frac{c}{v}\right)\\[2mm]\left(\dfrac{k}{\rho C_p}+\dfrac{16\sigma^* T_\infty^3}{3k^*}\right)\end{array}\right]\div bcx^2 \tag{C.42}$$

$$2f'(\eta)\theta(\eta) - f(\eta)\theta'(\eta) = \frac{\theta''(\eta)}{v}\left(\frac{k}{\rho C_p}+\frac{16\sigma^* T_\infty^3}{3k^*}\right) \tag{C.43}$$

$$2f'(\eta)\theta(\eta) - f(\eta)\theta'(\eta) = \frac{\theta''(\eta)k}{v\rho C_p}\left(1+\frac{16\sigma^* T_\infty^3}{3k^*}\right) \tag{C.44}$$

$$\Pr = \frac{v\rho C_p}{k} \quad \text{(Prandtl number)} \tag{C.45}$$

$$2f'(\eta)\theta(\eta) - f(\eta)\theta'(\eta) = \frac{1}{\Pr}\theta''(\eta)\left(1+\frac{4}{3}\frac{4\sigma^* T_\infty^3 \rho C_p}{k^* k}\right) \tag{C.46}$$

$$Nr = \frac{4\sigma^* T_\infty^3 \rho C_p}{k^* k} \quad \text{(thermal radiation parameter)} \tag{C.47}$$

$$2f'(\eta)\theta(\eta) - f(\eta)\theta'(\eta) = \frac{1}{\Pr}\theta''(\eta)\left(1+\frac{4}{3}Nr\right) \tag{C.48}$$

119

we assume

$$f'(\eta) = f'$$
$$\theta'(\eta) = \theta'$$

C.49

therefore we get,

$$2f'\theta - f\,\theta' = \frac{1}{\mathrm{Pr}}\,\theta''\left(1 + \frac{4}{3}Nr\right)$$

C.50

now the equation becomes

$$\theta''\left(1 + \frac{4}{3}Nr\right) - \mathrm{Pr}\left(2f'\theta - f\,\theta'\right) = 0$$
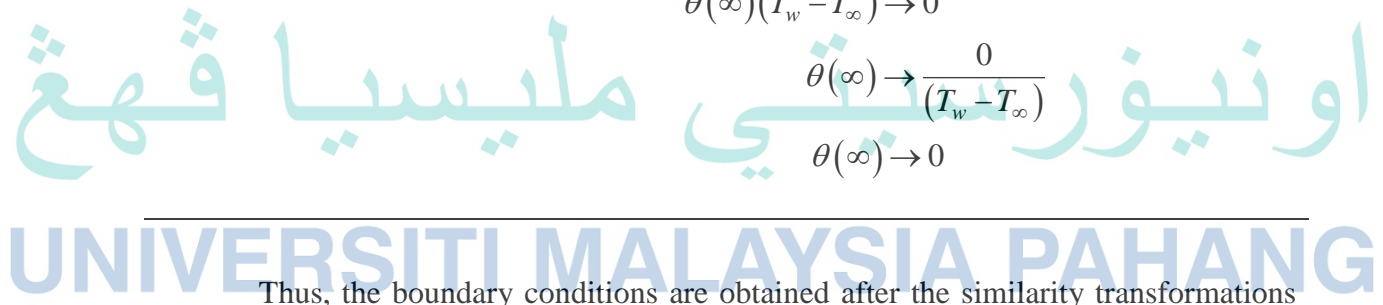
C.51

The boundary conditions (C.4) for the variables are carried out as follows when $y = 0$, is detailed out as in Table C.1

Table C.1 Formulation of Boundary Conditions

Boundary condition	Transformed Boundary Condition
$v = 0$	$v = 0$
	$-(c\nu)^{1/2} f(0) = 0$
	$f(0) = \dfrac{0}{-(c\nu)^{1/2}}$
	$f(0) = 0$
$u = u_w(x)$	$u = u_w(x)$
	$cxf'(0) = c\,x$
	$f'(0) = \dfrac{c\,x}{c\,x}$
	$f'(0) = 1$

Table C.1 (continued)

Boundary condition	Transformed Boundary Condition
$T = T_\infty$	$\theta(\infty)bx^2 = T_\infty + bx^2 - T_\infty$
	$\theta(\infty)bx^2 = T_\infty - T_\infty + bx^2$
	$\theta(\infty)bx^2 = bx^2$
	$\theta(\infty) = \dfrac{bx^2}{bx^2}$
	$\theta(\infty) = 1$
$u \to u_e(x)$	$u \to u_e(x)$
	$cxf'(\infty) \to ax$
	$f'(\infty) \to \dfrac{a}{c}$
	$f'(\infty) \to \varepsilon$
$T \to T_\infty(x)$	$T \to T_\infty(x)$
	$\theta(\infty)bx^2 + T_\infty \to T_\infty$
	$\theta(\infty)bx^2 \to T_\infty - T_\infty$
	$\theta(\infty)(T_w - T_\infty) \to 0$
	$\theta(\infty) \to \dfrac{0}{(T_w - T_\infty)}$
	$\theta(\infty) \to 0$

Thus, the boundary conditions are obtained after the similarity transformations
as follows:

$$f(0) = 0, \; f'(0) = 0, \; \theta(0) = 0 \text{ at } \eta = 0 \qquad \text{C.52}$$

$$f'(\infty) \to \varepsilon, \; \theta(\infty) \to 0 \text{ as } \eta \to \infty$$

APPENDIX D

LIST OF PUBLICATIONS

Proceeding

Presented

1. **Hashim, H.,** Mohamed, M. K. A., Hussanan, A., Ishak, N., Sarif, N. M. and Salleh, M. Z. 2015. The effects of slip conditions and viscous dissipation on the stagnation point flow over a stretching sheet. AIP Conference Proceedings.1691: 040007. (Scopus Indexed)

2. **Hashim, H.,** Mohamed, M. K. A., Hussanan, A., Ishak, N., Sarif, N. M. and Salleh, M. Z. 2016. Flow and heat transfer analysis of Williamson fluid on the stagnation point past a stretching surface with viscous dissipation and slip conditions. The National Conference for Postgraduate Research 2016, 725-738. (Indexed Proceeding)

3. **Hashim, H.,** Mohamed, M. K. A., Ishak, N., Sarif, N. M. and Salleh, M. Z. 2019. Thermal radiation effects on MHD Stangnation point flow of Williamson fluid over a strecthing surface.IOP Publishing, Journal of Physics: Conference Series, Volume.1366, No.1, pages 012011.

Journal

Published

1. Hussanan, A., Khan, I., **Hashim, H.,**Mohamed, M. K. A., Ishak, N., Sarif, N. M. and Salleh, M. Z. 2016. Unsteady MHD flow of some nanofluids past an accelerated vertical plate embedded in a porous medium. Jurnal Teknologi.78(2): 121-126. (Scopus)

2. Ishak, N**., Hashim, H.**, Mohamed, M. K. A., Sarif, N. M., Khaled, M., Rosli, N. and Salleh, M. Z. 2015. MHD flow and heat transfer for the upper-convected Maxwell fluid over a stretching/shrinking sheet with prescribed heat flux. AIP Conference Proceedings.1691: 040011. (Scopus)

3. M.K.A. Mohamed,**H. Hashim**, N.A.M. Noar, N.M. Sarif, M.Z. Salleh, A. Ishak (2016), Suction/Injection Effect on a Boundary Layer Flow past a Stretching Cylinder with Slip Condition. The National Conference for Postgraduate Research 2016, 739-746. (Indexed Proceeding)